Precipitation of Hematite and Recovery of Hydrochloric Acid from Aqueous Iron(II, III) Chloride Solutions by Hydrothermal Processing

Sebastian Johannes Hock

Department of Mining and Materials Engineering
McGill University, Montreal, Canada
June 2009

A thesis submitted to McGill University
in partial fulfillment of the requirements of the degree of
Master of Engineering

Abstract

Regeneration of HCl from process solutions is an important unit operation in chloride hydrometallurgy. Currently, it is accomplished by the highly capital and energy intensive technology of pyrohydrolysis. The research described in this thesis, has focused on an alternative HCl regeneration system from iron(II, III) chloride solutions that has been coined "Hydrolytic Distillation". This system relates to the earlier developed (in the 1970s) PORI Process. Basically this system involves two steps: (1) the oxidation of ferrous chloride solution by oxygen sparging under reflux conditions (atmospheric pressure) at 150ºC; and (2) the hydrolytic decomposition under atmospheric pressure of ferric chloride solution by continuous controlled water addition at 180ºC. As a result of the latter step iron is recovered as hematite and chloride units as superazeotropic (8-9 M) hydrochloric acid in the vapor phase condensate.

The study on oxidation determined that $^2/_3$ of $FeCl_2$ is converted to $FeCl_3$ and $^1/_3$ to Fe_2O_3 at a rate that is controlled by oxygen mass transfer. The hematite product from the oxidation step proved to be crystalline but nanostructured consisting of 1-2 μm porous aggregated particles possessing 12-28 m^2/g specific surface area and to be essentially pure α-Fe_2O_3 (70% Fe, <0.1% Cl^-). With reference to the hydrolytic precipitation/distillation step it was determined that at 180ºC, the temperature at which superazeotropic HCl (8-9 M) was consistently produced, the composition of the liquid phase is "$FeCl_3 \cdot 2H_2O$". Controlled continuous addition of H_2O (or feed solution) was found to be critical in maintaining pseudo-steady state and driving the reaction to ~95% conversion efficiency. The hematite consisted of coarse spherical compact aggregated particles (~40 μm) that exhibited excellent filtration and washing properties. Its %Fe content was 68.5% and it contained ~4% H_2O and ~3% Cl^- that could be removed by thorough washing.

Résumé

Le recyclage d’acide chlorhydrique à partir de solutions industrielles chlorées constitue une étape importante des procédés hydrométallurgiques. A l’heure actuelle cette opération est effectuée par pyrohydrolyse, une technique très couteuse d’un point de vue économique ou énergétique. La recherche présentée dans ce manuscrit se concentre sur un système de recyclage d’acide chlorhydrique à partir de solutions de chlorure de fer (II, III), baptisé "Distillation Hydrolytique". Ce système est issu du procédé PORI, préalablement développé (dans les années 1970). Le système inclus principalement deux étapes : (1) l’oxidation d’une solution de chlorure de fer (II) ($FeCl_2$) par barbotage d’oxygène et utilisation d’une colonne à reflux (sous pression atmosphérique), à une température de 150°C ; (2) la décomposition hydrolytique sous pression atmosphérique d’une solution de chlorure de fer (III) ($FeCl_3$) à 180 °C par ajout d’eau contrôlé et continu. A la fin de cette dernière étape, le fer est récupéré sous forme d’hématite et les dérivés chlorés sous forme d’acide chlorhydrique super-azéotropique (8-9 M) dans le condensat provenant de la phase gazeuse.

L’étude sur l’oxidation a permis de déterminer que $^2/_3$ du $FeCl_2$ était converti sous forme de $FeCl_3$ et le reste sous forme d’hématite Fe_2O_3, la vitesse de réaction étant contrôlée par le transfert de masse de l’oxygène. L’hématite produite lors de l’étape d’oxidation s’est avérée de nature cristalline, nano-structurée, constituée d’agrégats de particules poreuses, d’une taille moyenne de 1-2 μm avec une aire de surface de 12-28 m^2/g et de composition chimique α-Fe_2O_3 quasi pure (70% Fe, < 0.1% Cl^-). Quant à l’étape de précipitation/distillation hydrolytique, il a été déterminé qu’à 180°C, température à laquelle l’acide chlorhydrique super-azéotropique était continuellement produit, la composition de la phase liquide résultante était "$FeCl_3 \cdot 2H_2O$". L’ajout continu et contrôlé d’eau s’est avéré essentiel au maintient d’un régime pseudo-permanent et à l’obtention d’un rendement de réaction d’environ 95%. L’hématite produite lors de cette étape était constituée d’agrégats (~40 μm) de large particules sphériques fortement agglomérées, facilitant considérablement les étapes de filtration et de rinçage. Pour la composition chimique de ce produit d’hématite, des taux molaires de 68.5% en fer et de

~ 4% en eau ont été calculés, ainsi que ~ 3% d’ions chlorures qu’il a été possible de rincer ultérieurement.

Acknowledgements

First and foremost I would like to thank my supervisor, Professor Dr. George Demopoulos, for giving me the chance to work in his group. Without his offer to let me work for him in the Hydrometallurgy Laboratories at McGill University, I would have never experienced such wonderful two years of excellent research and friendship in Montreal. Furthermore, I would like to thank him for his invaluable guidance and especially for the interesting conversations during our meetings, that were not always about science but deeper.

This work would not have been possible without the support of Starfield Resources and Dr. Bryn Harris. Their sponsorship is enthusiastically acknowledged. The generous support of the Natural Sciences and Engineering Research Council of Canada (NSERC) is also recognized.

Moreover, I would like to thank members of the Hydrometallurgy Group at McGill, who helped me a lot with my time at McGill in the form of discussions, advice and friendship. Special thanks go to Cecile for help in translating the abstract, but also (and even more) for the nice conversations we had almost every day and our beautiful adventure in Edmonton. Thank you to Karl for everything. The help of Levente is gratefully acknowledged for his in depth advice and for sharing the benefit of his experience, but also for watching the experiment when I went for lunch. Thanks go to Guobin, Kee Eun, Derek (for his priceless workout and nutrition tips), Jeff, Lydia, Nick (for helping me to understand Québecois), Mario (for conducting vibrational spectroscopy), Renaud (for making my day in the office), Richard and Vincent (especially for the golf lessons!).

Special thanks to Ranjan Roy and Andrew Golsztajn for method development, troubleshooting and general advice in solution analysis by ICP-AES. I would also like to acknowledge the invaluable help of Helen Campbell, Monique Riendeau and Petr Fiurasek for solids characterization using a variety of techniques.

A big thank you goes to Barbara Hanley, who supported me a lot during my adventure at McGill here in Canada. Her help with the paper work and her patience on

the phone answering all the questions I had before arriving in Montreal are gratefully acknowledged.

Thanks go to all my friends outside of my Group at McGill, at Concordia, HEC, UdM and UQàM who have given me general advice and have always been there to encourage me over the last two years. I would also like to recognize my friends in the Department of Materials Engineering who were always willing to stop in the halls for a quick chat and to go out for a few drinks at the end of a long week. Thanks go to Max, Nathan, Pascale, Patrick, Per, Phil, Ryan and to the others that are too many to name! Thanks to the Ice Hockey Team “Blades of Wood”, for teaching me how to skate without breaking a bone, and to our Softball Team for the nice games on the field.

Last, but certainly not least, a very big thank you to my parents Beate and Peter as well as to Rosalinde and Paulus for their love, support and advice over the past few years of my studies. Without their generous help and encouragement, I would have certainly never made it over the Atlantic Ocean during my studies. God bless you and “Vielen Dank!”.

„Was ist das Leben voller Müh'n,
wenn uns die Zeit fehlt staunend still zu steh'n?“

Table of Contents

Chapter 4: The Oxidation of Ferrous Chloride 35

List of Figures

List of Tables

Chapter 1: Introduction

High energy costs and rising environmental awareness have, amongst other factors, prompted the extractive industry to develop cheaper, more efficient and cleaner processes for HCl regeneration from liquors generated in the leaching of mineral feedstocks or the finishing of metals. As an example, the steel industry has to deal with large amounts of waste pickle liquors from galvanization plants, containing 18%-25% ferrous chloride, 1% ferric chloride and about 1% of free HCl [1]. Another key operation is the chloride leaching of metal sulphide ores. In both cases the iron chloride liquors need to be treated in order to regenerate the hydrochloric acid [2]. Several approaches to recover the HCl and convert the ferrous and ferric chloride to iron oxide have been exploited. Currently the predominant technology by which this is accomplished is the capital- and energy intensive process of pyrohydrolysis.

In the current research a new low temperature approach to HCl regeneration from Fe(II)-Fe(III)-Cl solutions by “Hydrolytic Distillation” is investigated, as an alternative to pyrohydrolysis. Hydrolytic distillation [2] involves the hydrolytic decomposition under atmospheric pressure of boiling ferric chloride solution leading to precipitation of hematite and simultaneous recovery of HCl in the vapor phase as condensate. Prior to hydrolytic distillation any ferrous chloride is oxidized to ferric chloride. Typically the oxidation operation takes place at ~150ºC and the hydrolytic distillation operation at ~180ºC.

This thesis is divided into seven chapters. After this introduction chapter a literature review is presented in chapter 2 setting the theoretical background on which the complex system investigated in this work relates. It covers briefly the theory of iron oxidation, complex formation and hydrolysis as well as iron oxide precipitation and HCl regeneration. The third chapter summarizes the procedures that were applied to conduct the experiments. Moreover it shows how the samples were prepared before characterizing them with all the different methods. The chapters four, five and six discuss the results of the different experiments. Chapter four deals with the oxidation of aqueous ferrous chloride solutions and chapter five with the iron oxychloride-water system. Chapter six deals with the hydrolytic distillation experiments. Finally chapter seven concludes the total work conducted for this thesis and gives an outline of future work that could be undertaken.

Chapter 2: Literature Review

2.1. The Oxidation of Ferrous Chloride to Ferric Chloride

At the beginning of the last century, *McBain* was the first one to study the oxidation of ferrous chloride solutions by free oxygen [3]. Ever since then, the oxidation of ferrous iron has been the topic of many R&D investigations [4-7]. Basically the kinetics of ferrous ions in solution consists of two physicochemical steps:

First, the oxygen mass transfer from the gaseous into the liquid phase:

$$O_2\,(g) \longrightarrow O_2\,(aq) \qquad (1)$$

Second, the homogeneous oxidation of the ferrous ion with dissolved molecular oxygen:

$$4\,Fe^{2+}\,(aq) + O_2\,(aq) + 4\,H^+\,(aq) \longrightarrow 4\,Fe^{3+}\,(aq) + 2\,H_2O \qquad (2)$$

Equation 3 is the rate equation that applies to the gas-liquid mass transfer step:

$$r_{O_2} = k_L a (C^*_{O_2} - C_{O_2}) \qquad (3)$$

Where: r_{O_2} = rate of oxygen transfer ($mol{\cdot}m^{-3}{\cdot}t^{-1}$)
$k_L a$ = volumetric mass transfer coefficient (t^{-1})
$C^*_{O_2}$ = solubility of oxygen ($mol{\cdot}m^{-3}$)
C_{O_2} = concentration of oxygen ($mol{\cdot}m^{-3}$)

From Equation 3 is deduced that the rate of oxygen mass transfer depends on the solubility of oxygen and on its volumetric mass transfer coefficient. First the solubility of oxygen is discussed. Oxygen is a non-polar gas and thus exhibits a very low solubility in water. Its solubility data is given in a comprehensive IUPAC compilation [8]. The solubility of oxygen in water decreases constantly as temperature rises from 0 to 100ºC, but increases above 100°C with increasing temperature. Moreover, an increase of the oxygen partial pressure leads to an increase in oxygen solubility. This is described in *Henry's* law:

$$H = \frac{P_{O_2}}{C^*_{O_2}} \tag{4}$$

Where: H = Henry's constant
P_{O_2} = partial pressure of oxygen (Pa)
$C^*_{O_2}$ = solubility of oxygen ($mol \cdot m^{-3}$)

Tromans [9] determined H as a function of T and published a comprehensive expression regarding the solubility of O_2 in water as given in Equation 5:

$$C^*_{O_2} = \frac{P_{O_2}}{101325} \cdot \exp\left(\frac{0.046T^2 + 203.357T \ln\left(\frac{T}{298}\right) - (299.379 + 0.092T)(T - 298) - 20591}{RT} \right) \tag{5}$$

Where: $C^*_{O_2}$ = solubility of oxygen ($mol \cdot m^{-3}$)
P_{O_2} = oxygen partial pressure (Pa)
T = Temperature (K)

Equation 5 is valid for $T \leq 616K$ and $Po_2 \leq 6.1 \cdot 10^6 Pa$ (~60atm). The accuracy of this equation was claimed to be within the range of ±1%.

Due to the so called "salting-out effect", the solubility of oxygen is lower in aqueous electrolyte solutions than in pure water. At the end of the 19th Century, *Sechenov* [10] expressed this phenomenon mathematically:

$$KC_e = \log(C^*_{O_2,w} / C^*_{O_2,e}) \tag{6}$$

Where: K = Sechenov constant ($mol^{-1} \cdot m^3$)
C_e = electrolyte concentration ($mol \cdot m^{-3}$)
$C^*_{O_2,w}$ = solubility of oxygen in pure water ($mol \cdot m^{-3}$)
$C^*_{O_2,e}$ = solubility of oxygen in electrolyte solution ($mol \cdot m^{-3}$)

As far as it concerns the volumetric mass transfer coefficient k_La this includes the liquid-side mass transfer coefficient k_L ($^m/_t$) and the specific gas/liquid interfacial area α (m^{-1}). As such k_La heavily depends on the gas sparging and agitation conditions that govern the specific reactor.

With reference to the homogeneous oxidation reaction (Equation 2) the kinetics are reported to be in most studies second order with reference to $C_{Fe(II)}$ and first order in terms of Co_2 and Po_2:

$$r_{O_2,eq} = -k \cdot C^2_{Fe(II)} \cdot P_{O_2} \tag{7}$$

Where: r = rate of oxygen transfer ($mol \cdot m^{-3} \cdot t^{-1}$)
k = solubility constant
$C^2_{Fe(II)}$ = concentration of ferrous ion ($mol \cdot m^{-3}$)
P_{O_2} = partial pressure of oxygen (Pa)

Depending on the particular reactor setup used and reaction parameters applied the overall kinetics of the oxidation of ferrous ions can be controlled by Equation 1–this is the case of mass transfer control or by Equation 2–this is the case of chemical reaction control.

In 1971 Kovacs invented a process to produce ferric chloride from concentrated ferrous chloride solutions, which he patented in several countries [11-14]. The process involves pre-concentration of the $FeCl_2$ solution by evaporation to approximately 36% $FeCl_2$ followed by oxidation with air in an autoclave operating at 150ºC under 1-8 atm pressure over a period of 2 hours [15]. Under the applied conditions the oxidation process was found to consist of two chemical steps.

The first step involves the oxidation of the ferrous chloride with the help of oxygen and hydrochloric acid:

$$12\ FeCl_2\ (aq) + 3\ O_2\ (g) + 12\ HCl\ (aq) \longrightarrow 12\ FeCl_3\ (aq) + 6\ H_2O \tag{8}$$

This step is followed by the hydrolysis of the ferric chloride to hematite with simultaneous formation of hydrochloric acid. The formed acid is consumed by reacting again in the above shown first step:

$$4\ FeCl_3\ (aq) + 6\ H_2O \longrightarrow 2\ Fe_2O_3\ (s) + 12\ HCl\ (aq) \qquad (9)$$

These two steps can be written as the following overall equation:

$$12\ FeCl_2\ (aq) + 3\ O_2\ (g) \longrightarrow 8\ FeCl_3\ (aq) + 2\ Fe_2O_3\ (s) \qquad (10)$$

This reaction constitutes the subject of the investigation described in chapter 6.

2.2. The Hydrolysis of Iron (III)

One of the characteristics of the ferric ion is its ability to hydrolyze. In dilute aqueous solutions, iron(III) exists as the hexa-aqua complex. Its shape is octahedral, as shown in Figure 1:

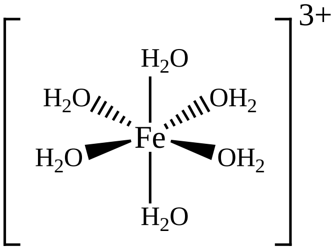

Figure 1: The Hexa-Aqua Iron (III) Complex.

The iron(III) inner core of this complex can undergo a deprotonation reaction with the water of the primary hydration shell and dissociate:

$$[Fe(H_2O)_6]^{3+} \longrightarrow [Fe(OH)(H_2O)_5]^{2+} + H^+ \qquad (11)$$

This process is stepwise until all six water molecules are deprotonated, so that iron(III) oxyhydroxide (either ferrihydrite or α-, β-, γ-FeOOH), water and protons (H^+) form [16]:

$$[Fe(H_2O)_6]^{3+} \longrightarrow FeOOH\ (s) + 4\ H_2O + 3\ H^+ \qquad (12)$$

Another path of the hydrolysis reaction may lead to hematite as a product:

$$2\ [Fe(H_2O)_6]^{3+} \xrightarrow{\qquad\qquad} Fe_2O_3\,(s) + 9\ H_2O + 6\ H^+ \tag{13}$$

In ferric chloride solutions, different kinds of complexes occur, depending on the temperature and the chloride concentration. The formation of chloro-complexes is described by the following general reaction [17]:

$$M^{z+} + nCl \rightleftharpoons MCl_n^{(n-z)-} \tag{14}$$

The solubility constant of a complex, β_n, is given in the following equation:

$$\beta_n = \frac{\alpha_{MCl_n^{(n-z)-}}}{\alpha_{M^{z+}}\alpha^n_{Cl^-}} \tag{15}$$

The magnitude of β_n reflects the strength of the n^th chloro-complex [18]. In addition to the respective value β the abundance of the various chloro-complexes depends on the activity of the chloride ion [17].

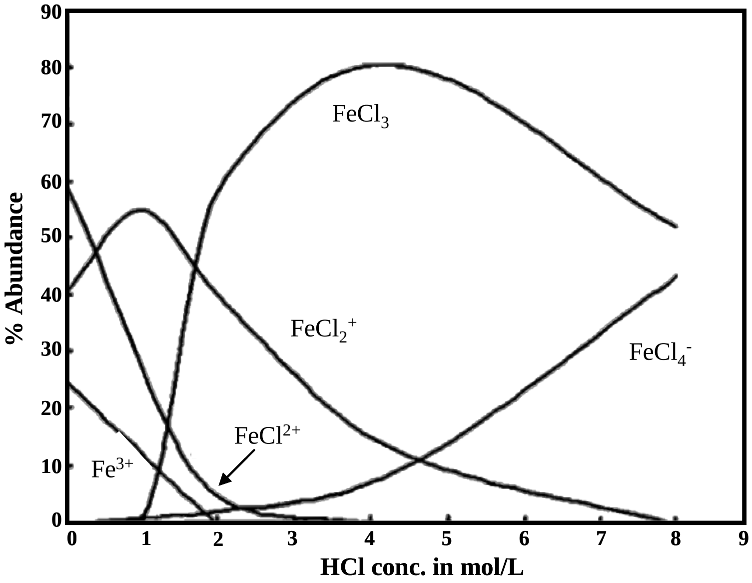

Figure 2: Distribution of Ferric Chloride Complexes as a Function of HCl Concentration. Conditions: 20ºC, Fe(III) =10^{-3} M, (Non-Corrected Ionic Strength) [19].

Speciation diagrams are used in the literature to graphically represent the abundance of those complexes. Figure 2 shows the distribution of ferric chloride complexes as a function of hydrochloric acid concentration.

The hydrolysis of iron (III) may take different paths leading to formation of a wide variety of iron (III) oxides. The type of oxide formed depends on temperature, solution composition (especially pH and anion) and kinetics. Figure 3, reproduced from *Cornell* and *Schwertmann* [20] provides a comprehensive picture of the different reaction pathways of Fe^{3+} and Fe^{2+} and different types of iron oxides and oxy-hydroxides that are known to form.

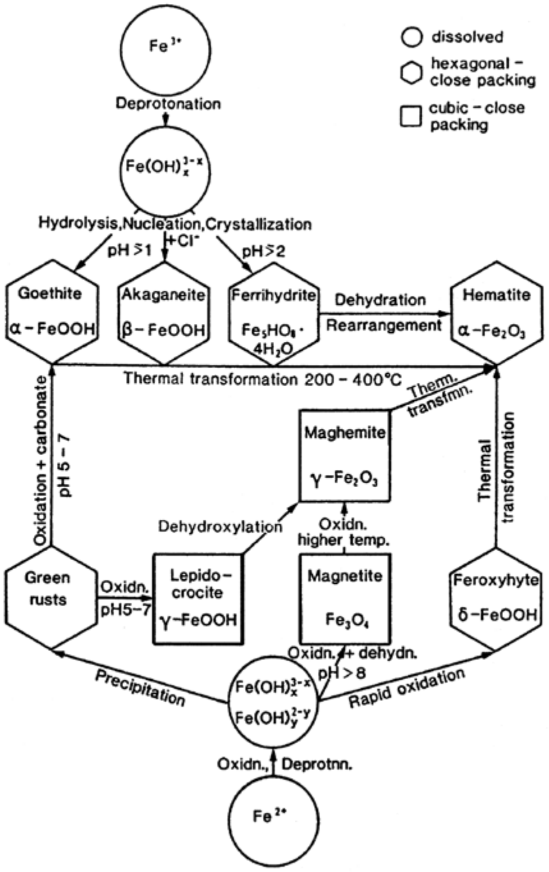

Figure 3: Schematic Representation of Major Formation and Transformation Pathways of Common Iron Oxides [20].

2.3. Precipitation of Iron Oxides

The precipitation of iron oxide phases from solution by hydrolysis has attracted a lot of attention over the years as it is manifested by the series of conferences devoted to this subject in hydrometallurgy [21-23]. The bulk of these previous studies, however, have dealt with sulphate solutions that dominate the hydrometallurgical processes. Typically iron is precipitated from concentrated sulphate solutions (commonly encountered in zinc and other non-ferrous metal extraction plants) either as jarosite ($MFe_3(SO_4)_2(OH)_6$), goethite (α-FeOOH) or hematite (α-Fe_2O_3). With reference to the subject of the present work of interest is the industrial production of hematite from $FeSO_4$-$ZnSO_4$ solution as produced by Akita Zinc in Japan [24-26]. In this process a concentrated ferrous sulphate solution (approximate concentration 40g/L Fe(II) and 80g/L Zn) is oxidized (Equation 16) and simultaneously hydrolyzed (Equation 17) at 190-200ºC:

$$2\ FeSO_4\,(aq) + \tfrac{1}{2}\ O_2\,(g) + H_2SO_4\,(aq) \longrightarrow Fe_2(SO_4)_3\,(aq) + H_2O\,(l) \quad (16)$$

$$Fe_2(SO_4)_3\,(aq) + 3\ H_2O\,(l) \longrightarrow Fe_2O_3\,(s) + 3\ H_2SO_4\,(aq) \quad (17)$$

In reality, however, the hematite product is contaminated with significant SO_4 content due to jarosite and to a lesser extent basic ferric sulphate ($Fe(OH)(SO_4)$) co-precipitate that is kinetically favored by the prevailing supersaturation conditions [26].

In analogy to the Fe(III) phases (with the exception of jarosite) precipitated in sulphate media iron precipitates from Fe(II)-Fe(III)-Cl media either as akaganeite (β-FeOOH) or hematite (α-Fe_2O_3). Of these ferric ion phases, hematite (Fe_2O_3) is the preferred one because it yields a stable high-density product with high iron content (theoretically 70% Fe), ideal for disposal or marketing. Akaganeite (also written as $Fe(OH)_{2.7}Cl_{0.3}$ [27] or $Fe_8(OOH)_{16}Cl_{1.3}$ [28]), though, appears to be the kinetically favored phase under normal neutralization/precipitation conditions. However, if akaganeite is formed it tends to contain a significant chloride component (as high as 7% Cl), leading to chloride losses, solid/liquid separation problems and consequent difficulty in satisfactorily disposing of the residue. Work by *Dutrizac* and *Riveros* [29, 30] has clearly demonstrated that the formation of the undesirable akaganeite phase can be avoided if precipitation takes place in an autoclave, i.e. above the boiling point of the solution, or at atmospheric pressure, if hematite seed is used together with neutralization. *Filippou* and *Choi* [31] also showed that use of seed can be beneficial to suppress the formation of akaganeite during iron precipitation from ferrous (by oxidation) or ferric chloride (by controlled neutralization [32]) solutions. In this case, the formation of goethite as precipitate was reported. The work of *Dutrizac* and *Riveros*, because of its close relevance to the present study is discussed in more detail in the next section.

2.3.1. Autoclave Precipitation of Hematite

Riveros and *Dutrizac* studied the autoclave precipitation of hematite from various concentrations (up to 1.0 M) ferric chloride solutions, over the temperature range of 95ºC to 175ºC [29]. It was found that a minimum temperature of 125ºC is required to form hematite in the absence of seed –refer to Equation 18. Lower temperatures were found to lead under the applied conditions to the formation of akaganeite the β-Fe(III)-oxyhydroxide according to Equation 19. Similar results, i.e. production of hematite above 125ºC and akaganeite below this temperature had been reported earlier by *Voigt* and *Göbler* [33]. The latter work involved 1 M $FeCl_3$ solutions.

$$2\ FeCl_3\ (aq) + 3\ H_2O\ (l) \longrightarrow Fe_2O_3\ (s) + 6\ HCl\ (aq) \qquad (18)$$

$$2\ FeCl_3\ (aq) + 4\ H_2O\ (l) \longrightarrow 2\ \beta\text{-}FeOOH\ (s) + 6\ HCl\ (aq) \qquad (19)$$

At temperatures greater than 125ºC, the presence or absence of hematite seed plays no role on precipitation. The only precipitated product is hematite. The precipitation of hematite may here take place directly as suggested by Equation 17 or via intermediate formation and redissolution of akaganeite [34, 35]:

$$2\ \beta\text{-}FeOOH\ (s) \longrightarrow Fe_2O_3\ (s) + H_2O \qquad (20)$$

It was found further that if hematite seed is present, the formation of hematite is favored at temperatures even below 125ºC. Seed did not only influence the type of oxide formed but also the filterability of the final product. Seed in the reaction slurry was found to lead to heterogeneous nucleation and growth of particles with diameters of 10-20 μm were formed while particles of 1 μm size were formed by homogeneous nucleation without seed.

The effect of the initial $FeCl_3$ concentration on the amount of hematite precipitated at 150ºC was another parameter studied by *Riveros* and *Dutrizac* [29]. Figure 4 shows the results for both cases in the presence or absence of hematite seed. For concentrations lower than 0.4 M $FeCl_3$, the product yield increases with increasing $FeCl_3$ concentration and remains constant afterwards. The hydrochloric acid generated during the reaction (refer to Equation 18) accumulates in the aqueous solution ultimately reaching pseudo-equilibrium and stoppage of the formation of hematite.

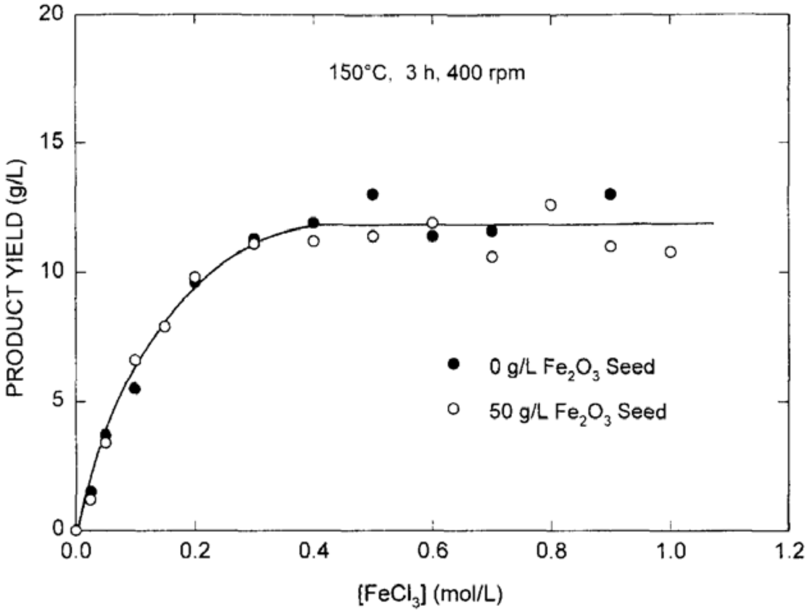

Figure 4: Effect of the Initial Ferric Chloride Concentration on the Amount of Hematite Precipitate at 150ºC in the Absence and Presence of 50 g/L of Hematite Seed [29].

2.3.2. Precipitation of Hematite at Atmospheric Pressure

In a subsequent study, *Dutrizac and Riveros* investigated the precipitation of hematite at atmospheric pressure [30] at temperatures lower than 100ºC and at concentrations of up to 1 M $FeCl_3$. In this case precipitation was forced by preneutralization (ZnO was used as a base) rather than simple heating. According to this study the reaction time at 100ºC is an important parameter in determining whether hematite or akaganeite (β-FeOOH) is formed.

In the absence of hematite seed, the reaction during the first 16 hours favored the production of akaganeite. At longer times, the precipitates were observed slowly to transform to hematite. The transformation is completed after 96 hours. This confirms that akaganeite is a metastable phase relative to hematite. In the presence of hematite seed, heterogeneous nucleation takes place and the transformation of akaganeite to hematite is promoted. Thus, the formation of hematite is accelerated and after five hours, just hematite is present [30].

This shows that Fe_2O_3 seeding has a significant influence on the precipitation and the composition of the product. Thus, experiments with varying amounts of seed at a temperature of 100ºC were conducted. It turned out, that 5 g/L hematite seed are sufficient to avoid akaganeite formation at 18 h or longer reaction time. Shorter reaction times (2 h) require larger amounts of seed (20 g/L) for the same solution concentration (0.4 M) to precipitate hematite only [30].

In addition to seeding, the effect of the $FeCl_3$ concentration on the composition and amount of the precipitated products at 100ºC and 5 h of reaction was investigated. The yield of precipitate formed increases with increasing initial $FeCl_3$ concentrations to about 0.2 M solutions and then stays constant for higher concentrations [30].

2.4. Thermal Decomposition of $FeCl_3 \cdot nH_2O$ Crystals

The hydrolytic distillation process investigated in this work involves evaporation of most of the water in the original solution as such it may be thought to be equivalent to thermal decomposition of the hydrated ferric chloride salt ($FeCl_3 \cdot 6H_2O$) hence the relevant literature is reviewed here. This section deals with the reactions the iron(III) chloride hexahydrate salt can undergo upon heating at atmospheric pressure and in particular the formation of FeOCl.

Iron oxychloride (FeOCl) was first identified in 1881 by *Thorpe et al.* [36] and characterized in 1890 by *Rousseau* [37] but by far the biggest contribution made to the study of the $FeCl_3$-FeOCl-H_2O system are those of S*chäfer* and co-workers [38-47].

According to *Schäfer* the production of FeOCl by thermal decomposition of $FeCl_3 \cdot nH_2O$ crystals (Equation 21) depends on the degree of hydration (the value of n) and if the system is open or closed:

$$FeCl_3 \cdot nH_2O\ (s) \longrightarrow FeOCl\ (s) + (n-1)\ H_2O\ (g) + 2\ HCl\ (g) \qquad (21)$$

Thus if the system is closed Equation 21 yields FeOCl, otherwise (at higher n) Fe_2O_3 is produced. This is exemplified with the data summarized in Table 1 originally published by *Schäfer et al.* [42]. If on the other hand the system is open and the release of water vapor is possible the production of FeOCl is favored even from the $FeCl_3 \cdot 6H_2O$ salt.

Table 1: Thermal Decomposition of Different Ferric Chloride Hydrates at 270ºC (Tests Done in Sealed Glass Tubes for 20 Hours) [42].

Reactant	**Composition of the Products**	
$FeCl_3 \cdot n\ H_2O$	**% FeOCl**	**%Fe_2O_3**
$FeCl_3 \cdot 0.45\ H_2O$	100	0
$FeCl_3 \cdot 0.7\ H_2O$	100	0
$FeCl_3 \cdot 0.9\ H_2O$	100	0
$FeCl_3 \cdot 1.8\ H_2O$	10-20	90-80
$FeCl_3 \cdot 3.6\ H_2O$	2-5	98-95

In 2006, *Marinovic et al.* [48] described the formation of α-hematite and FeOCl colloids by forced hydrolysis of $FeCl_3$. The procedure involved slow addition (dropwise) of ferric chloride solution under reflux conditions into boiling distilled water. Depending on the initial iron chloride concentration, different colloids were obtained. The produced particles had a size of about 10 nm in average. This data suggests that the reaction system is complex hence better understanding and control is required to obtain the desired product – in this case hematite.

2.5. Regeneration of HCl

The commercially practiced technology for regeneration of HCl from aqueous ferric and ferrous chloride solutions or other metal chloride solutions is pyrohydrolysis. However, on recent years R&D efforts have been devoted to development of lower temperature and potentially lower cost alternatives to pyrohydrolysis. These various HCl regeneration options are reviewed in this section.

2.5.1. Pyrohydrolysis

Currently, the key process for the regeneration of HCl is pyrohydrolysis of the metal chloride solution [49]. It involves the conversion of metal halides into metal oxides at temperatures up to 850ºC and the presence of water vapor/air. The products of the reaction, in case of $FeCl_2/FeCl_3$ solutions are hematite and hydrochloric acid with almost azeotropic strength (4.9 mol/L or 18.5%) [50]. Fuel combustion provides the required energy for water evaporation. The relevant reactions for the case of $FeCl_2$ (Equation 22) and $FeCl_3$ solutions (Equation 23) are [51, 52]:

$$4\,FeCl_2\,(aq) + 4\,H_2O\,(g) + O_2\,(g) \longrightarrow 2\,Fe_2O_3\,(s) + 8\,HCl\,(g) \qquad (22)$$

$$2\,FeCl_3\,(aq) + 3\,H_2O\,(g) \longrightarrow Fe_2O_3\,(s) + 6\,HCl\,(g) \qquad (23)$$

There are two types of pyrohydrolysis reactors, the Spray Roaster (SR) and the Fluidized Bed Reactor (FBR). The spray roaster is the most widely used pyrohydrolysis reactor in the world, with over 200 units operating [42-44]. The chloride solution is sprayed from the top of a cylindrical vessel into a stream of 600-700ºC hot combustion gases. Very small and hollow iron oxide particles form, while the off-gas contains the gaseous HCl, which can be dissolved in water as azeotropic acid and used in the leaching or pickling process again.

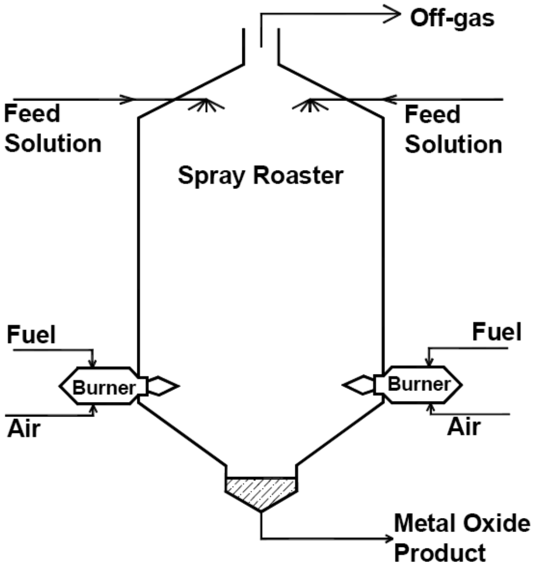

Figure 5: Sketch of a Spray Roaster [53].

In the FBR, the chloride solution is not sprayed but poured on top or into a large bed of hot metal oxide particles, while the heat is provided by the fluidizing combustion gases. The liquid wets the hot outer layer of the oxide particles and is quickly evaporated, forming a new layer of iron oxide solid, which is continuously removed. The generated HCl gases are separated from the off gas, to generate new hydrochloric acid.

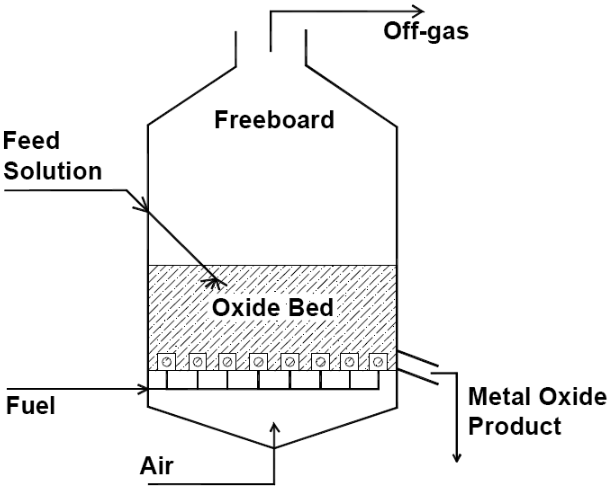

Figure 6: Sketch of a fluidized bed reactor [53].

The fluid bed reactors have some advantages over spray roasters. The iron oxide product is a non-hollow granular solid and, because of the onion layer-like growth of the particles, dust-free. FB pyrohydrolyzers are smaller that spray roasters and the mixing and temperature control inside the reactor are generally better. Particle size can be manipulated via residence time control [53]. Table 2 provides a comparison between spray roasters and fluidized bed reactors in the case of pickle liquor treatment.

Table 2: Comparison of SR and FB for a Simulated Waste Pickle Liquor [53].

	Spray Roaster	**Fluid Bed**
Feed Characteristics		
$FeCl_2$ Concentration (g/L)	205	205
HCl Concentration (g/L)	29.8	29.8
Energy Consumption for 1 t Feed		
Natural Gas Input (Nm^3)	59.8	75.7
Electricity (kW, excluding pumps)	19.1	28
Dilution Water Required (kg)	0	175
Relative Reactor Size for 1 t/h Feed		
Inside Diameter (m)	1.3 to 2.3	0.9 to 1.0
Roaster Height (m)	5-8	5-6
Product Properties (Oxides)		
Shape	Hollow, fluffy	Granular
Particle Size (μm)	30-40	200-2000
Bulk Density (kg/L)	0.4-0.6	3.8
Typical Chloride Content (%)	0.07-0.15	0.01
Specific Surface Area (m^2/g)	3-5	<1
Retention Time in Roaster	<10 sec	Hours
Product Properties (Acid)		
Regenerated HCl (mol/L)	4.9	4.9

2.5.2. Low Temperature HCl Regeneration Alternatives

Pyrohydrolysis, despite its effectiveness and proven record, remains a highly capital- and energy-intensive technology that makes it in many cases not an economically viable option. This is for example the case of $MgCl_2$ pyrohydrolysis which has been previously proposed in connection to the leaching of laterites in HCl-$MgCl_2$ media [54] or the HCl-O_2 leaching of complex zinc sulphate concentrates [55]. Therefore the search for HCl regeneration techniques operating at low costs has recently attracted a lot of attention. One of the options investigated at McGill University [56, 57] in the recent past is based on the reaction of spent calcium chloride leach solution with sulfuric acid to crystallize calcium sulphate with simultaneous production of azeotropic strength hydrochloric acid. This reaction is a part of the Intec laterite leaching process [58]. A similar concept is proposed by others for the regeneration of hydrochloric acid by crystallization of metal sulphate salts like those of ferrous ion, magnesium or zinc from their acid metal chloride solutions by the addition of sulphuric acid [59-61].

In addition to HCl regeneration by metal sulphate salt crystallization, hydrolytic distillation is a new low temperature HCl regeneration process [2, 62]. This process involves the hydrolytic precipitation of iron as hematite and the concomitant recovery of HCl in the vapor phase via distillation. Hydrolysis is conducted in this case under atmospheric pressure while the brine solution is partially evaporated. The hydrolytic distillation process builds on work associated with an invention developed in the early 1970s called the PORI Process [11, 15, 63] from steel pickling liquors (essentially ferrous chloride) hence a description of the latter is provided in the following section before the recent hydrolytic distillation work preceding the current thesis is described.

2.5.3. The PORI Process

The PORI Process, patented in 1972 [11-13] is an unconventional hydrometallurgical method that achieves HCl regeneration via the precipitation of hematite from ferrous/ferric chloride solutions. The process is divided into two major steps, involving (1) evaporation of excess water and oxidation of ferrous to ferric iron, and (2) the conversion of ferric chloride in presence of water to hematite and hydrochloric acid [15, 63, 64].

In the first step ("oxidation step") of the process, an aqueous solution of ferrous chloride, such as waste HCI pickle liquor, is oxidized. The reaction takes place in an autoclave, according to the following equation as already discussed in section 2.1:

$$12\ FeCl_2\,(aq) + 3\ O_2\,(g) \longrightarrow 8\ FeCl_3\,(aq) + 2\ Fe_2O_3\,(s) \qquad (24)$$

Air is sparged into the ferrous chloride solution at ~150ºC and ~7 atm producing simultaneously ferric chloride and hematite at a Fe molar ratio of 2:1. The average retention time for the oxidation of ferrous chloride was reported to be two hours. This step produces one third of the total hematite in the process.

The next step ("hydrolysis step") involves the transformation of the above produced ferric chloride to hydrochloric acid and hematite under atmospheric conditions:

$$2\ FeCl_3\,(aq) + 3\ H_2O\,(l) \longrightarrow 6\ HCl\,(g) + Fe_2O_3\,(s) \qquad (25)$$

Hereby, the $FeCl_3$ solution is pumped into another vessel and heated up to ~180ºC at atmospheric conditions. $FeCl_3$ converts completely to HCl (g) according to the above equation. The produced HCl gas is condensed as acid with a concentration of ~30% (superazeotropic strength). The produced hematite is black and has a mean particle size of 20–40 μm. Conducted X-Ray analysis indicated that the product is α-hematite [15]. Figure 7 shows a simplified flow sheet of the PORI HCl Regeneration process [15, 64]:

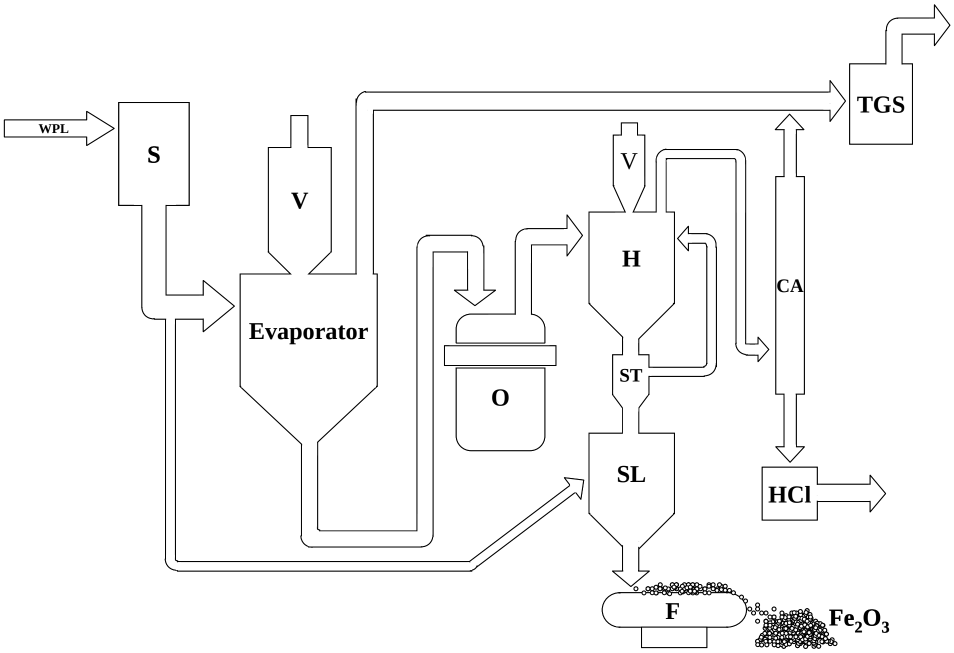

Figure 7: The PORI HCl Regeneration Process. (WPL, Waste Pickle Liquor; S, Storage; O, Oxidizer-Autoclave; H, Hydrolyzer, CA, Adiabatic Absorber; ST, Settling Tank; SL, Slurry Tank; F, Filter; TGS, Tail Gas Scrubber, V, Venturi Nozzle [64]).

2.5.4. Hydrolytic Distillation

The initial hydrolytic distillation work was carried out involving iron containing $MgCl_2$ solutions advocated as leaching medium for the processing of Cu-Ni sulphide ores [65-67] and/or laterite ores [68]. This preliminary test work involved both oxidation and hydrolytic distillation tests [69, 70]. Oxidation was effected by continuous sub-aqueous sparging of oxygen gas in a hot (120-130ºC) 0.5 M $FeCl_3$-3.8 M $MgCl_2$ solution. During the experiment the water evaporated was collected with the aid of a condenser while hot water was added as needed to avoid solidification of the slurry. It was observed during these preliminary tests [69] that oxidation was possible only when very vigorous agitation was applied (2400 rpm). A typical oxidation profile is shown in Figure 8:

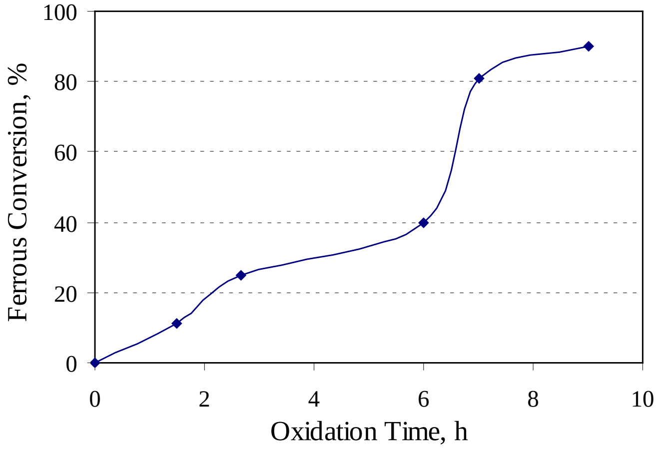

Figure 8: Oxidation of a 0.5 M $FeCl_3$-3.8 M $MgCl_2$ Solution at 120-130°C by Oxygen Sparging [69].

It can be seen that 90% of Fe^{2+} was converted to Fe^{3+} after approximately 9 hours. Via mass balance calculations the oxidation of $FeCl_2$ from the mixed $FeCl_2$-$MgCl_2$ solution was found to follow the stoichiometry of Equation 24 (first step of the PORI process).

Hydrolytic distillation from the mixed $FeCl_2$-$MgCl_2$ solution proved much more challenging than oxidation itself. It was determined that the $MgCl_2$-$FeCl_3$ solution (typical initial composition 0.5 M $FeCl_3$ and 3.8 M $MgCl_2$) upon heating to 200-220ºC under atmospheric pressure while adding water resulted in the precipitation of hematite and the recovery of hydrochloric acid with ~5.5 M concentration.

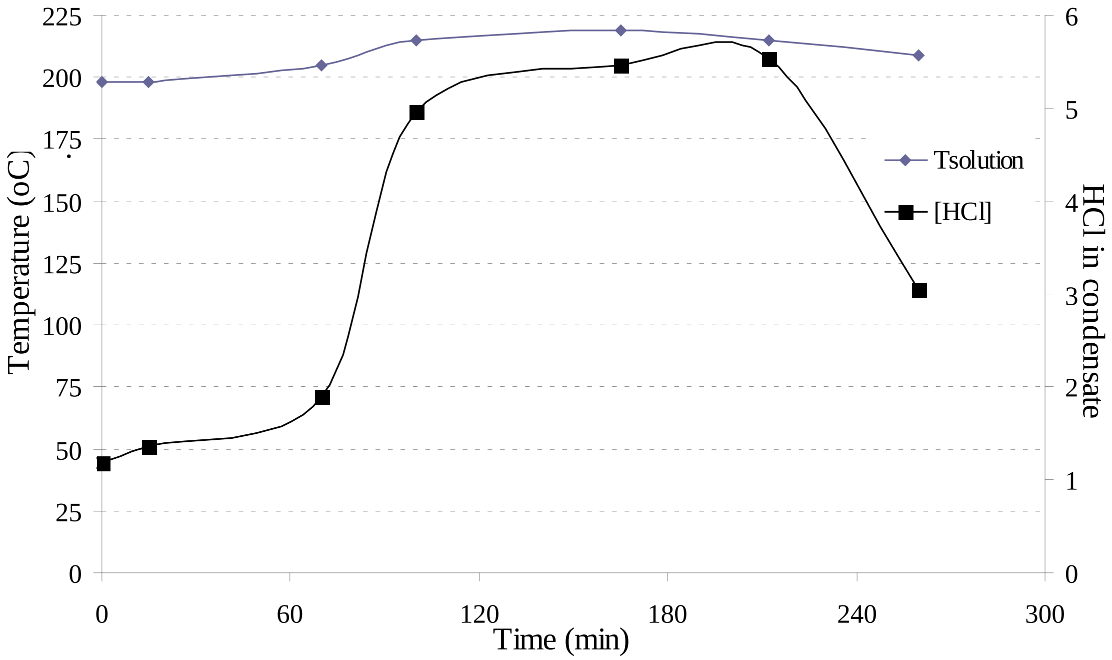

Figure 9: Hydrolytic Reaction Profile of 0.5 M $FeCl_3$-3.8 M $MgCl_2$ Solution at >200ºC [70].

Figure 9 provides the HCl and temperature profiles of one of the successful hydrolytic distillation tests conducted at the McGill Hydrometallurgy Laboratory [70]. It can be seen that essentially azeotropic strength acid suitable for recycling to the leaching operation was produced. Hydrolytic distillation was also successfully performed in another configuration [65], where instead of water feed solution was added at temperatures up to 250ºC. This new concept and its integration into the leaching of sulphidic and laterite ores is the subject of two patents [71, 72].

Figure 10 illustrates the integration of the hydrolytic distillation process into a new leaching process currently under development for the treatment of Fergusson Lake massive Cu-Ni sulphide ore deposit located in Northern Canada [65, 66]. The magnesium chloride/ferrous chloride leach liquor is oxidized by oxygen (see Figure 8) [62] to form $FeCl_3$ of which part is employed as the Lixiviant in the second stage leach, and the balance is processed by the hydrolytic distillation unit. The oxidation of ferrous chloride is associated with partial precipitation of hematite (see Equation 22) under the applied conditions (120-150ºC). This iron oxide precipitates in the hydrolytic distillation unit (operating at 200-250ºC), where hydrochloric acid is recovered and returned to the primary leach step upon recombining with the spent $MgCl_2$ solution.

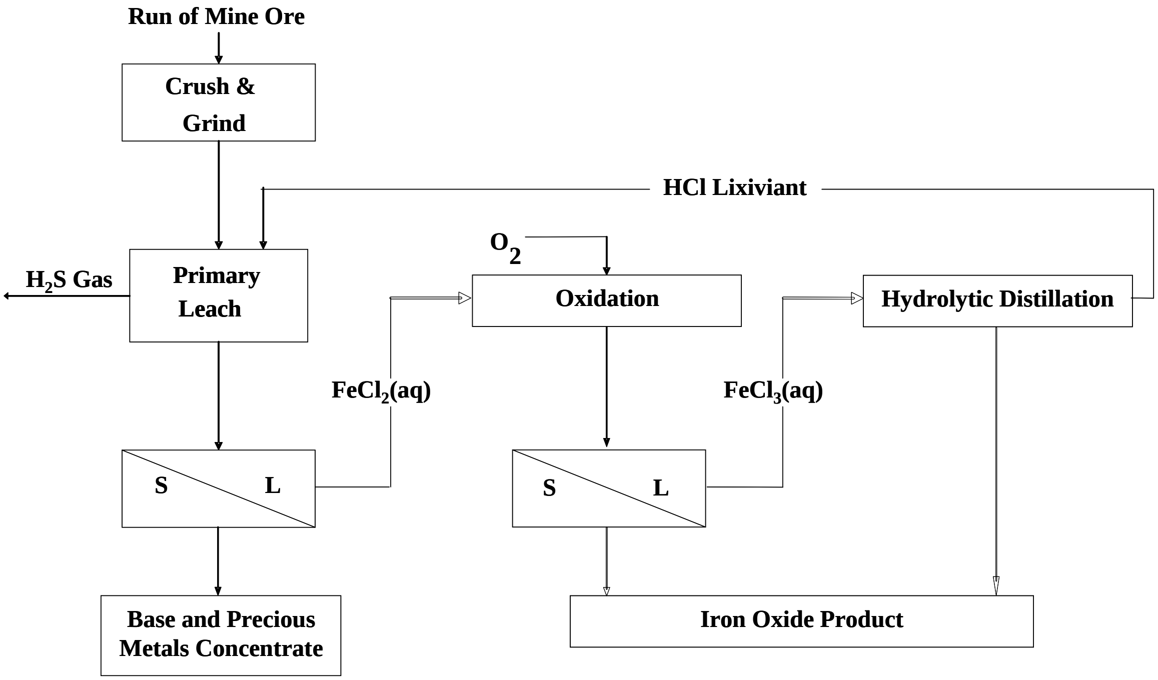

Figure 10: Proposed HCl-$MgCl_2$ Leaching Circuit for the Treatment of Starfields Massive Sulphide Ore Incorporating Lixiviant Regeneration by Hydrolytic Distillation (adapted from [65]).

Despite the initial encouraging results described above it became evident with the progress of the work [70, 73] that the presence of $MgCl_2$ greatly complicates the hydrolytic distillation operation. It was observed that at temperatures above ~195ºC magnesium chloride crystallized out of the solution and partially hydrolyzed (see Equation 26 and Equation 27) causing significant scale formation and low grade hematite product (typically ~50% iron) due to Mg(OH)Cl occurrence.

$$MgCl_2\,(aq) + x\,H_2O \longrightarrow MgCl_2\cdot xH_2O\,(s) \qquad (26)$$

$$MgCl_2\cdot xH_2O\,(s) \longrightarrow Mg(OH)Cl\,(s) + HCl\,(g) + (x-1)H_2O\,(g) \qquad (27)$$

In order to avoid the complications from the presence of $MgCl_2$, *Demopoulos* and co-workers [2, 69] proposed its replacement by $FeCl_2$ as described in Figure 11. Employment of the $FeCl_2$-HCl leaching system means that HCl regeneration can be effected as in the PORI Process (refer to section 2.5.3). Given, therefore, this renewed interest in the PORI Process as HCl regeneration/hematite precipitation option and the lack of detailed studies on it the present research was undertaken the results of which are described in the subsequent chapter of this thesis.

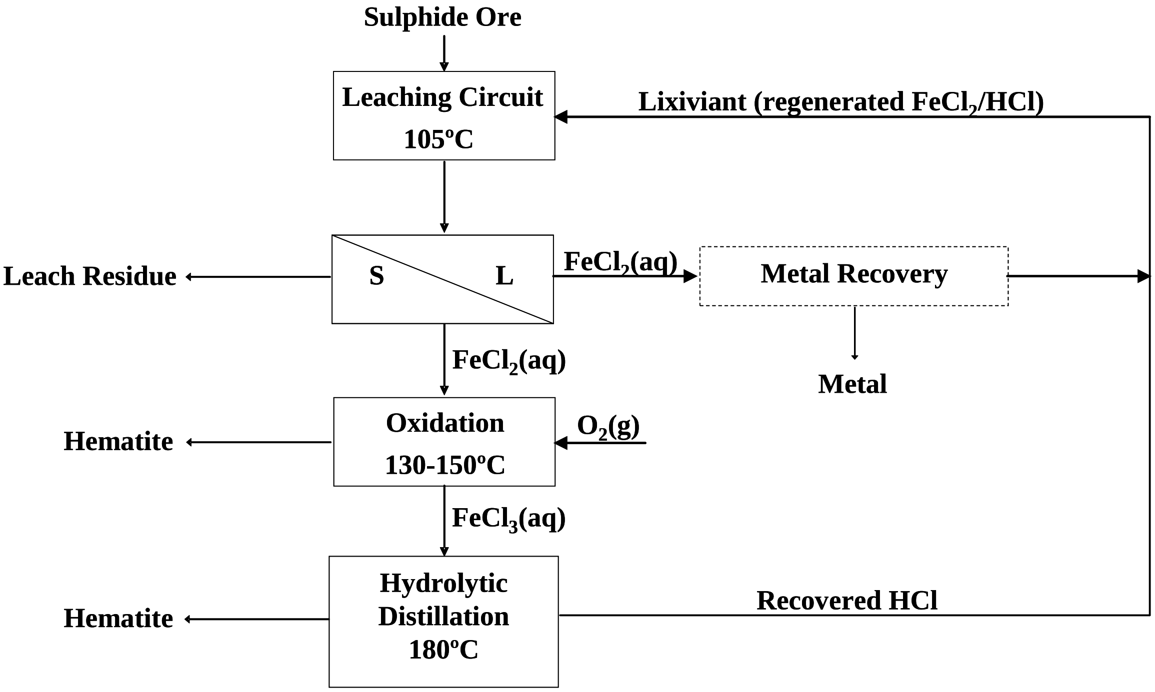

Figure 11: Conceptual Flow Sheet of an HCl-$FeCl_2$ Lixiviant Process Incorporating Non-Oxidative Leaching of a Sulphidic Ore and HCl Regeneration via Hydrolytic Distillation (reproduced from [2]).

Chapter 3: Methods and Materials

In this chapter the experimental methods, chemicals and characterization techniques used in this work are described.

3.1. Chemicals

All chemicals used along some key information about them are listed in Table 3. Solutions were made using deionized water prepared with the help of a Biolab 2200 portable reverse osmosis apparatus.

Table 3: Chemicals, their Grade, Source, Physical Form and Hazard Symbols.

Chemical	Grade	Supplier	Physical Form	Symbol
Iron Salts				
$FeCl_3 \cdot 6\ H_2O$	Technical	Fisher	Lumps	Xn
$FeCl_2 \cdot 4\ H_2O$	Certified	Fisher	Crystalline	Xn
Fe_2O_3	Certified	Fisher	Red Powder	--
Potassium Salts				
$K_3[Fe(CN)_6]$	ACS	Sigma-Aldrich	Crystalline	--
$K_4[Fe(CN)_6] \cdot 3\ H_2O$	ACS	Fisher	Crystalline	--
Other Salts				
$AgNO_3$	ACS	Fisher	Crystalline	C, N
$MgCl_2 \cdot 6\ H_2O$	USP/FCC	Fisher	Crystalline	Xi
Acids				
HCl	ACS	Fisher	Liquid	C
HNO_3	ACS	Fisher	Liquid	O, C
HF	ACS	Fisher	Liquid	T+, C
H_2SO_4	ACS	Fisher	Liquid	C
Titrants				
$K_2Cr_2O_{7,}$ 0.1 N	ACS	LC	Solution	T+, N, O
NaOH, N/10	ACS	Fisher	Solution	C
Indicators				
Phenole Red	ACS	Fisher	Powder	--
Sodium-Diphenylaminesulfonate	ACS	Fisher	Powder	--

Organic Solvents				
Hexanes	Optima	Fisher	Liquid	F, Xn, N
Acetone	ACS	Fisher	Liquid	F, Xi

3.2. Experimental Setup and Procedure

3.2.1. $FeCl_2$ Oxidation

The study of $FeCl_2$ oxidation that constitutes the first step in the PORI process (refer to Equation 28 and section 2.5.3) was carried out at the boiling temperature (unless otherwise stated) of concentrated $FeCl_2$ (with or without $FeCl_3$ or $MgCl_2$) solutions and atmospheric pressure under reflux conditions:

$$12\ FeCl_2\,(aq) + 3\ O_2\,(g) \longrightarrow 8\ FeCl_3\,(aq) + 2\ Fe_2O_3\,(s) \qquad (28)$$

After the initial investigation of different reactor setups the one schematically described in Figure 12 was used. The double wall Applicon$^{®}$ glass reactor (1.6L volume capacity) seen on Figure 13 was heated with a circulating oil bath.

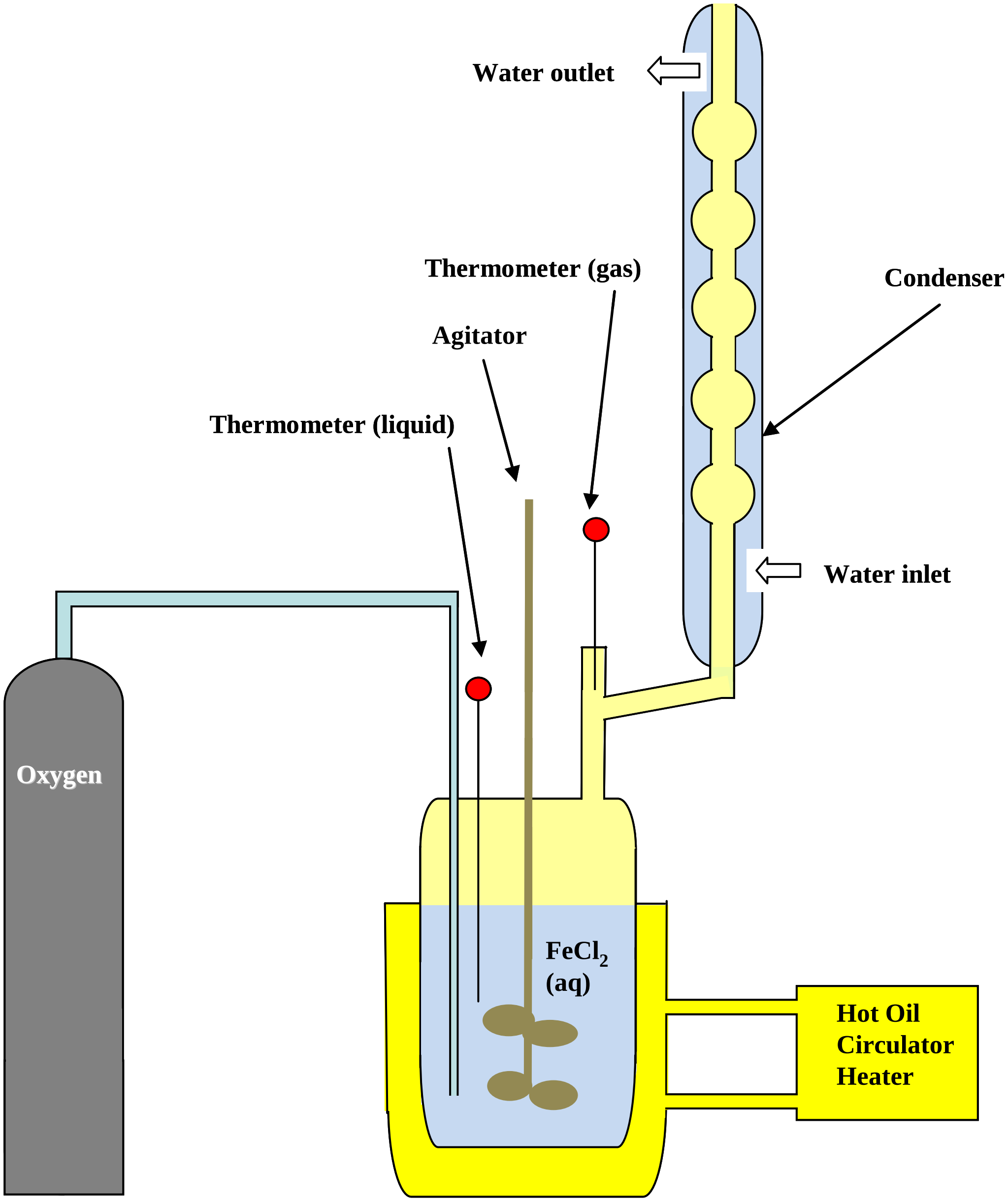

Figure 12: Reactor Setup of Ferrous Chloride Oxidation with a Reflux Apparatus.

The reactor was equipped with a mechanical agitator. The stirring shaft made of 316 stainless steel was fit with two impellers made of titanium. The whole stirring shaft/dual impeller mixer was custom Teflon coated[1] to prevent/minimize corrosion attack. The diameters and positioning of the impellers are given in Figure 13.

---

[1] Canadian Coating Industries Ltd., 7498 19E Av., Montreal, QC, H2A 2L7, 514-728-9229.

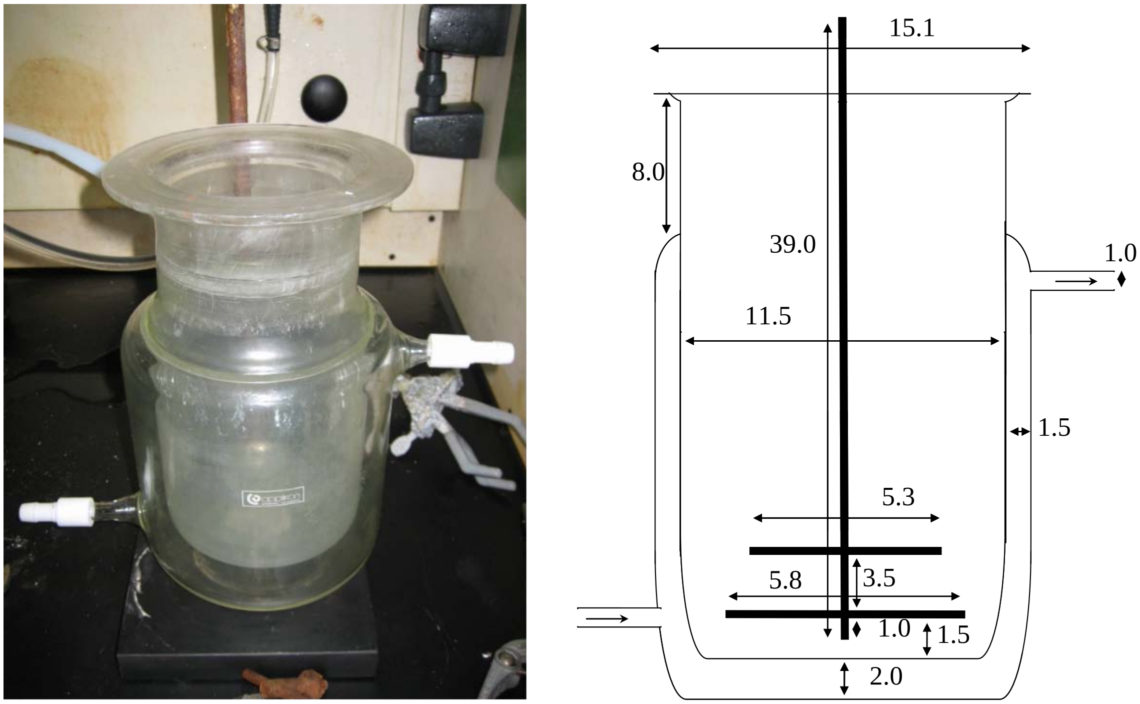

Figure 13: Double Wall Applicon® Glass Reactor (1.6L volume capacity) with Dimensions (in cm).

Based on a previous laboratory study [74] the axial impeller was placed below the radial impeller for better (k_La) oxygen mass transfer kinetics. The stirring shaft with the impellers is shown in Figure 14.

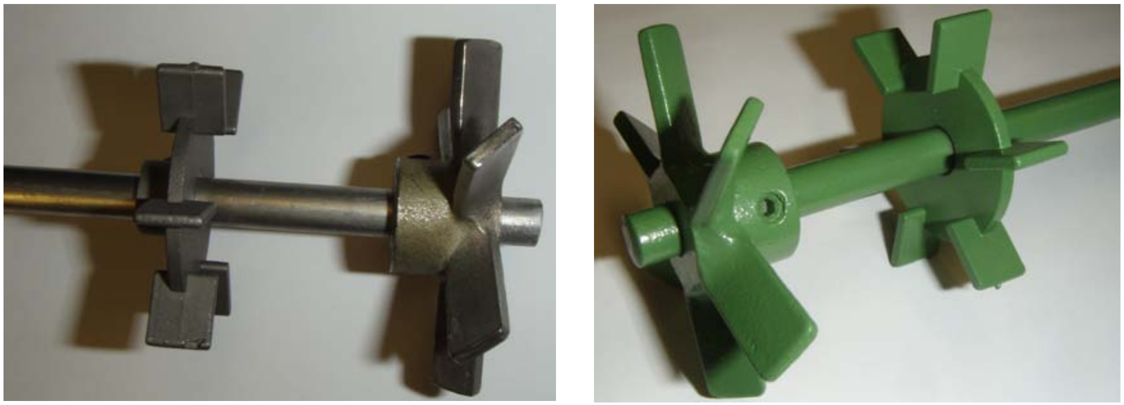

Figure 14: Stirrer with Dual Impellers (Radial Top, Axial Bottom) before Teflon Coating (left) and after (right).

This reactor setup was operated in a semi-batch mode by continuous oxygen sparging. Because of the viscosity and density of the concentrated solution a minimum

(1.5 L/min) oxygen flow rate was required to prevent the sparger from clogging. 1L of solution was loaded in the reactor for a typical test and agitated at various speeds using the Teflon coated dual impeller stirrer (Figure 14 (right)). The solution was heated to its boiling temperature (typically 113ºC for a 2 M $FeCl_3$-2 M $FeCl_3$ solution) and allowed to concentrate via evaporation until the target temperature (most commonly 150ºC) was reached. After that point oxygen sparging started while the temperature was kept constant via refluxing. This involved water vapor condensation and return to the reactor via a perpendicularly arranged distillation column, thus maintaining the volume of the solution practically constant (refer to Figure 12). Among the parameters studied were: oxygen flow rate, agitation speed and the effect of addition of salts like $MgCl_2$ or $FeCl_3$ (to elevate the boiling point of the solution). The precipitates were filtered through a 0.1μm nitro cellulose filter under 50psi pressure, washed with 1L of water to remove the residual soluble material (unreacted chlorides) and subsequently dried over night at ambient pressure in a heated oven (55˚C), losing 2.1-5.5% of their weight

3.2.2. FeOCl Preparation

During the course of this investigation it was realized that FeOCl forms as an intermediate product. In order to assist in the characterization of the products and the interpretation of the results it was necessary to study the preparation of FeOCl via thermal decomposition of $FeCl_3{\cdot}nH_2O$ salts. The design of the experiments (selection of conditions) was based on the work of *Schäfer* [37-45].

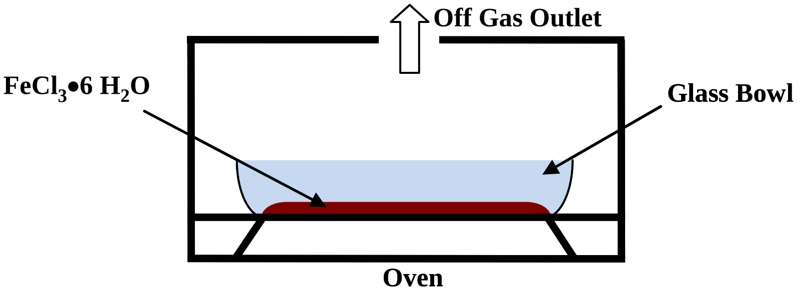

Figure 15: Experimental Setup for FeOCl Production.

Iron oxychloride was produced using an oven as depicted in Figure 15. Prior to the experiment, the drying oven was heated to 100-250ºC. When the oven reached the target temperature, $FeCl_3 \cdot 6H_2O$ (30-300 g) was placed into a glass bowl. The thermal treatment time applied depended on the used temperature, being longer at lower temperature and vice versa. The powder-crystals melted upon heating and started to lose water. After several minutes, gases (assumed to be hydrogen chloride) began to flash off. In a typical test, after one hour, the reaction mixture was liquid with a water-like viscosity and the rate of HCl evaporation was at its maximum. After two hours small crystals formed at the surface that evolved to a thick crust, which had to be crushed with a spatula from time to time. The overall process took up to ten hours. Eventually the bowl content dried out and the ferric chloride salt had transformed to iron oxychloride - confirmed by proper analysis. Then, the oven temperature was held at 50ºC for several hours (over night). The following day, the crystals were removed and ground to a fine powder. This fine powder was stored over phosphorous pentoxide in a dessicator, to keep it dry and avoid any reaction with humidity/water.

3.2.3. Hydrolytic Distillation

The main focus of this research was to investigate the hydrolytic distillation reaction, or otherwise the hydrolytic decomposition of $FeCl_3$ solution with simultaneous precipitation of Fe_2O_3 and recovery-distillation of HCl as per Equation 29:

$$2\,FeCl_3\,(aq) + 3\,H_2O\,(l) \xrightarrow{\qquad\qquad} 6\,HCl\,(g) + Fe_2O_3\,(s) \tag{29}$$

In designing and performing the hydrolytic distillation experiments the author benefited from the work that had been done within the Hydrometallurgy Group at McGill University [69, 70, 73, 75]. A schematic of the setup for the hydrolytic distillation experiments is shown in Figure 16. The setup consisted of a double wall reactor vessel – the same one used for the oxidation tests (refer to Figure 13 section 3.2.1)– that was mechanically agitated and heated with a circulating oil bath. In this case the agitation was effected with a glass-made impeller (axial type) stirrer depicted in Figure 17.

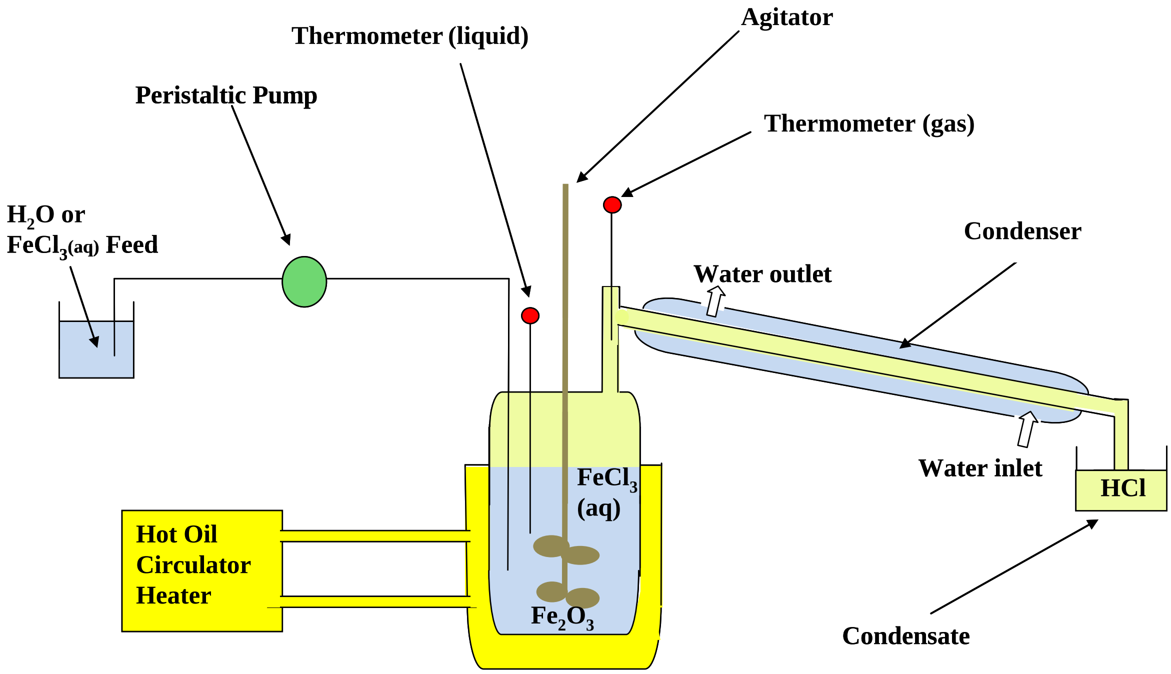

Figure 16: Schematic of Experimental Setup of Hydrolytic Distillation.

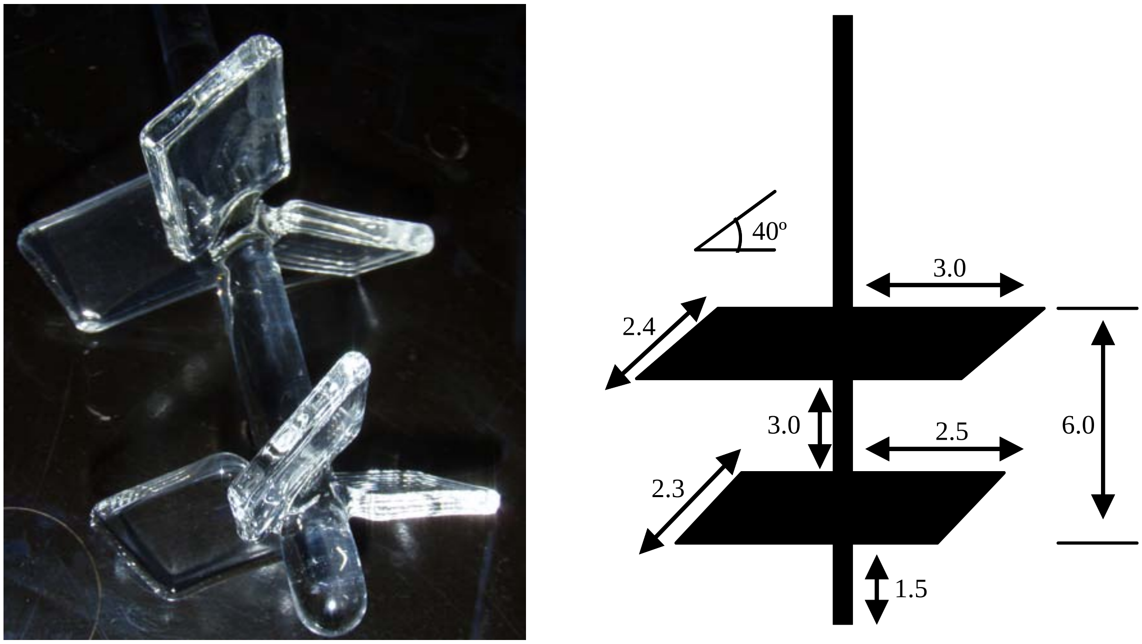

Figure 17: Glass Stirrer with Dual Impellers and Dimensions (in cm).

A fixed agitation speed of 400 rpm was employed in all hydrolytic distillation tests. The reactor (Figure 13) was fitted with a condenser to collect the volatile HCl and water vapor. A picture of the overall experimental setup is shown in Figure 18.

Figure 18: Experimental Setup of Hydrolytic Distillation.

A typical test involved placing 1L of solution in the reactor and heating it to its boiling point. The composition of the solution ranged between 30-315 g/L (0.54-5.67 M) Fe as $FeCl_3$. Upon continuous boiling, water evaporation resulted in concentration of the solution having as result the increase of its boiling point. At a certain critical temperature (~180ºC) that coincided with the distillation of HCl(g), water or $FeCl_3$ feed solution started being added continuously with the aid of a peristaltic pump (1-3 mL/min) to maintain the temperature constant. After several hours of operation, when no more HCl-condensate formed, the experiment was stopped by shutting off the supply of heat. At that point, before cooling starts, water was added to bring the volume of the solution inside the reactor to its original level. Failure to do so resulted in solidification of the remaining slurry. The slurry was stirred continuously overnight while cooling. The following day the reaction slurry was filtered and the solids were washed three times with 1 L of water and dried at 50ºC until they had a constant weight.

3.3. Analysis and Characterization Methods

The different methods used to characterize the physical (e.g. phase, surface area, morphology, size) and chemical (e.g. oxidation state, composition) properties of the solutions and solids are described in the following paragraphs.

3.3.1. Solid Product Characterization

XRD Analysis: The products of all experiments were characterized with the help of powder X-ray diffraction measurements using a Philips PW 1710 X-Ray Diffractometer which operated at 20 mA and 40 kV. The Cu-Kα1 radiation (λ = 1.5405 Å) was Ge monochromated. All measurements were carried out at room temperature. The diagrams were collected over a period of 1 hour in the 2θ range of 10-100°. Coarse solid reaction products were ground with a mortar to obtain a homogeneous fine powder. The fine powders were pressed into an aluminum sample holder. With the help of a flat glass piece, a smooth and flat surface was created. The collected XRD powder patterns were indexed and compared with relevant structures from online databases.

Raman Spectroscopy: The samples were dried, ground and prepared as mentioned above in the XRD section and then mounted on the sample holder. Less than a gram of sample was required to conduct a measurement. The instrument used was a Renishaw Invia microscope with a 50x distance objective. The energy/light source was a polarized Helium Neon laser, operated at 632.8 nm wavelength and 10% power.

Microprobe Analysis: Microprobe Analysis was applied to determine the chlorine content of the precipitates. A small amount of the powder (several milligrams) was embedded in a polyurethane resin matrix. After hardening over 48 hours, the samples were ground and eventually polished. It was important to have an area of at least 1 cm in diameter of precipitate on the surface. The samples were then carbon coated and analyzed.

Thermogravimetric Analysis (TGA): TGA analysis was conducted using a TA Instruments Q500 TGA. The product was heated by a rate of 10ºC per minute from ambient temperature up to 1000ºC under inert gas atmosphere (Nitrogen). The samples prior to TGA analysis were dried in the oven at 50ºC and then a small amount was directly fed to the machine.

Particle Size Analysis: The Horiba LA-920 Laser Scattering Analyzer was used to collect particle size data. Before determining the particle size, it was very important to ensure that a representative sample was used. Such sample was collected after finishing the experiment, directly out of the agitated reaction slurry. The collected slurry samples were stored in plastic sample tubes until analysis could be performed. For the analysis, a small amount (1-3 mL) of the well mixed slurry was taken with a pipette and injected into the analyzer. After sonicating for 2 minutes to reduce the incidence of aggregation measurements were made.

BET Surface Area Analysis: Multi-point BET surface are analysis was done on a Micromeritics TriStar Surface Area and Porosity Analyzer. To degas the samples before analysis a Micromeritics FlowPrep 060 Sample Degas System was used. Precipitates had to be ground gently prior to analysis to break down large aggregates formed upon drying of the products.

Scanning Electron Microscope Imaging (SEM): Pictures of the surface morphology of selected solid samples were taken with the help of a Hitachi S-3000N Variable Pressure Scanning Microscope (VP-SEM) operated at 10.0 kV. The precipitates were ground with the help of a mortar to obtain a fine powder. A tiny amount of the resulting powder was mounted on a sample holder with help of double sided carbon tape. Superfluous powder was removed with compressed air spray. The samples were subsequently coated with a Pd/Au alloy for 2 minutes with a sputtering machine.

3.3.2. Chemical Analysis

Inductively Coupled Plasma Spectroscopy (ICP): ICP-AES was used to determine the total iron content of the condensates, the filtrates and the solids after acid digestion. For condensates, 1 mL was pipetted into a plastic sample tube and diluted with deionized water to 10 mL. The filtrates were diluted by 1:50 and the initial solutions by 1:2500 (20 µl in 50 mL). 1 g of the solids was digested in 25 mL HCl for several days and then diluted by a factor of 1:2000 before analyzing. After preparing the samples, standards of 0.5 ppm, 5 ppm, 50 ppm and 150 ppm iron were used to calibrate the machine.

Gravimetric Analysis: This method was used to determine the chlorine content of the precipitates following their digestion. Prior to analysis 3 g of the dried precipitate were digested with 10 mL concentrated hydrofluoric acid (38%) over night. Hematite transformed to iron(III)-fluoride and chloride ions were released in the solution. The solution was filtered with a vacuum filter and the filtration cake was rinsed with deionized water. Subsequently to that a concentrated solution of silver nitrate in 4% nitric acid was added to the filtrate to cause the quantitative precipitation of silver chloride. Once more, the slurry (AgCl) was filtered and the cake was dried in an oven at 55ºC over night and weighed.

Potassium Dichromate Titration: Potassium dichromate titration was used to determine the iron (II) content of aqueous solutions or solids, the latter after digestion in concentrated HCl solution (10 M). The procedure followed these steps: Into a 250 mL Erlenmeyer flask between 50 and 100 mL of deionized water was added. Afterwards 10 mL of the sample was pipetted into the water followed by addition of 20 mL of concentrated HCl and 25 mL of mixed acid (15%v H_3PO_4, 15% H_2SO_4) and a few drops of indicator solution (aqueous sodium diphenylamine sulfonate). The solution was stirred with a magnetic bar and turned from grey to purple at the titration point. The concentration of iron (II) in g/L was calculated afterwards with the following formula:

$$c_{[Fe(II)]} = MW_{Fe} \cdot N_{K_2Cr_2O_7} \cdot \left(\frac{Vol_{Titrant}}{Vol_{Sample}} \right) \tag{30}$$

Where MW_{Fe} equals 55.85 g/mol and $N_{K2Cr2O7}$ equals 0.2 mol/L.

Acid – Base Titration: Acid-base titration was used to determine the strength of the collected HCl-H_2O condensate. With a pipette, 2-10 mL of the condensate was transferred in a 200 mL Erlenmeyer flask. The solution was diluted to 100 mL with deionised water. Afterwards, 2-3 drops of the indicator (methyl orange) were added. A burette was filled with N/5 sodium hydroxide solution (c = 0.2 mol/L). During the titration, the solution was stirred with the help of a magnetic bar. The base (NaOH) was added until the indicator changed its color from yellow to purple. The amount (volume) of NaOH consumed was noted and converted to mol in order to calculate the concentration of the condensate (hydrochloric acid).

Chapter 4: The Oxidation of Ferrous Chloride

4.1. Introduction

In this chapter the oxidation of concentrated ferrous chloride solutions by continuous sparging of oxygen at the boiling point (110-150ºC) under reflux conditions is investigated. To the best of the author's knowledge, this approach to ferrous chloride oxidation is the first time that is undertaken. The previous work by *Kovacs* [11-13] that led to the development of the PORI Process, the subject of this thesis involved the oxidation of similar solutions in an autoclave under pressure using air. In the following pages a description of the performed oxidation experiments is given and the results obtained are analyzed.

4.2. Methodology

The experimental procedure and the reactor setup (depicted in Figure 12 of chapter 3) employed in this investigation were described in section 3.2. Under the applied conditions the oxidation of $FeCl_2$ is associated with partial hydrolysis of the produced $FeCl_3$ and iron(III) precipitation –refer to sections 5.3 and 3.2.1. Hence the goal of the investigation was to determine both the kinetics of oxidation and type of iron(III) precipitate forming ultimately, identifying optimum conditions for oxidation and hematite production. A summary of all oxidation tests performed is given in Table 4. The first set of experiments (RT50-RT54) was exploratory in nature involving solutions with different concentrations of $FeCl_2$ (and one time containing as well $MgCl_2$). These experiments were conducted in order to find the right solution composition for oxidation and also to identify the temperature (150ºC) that yields hematite as the solid oxidation product. A higher reaction temperature could be reached by adding $MgCl_2$ into the system. This series of tests concluded a high agitation speed (2400 rpm) and 150ºC are required to obtain high oxidation rates and production of hematite.

The second set of experiments (RT55-RT64) was conducted with ferrous-ferric chloride mixed solution with initial composition 2 M $FeCl_2$-2 M $FeCl_3$. The boiling point of this solution was found to be 113ºC for 1 L of the mixture of 2 M of each of the two salts. Upon concentration of the solution by evaporation 675 mL water were removed from the initial 1 L volume solution and the temperature rose to 150ºC. It was at this temperature that oxidation by continuous oxygen sparging under efflux conditions (refer to Figure 12 in 3.2.1 for details) was carried out. Due to the viscous nature of concentrated solutions sampling could not be effected. Hence for each set of solutions two oxidation times, 140 min or 300 min were chosen.

Table 4: Summary of the Ferrous Chloride Oxidation Experiments.

ID RT	Time (min)	Gas	RPM	Flow Rate (L/min)	Fe(II)/Fe(III) Conversion(%)	Temperature (ºC)	Initial Solution Composition
50	20	O_2	400	Not measured	---	~74	0.5 M $FeCl_2$
51	130	O_2	400	Not measured	---	98-109	3.2 M $FeCl_2$
52	202	O_2	400	Not measured	6.9	119-150	$FeCl_2/MgCl_2$[*]
53	450	O_2	400	Not measured	15.8	~115	4.48 M $FeCl_2$
54	165	O_2	2400	2.5	68.8	~115	4.17 M $FeCl_2$
55	140	O_2	2400	2.5	49.0	~150	$FeCl_2/FeCl_3$[=]
56	300	O_2	2400	2.5	88.8	~150	$FeCl_2/FeCl_3$[=]
57	140	O_2	2400	1.5	46.0	~150	$FeCl_2/FeCl_3$[=]
58	300	O_2	2400	1.5	85.9	~150	$FeCl_2/FeCl_3$[=]
59[+]	140	---	2400	---	2.2	~150	$FeCl_2/FeCl_3$[=]
60[+]	300	---	2400	---	13.5	~150	$FeCl_2/FeCl_3$[=]
61	300	Air	2400	2.5	13.3	~150	$FeCl_2/FeCl_3$[=]
62	300	Air	2400	2.5	17.7	~150	$FeCl_2/FeCl_3$[=]
63	300	O_2	1600	2.5	87.0	~150	$FeCl_2/FeCl_3$[=]
64	300	O_2	800	2.5	43.5	~150	$FeCl_2/FeCl_3$[=]

* 0.5 M $FeCl_2$ and 3.8 M $MgCl_2$
= 2 M $FeCl_2$ and 2 M $FeCl_3$
\+ No oxygen/air was sparged. Observed oxidation is due to atmospheric air intake by the agitation

4.3. Preliminary Oxidation Experiments (RT50-RT54)

The first tests (RT50 and RT51) were conducted with the reaction setup shown in Figure 16. As reaction medium 0.5 M and 3.2 M $FeCl_2$ solutions (initial composition) were used. The boiling point of the 3.2 M $FeCl_2$ solution was 108ºC (no reflux or water addition was practiced to compensate for the evaporated water). These experiments were not successful since the system dried out after the water had been evaporated. *Demopoulos and Li* [69] reported the almost complete oxidation (95%) of ferrous chloride (0.5 M Fe(II)) to ferric chloride in concentrated magnesium chloride medium (3.8 M $MgCl_2$) (refer to Figure 8 in section 2.5.4). However, the equivalent preliminary oxidation experiment, (RT52), yielded only 7% oxidation. This was traced to the lower agitation speed employed (400 rpm with the glass stirrer of Figure 17) as opposed to the 2400 rpm speed employed in the earlier work [69]. Nevertheless this test (RT52) showed that an oxidation temperature of about 150ºC is necessary to promote the formation of hematite as precipitate.

Since it is well known, that a higher concentration of a metal salt increases the boiling point of its solution, a concentrated (4.4 M)[2] aqueous solution of ferrous chloride was used as reaction medium for two experiments (RT53 and RT54). Experiment RT53 was operated at the boiling point of 115ºC using the glass stirrer of Figure 17 and a speed of 400 rpm. A brown precipitate was seen to form, which was difficult to filter (several hours using a pressure filter). This test yielded 15.8% oxidation after 450 min. The slow oxidation progress combined with the observation made earlier for the test RT52 led to the conclusion, that a higher agitation speed had to be applied to improve the oxidation kinetics. It was at this point that the Teflon coated stirrer described in section 3.2.1 (see also Figure 14) was used allowing the agitation speed to be increased from 400 rpm to 2400 rpm.

Experiment RT54 was a repetition of RT53 but this time the new stirrer at 2400 rpm was employed. As a result of the increased agitation speed the oxidation efficiency increased from 16% after 450 min with 400 rpm to 69% after 165 min with 2400 rpm. For this experiment, the oxygen flow rate was set to 2.5 L/min oxygen, which means that during the experiment 412.5 L (18.4 mol) O_2 were used to oxidize 4.17 mol Fe^{2+}. The molar ratio of oxygen to ferrous iron was therefore about 4.4:1. Interestingly enough the corresponding stoichiometric ratio $O_2/FeCl_2$ according to Equation 24 is 1:4, i.e. the actual oxygen consumption was 16 times the stoichiometric amount. Or, equivalently the utilization efficiency was only ~6%.

---

[2] This concentration was found to be the maximum that can be obtained in solution at room-temperature

As mentioned already tests RT53 and RT54 conducted at 115ºC resulted in a brown precipitate that was difficult to filter. This precipitate was identified to be goethite. The respective XRD-pattern is shown in Figure 19. The finding of goethite (α-FeOOH) was surprising as it is commonly known akaganeite (β-FeOOH) to form (as opposed to goethite, α-FeOOH) in chloride media [29]. *Filippou* and *Choi* [31] were the only other researchers that had previously reported the formation of goethite out of chloride solutions.

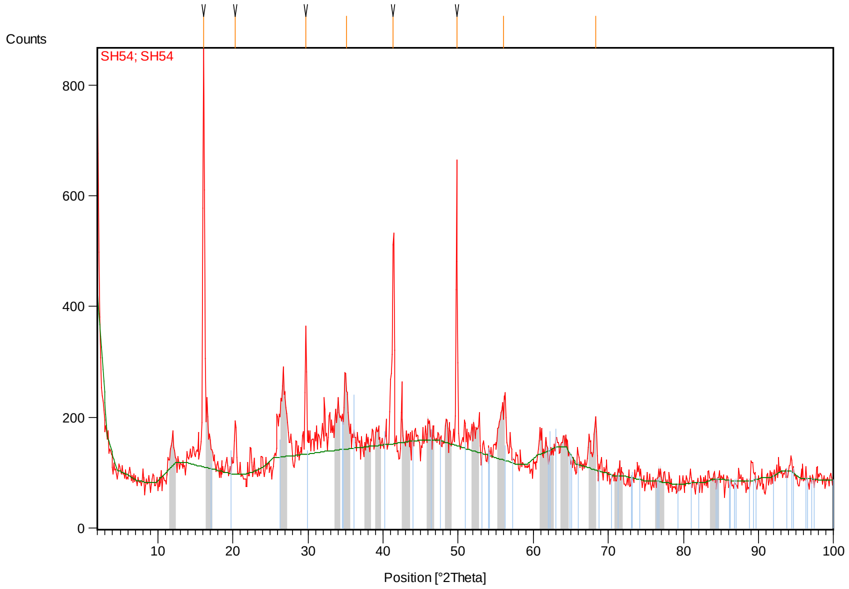

Figure 19: XRD pattern of the α-FeOOH product (Goethite) (Ref. #: 00-001-0662).

4.4. Oxidation of a $FeCl_2$-$FeCl_3$ Solution at 150ºC (RT55-RT64)

After having gathered experience from the preliminary oxidation experiments (see section 4.3) the reaction temperature was fixed at 150ºC, the agitation speed was set at 2400 rpm and the iron chloride composition of the initial solution was fixed to 2 M ferrous chloride and 2 M ferric chloride. This concentration-composition matched interestingly the solubility of the salt mixture in water at ambient temperature. At the temperature oxidation was effected (150ºC), the solution composition had been raised to approximately 6 M $FeCl_2$-6 M $FeCl_3$ due to water evaporation that led to boiling point elevation from 113ºC to 150ºC. It was under these conditions that the influence of the flow rate on oxidation was investigated as well as the influence of the agitation speed. Both pure oxygen and air were tested.

Investigation of the Oxygen/Air Flow Rate: Before the oxidation results are discussed it should be mentioned that upon oxidation of $FeCl_2$ at 150ºC the solution turned red as a result of the formation of hematite. The characterization of the precipitate is discussed in section 4.5.

Figure 20 shows the conversion of $FeCl_2$ for the two oxidation times. Interestingly, the oxidation rate for a sparging flow rate of 1.5 L oxygen per minute is almost the same as the rate for 2.5 L/min. No lower flow rate could be tested because of the clogging of the sparging tube at its tip. In order to evaluate a lower oxygen flow rate without having the sparging tube clogging problem oxygen was replaced by air (applied flow rate = 2.5 L air/min, tests RT61 and RT62). This air flow rate corresponds to 0.5 L oxygen/min. As it can be seen these tests yielded rather poor oxidation efficiency, only ~16±3%. This is 18% (i.e. approximately $^1/_5$) of the conversion efficiency (88.8%) obtained with 2.5 L pure oxygen/min flow rate. Although superficially this reached conversion efficiency seems to be proportional to the reduced oxygen flow rate ($^1/_5$), it is believed that this is due to the effect of oxygen partial pressure rather than flow rate (0.21atm in air vs. 1atm for pure O_2). This is so because even at 0.5 L O_2/min flow rate the amount of consumed oxygen was more that one order higher (3.3 mol O_2/mol $FeCl_2$) than the stoichiometric requirements (0.25 mol O_2/mol $FeCl_2$ according to Equation 28, section 3.2.1).

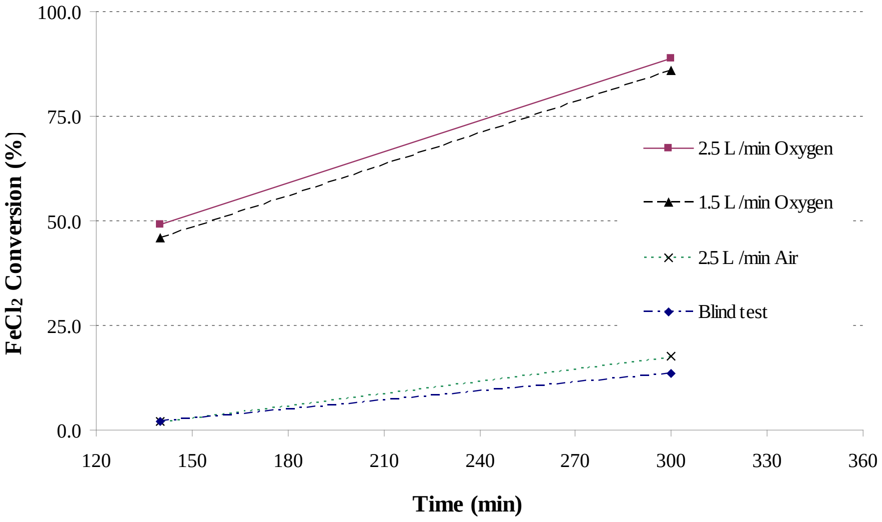

Figure 20: The Effect of Oxygen/Air Flow Rate on Ferrous Chloride Oxidation at an Agitation Speed of 2400 rpm. (Initial Solution Composition 2 M $FeCl_2$/2 M $FeCl_3$; 150ºC; Dual Radial/Axial Impeller System).

Investigation of the Agitation Speed: For these experiments (RT56, RT63 and RT64 –refer to Table 4), the oxygen flow rate was kept constant at 2.5L/min. Figure 21 shows the effect of various agitation speeds in percent conversion of ferrous to ferric chloride after five hours. It can be seen that oxidation kinetics strongly depends on the applied agitation speed pointing to a mass transfer controlled reaction process (refer to section 2.1). Among the three agitation speeds 1600 rpm appears to be the optimum for the given reactor setup. Further experiments with larger reactors are required to establish scale-up criteria.

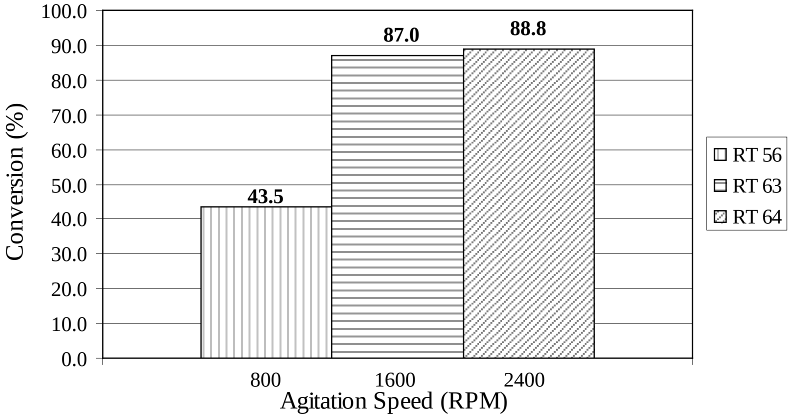

Figure 21: The Effect of the Agitation Speed Influence on Ferrous Chloride Oxidation at an Oxygen Flow Rate of 2.5 L/min.

Reaction Stoichiometry and Rate Limiting Step: In this section the oxidation reaction data are analyzed to verify/confirm the stoichiometry of Equation 24:

$$12\ FeCl_2\,(aq) + 3\ O_2\,(g) \longrightarrow 8\ FeCl_3\,(aq) + 2\ Fe_2O_3\,(s) \qquad (24)$$

As discussed later in the product characterization section 4.5 the precipitate obtained by oxidation at 150ºC was hematite (α-Fe_2O_3) with essentially the theoretical %iron content of 70%. The mass of collected hematite product at the end of each test was weighed (before and after drying) and the final solution analyzed for ferrous iron (by titration) and total iron (by ICP). The obtained data after proper conversions were compared to those expected (calculated) from the stoichiometry of Equation 24. Table 5 summarizes all these data. These data had an experimental error of ~5% compared to the values of the stoichiometry of Equation 24.

Table 5: Stoichiometric Data of Oxidation Experiments (For Conditions Refer to Table 4).

Test ID	Fe(II) Conversion (%)	$Fe^{(II)}_{reacted}$ (mol)	$Fe^{(III)}_{sol,calc}$ (mol)	$Fe^{(III)}_{sol,meas}$ (mol)	Difference (%)	$Fe^{(III)}_{hem,calc}$ (mol)	$Fe^{(III)}_{hem,meas}$ (mol)	Difference (%)
RT55	49.0	0.98	0.65	0.75	14.49	0.33	0.32	-3.13
RT56	88.8	1.78	1.18	1.18	±0.00	0.59	0.56	-7.14
RT57	46.0	0.92	0.61	0.53	-13.44	0.31	0.29	-6.90
RT58	85.9	1.72	1.15	1.09	-4.40	0.57	0.54	-5.56
RT62	17.7	0.35	0.35	0.18	-0.63	0.12	0.12	±0.00
Average					-0.55			-4.54

$Fe^{(II)}_{reacted}$ = Moles of $Fe^{(II)}$ that were oxidized

$Fe^{(III)}_{sol,calc}$ = $^{2}/_{3}\cdot Fe^{(II)}_{reacted}$ as per stoichiometry of Equation 28

$Fe^{(III)}_{sol,meas}$ = $FeCl_3$ generated by the oxidation of FeCl2 and remaining in solution

$Fe^{(III)}_{hem,calc}$ = $^{1}/_{3}\cdot Fe^{(II)}_{reacted}$ as per stoichiometry of Equation 28

$Fe^{(III)}_{hem,meas}$ = mass of iron in hematite

All units in mol; basis of calculation 1 L initial solution.

With reference to the kinetics of the process based on the data obtained it may be concluded that the rate-limiting step is the transfer of oxygen at the gas/liquid interface:

$$O_2\,(g) \longrightarrow O_2\,(aq) \qquad (1)$$

The corresponding rate equation as discussed in section 2.1 is:

$$r_{O_2} = k_L a(C^*_{O_2} - C_{O_2}) \qquad (3)$$

This equation is reduced to Equation 31 when C^*o_2 is replaced by Po_2/H (refer to Henry's law constant, in Equation 4 section 2.1) and Co_2 is taken to equal zero (the case of oxygen mass transfer being the rate limiting step):

$$r_{O_2} = \frac{k_L a}{H} \cdot P_{O_2} \qquad (31)$$

The effect of oxygen partial pressure discussed earlier is in accordance with Equation 31.

4.5. Product Characterization

In this section the characterization of the hematite precipitate produced by oxidation of $FeCl_2$-$FeCl_3$ solution at 150ºC as per Equation 24 is described. The precipitates were characterized by XRD and Raman spectroscopy for the purpose of phase identification; TGA and chemical analysis for determining their composition; and SEM, BET and Laser Scattering for determining their morphology, surface area and particle size determination.

Before the characterization results are presented it is important to comment on the filterability and washability characteristics of the precipitates which are important from an industrial point of view. The resulting slurry upon completion of the oxidation test was diluted back to its original volume of 1 L and filtered hot (~80ºC) using a pressure filter.

Typically a filtration took 10-15 min under 50psi pressure using a 0.1 μm pore size filter. Following filtration the cake was washed and dried at 55°C before subjecting it to characterization.

Figure 22: Image of the Precipitated Hematite by Oxidation at 150°C (RT56).

Phase Identification: The color of the precipitates was red. A picture of typical iron oxide product is shown in Figure 22. XRD analysis (a typical pattern is shown in Figure 23 revealed the product to be hematite (α-Fe_2O_3) of good crystallinity. The red color of the hematite according to *Cornell* and *Schwertmann* [20] is owed to its fine particle size. Since the detection limit of XRD is only 5% further fine characterization was done by using Raman Spectroscopy.

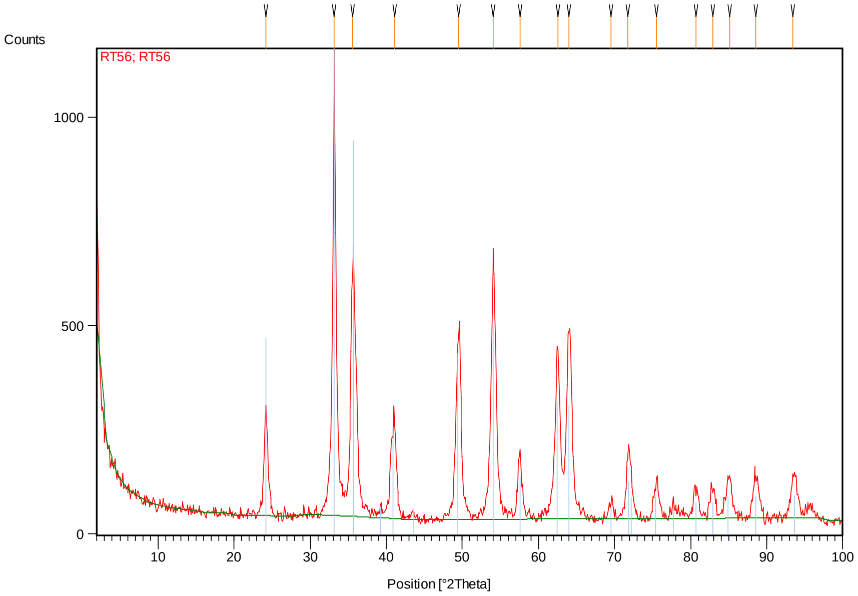

Figure 23: XRD Pattern for the Iron Oxide Precipitate Produced from Oxidation with Oxygen, Compared with the Reference Pattern of Hematite (α-Fe_2O_3) (Ref. #: 00-024-0072).

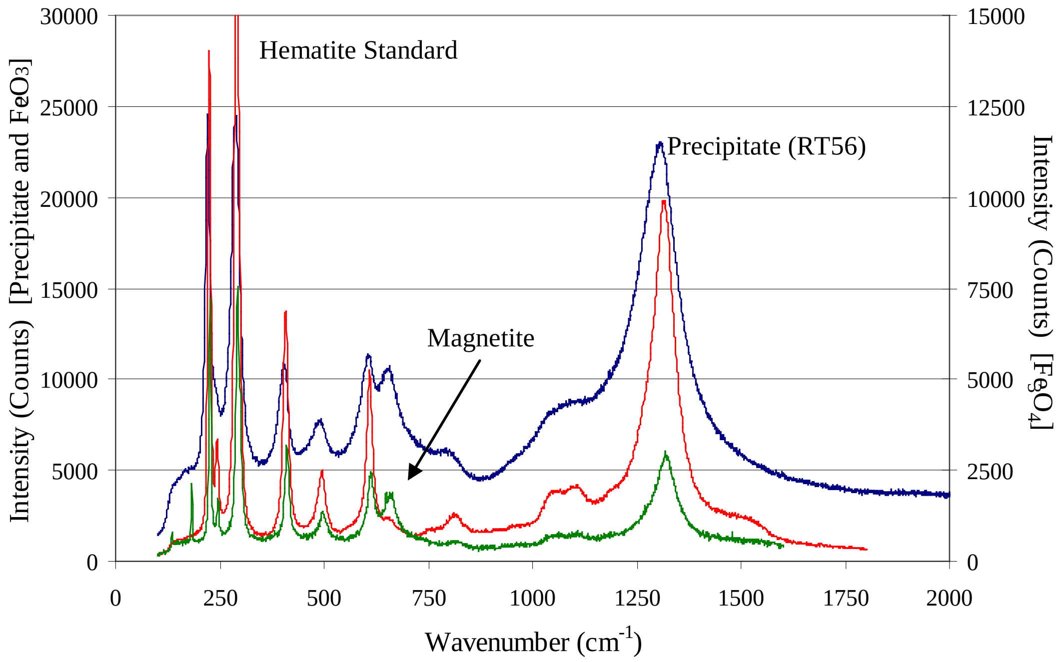

Figure 24: Raman Spectrum for the Iron Oxide Precipitate Produced from Oxidation Experiment RT56, Compared with Hematite and Magnetite Standards.

Figure 24 shows the Raman spectrum of the hematite produced from experiment RT56. This spectrum is compared to those of reference materials hematite and magnetite obtained from Fisher Scientific. There was a good match of the precipitate's spectrum with that of hematite. However, the characteristic magnetite peak at 680 cm^{-1} was found to be present as well [76]. Since the detection limit of the Raman spectrometer is ~1% and the detection limit of the XRD, which did not indicate the presence of magnetite, is ~5%, it is assumed that a small amount of magnetite somewhere between one and five percent is present in the final product. The formation of magnetite (which is characterized by an intermediate oxidation state: $Fe^{2+}Fe_2^{3+}O_4$) is not surprising as hematite was produced via oxidation of ferrous to ferric iron.

Composition: Table 6 provides a summary of chemical analysis data (%Fe) obtained by digestion of several precipitates. It can be seen that the %Fe content varies between 68.6 to 70.5%, i.e. is very close to the theoretical value of 69.94% for pure Fe_2O_3. The slightly higher %Fe content in some of the samples may reflect either experimental analytical error and/or the presence of the minor amount of magnetite

(72.3% Fe). The chlorine content of the product was measured with the help of silver nitrate and found to be as low as 0.1%.

Table 6: Chemical Composition Analysis and Surface Area of the Precipitated Hematite Product from Selected Representative Oxidation Experiments.

Sample ID	Gas Flow Rate (L/min)	Reaction Time (min)	Water Content (%)	Iron Content (%)	BET Surface Are (m^2/g)
RT55	2.5 O_2	140	4.8	68.6	12.3
RT56	2.5 O_2	300	4.6	69.7	13.7
RT57	1.5 O_2	140	4.6	69.2	19.6
RT58	1.5 O_2	300	3.9	70.2	28.2
RT62	2.5 Air	300	6.1	70.5	17.2

Thermo gravimetric analysis of the iron oxide products generated the weight loss vs. temperature curves shown in Figure 25. It can be observed that the precipitate lost 3.9-6.0% -this loss apparently representing surface (up to 2%-150ºC) and structural water (3-4%)

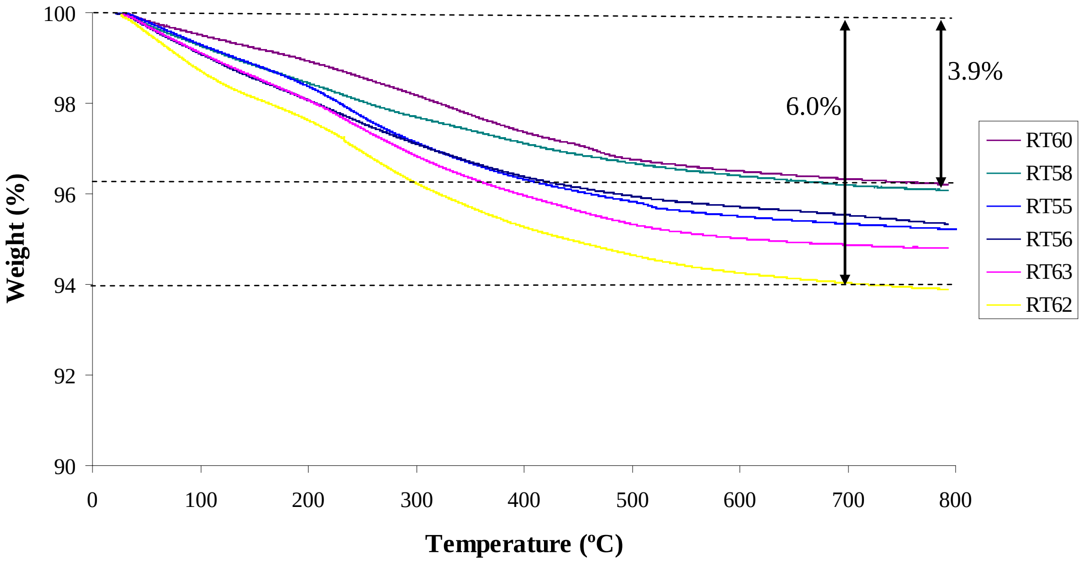

Figure 25: TGA of Iron Oxide Precipitates; Heating Rate 10˚C/min.

Physical Characteristics: The particle size distribution of a representative sample (RT56) is shown in Figure 26. The mean particle size of this sample was 1.7µm with a standard deviation of 0.1µm and the particle size mode was 1.6µm in diameter. Scanning electron microscope examination of the hematite product (refer to Figure 27) concluded that growth had been occurred through aggregation of sub-micron crystallites, hence confirming the particles size distribution data. The BET surface area measurements are summarized in Table 6. All the samples measured were found to have a BET surface area in a range of 12.3-28.2 m^2/g. By applying the formula presented in Equation 32 for an average specific area of 13.2 m^2/g it was determined this surface area to correspond to isometric dense particles of 0.08 μm. Compared with the volume based particle size of 1.7 μm this suggests that the hematite particles are porous agglomerates of nano crystallites in agreement with the morphology of Figure 27 and the relative slow filtration rate observed.

$$d_p = \frac{6 \times 10^4}{\rho \times S} = \frac{6 \times 10^4}{(5.2g/cm^3) \times (13.7 \times 10^4 cm^2/g)} = 0.08\mu m \tag{32}$$

Where: d_p = Equivalent Particle Size (μm)
ρ = Density (g/cm^3)
S = BET Surface Area (cm^2/g)

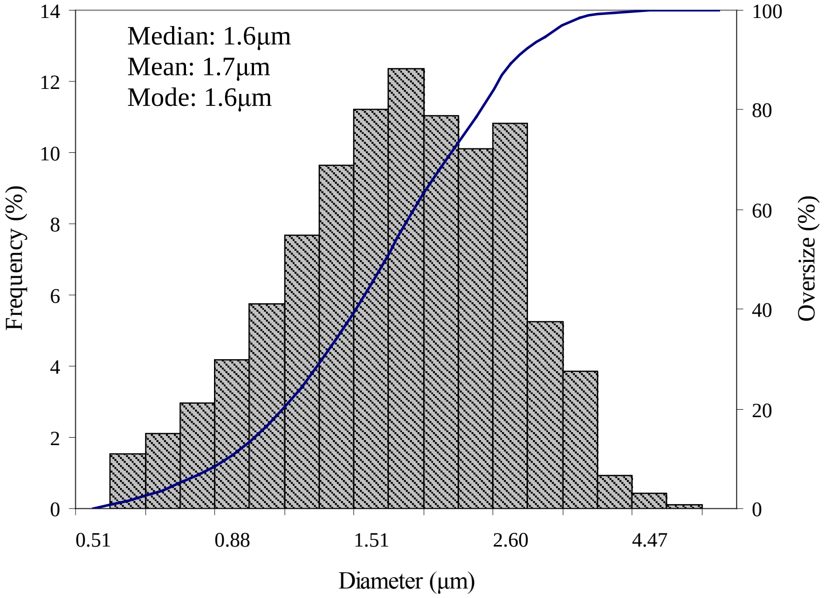

Figure 26: Volume Based Particle Size Distribution of the Precipitated Hematite Product. Median=1.6μm, Mean=1.7μm, Mode=1.6μm (RT56).

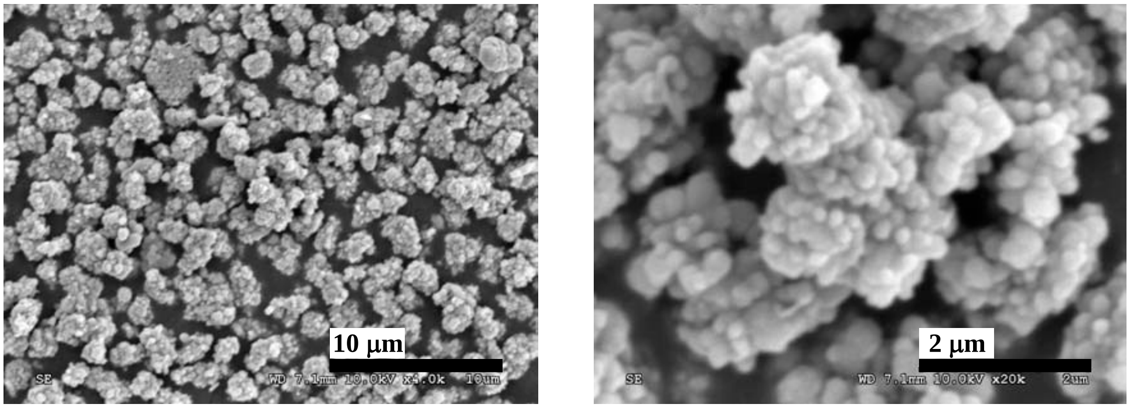

Figure 27: SEM Images of the Precipitated Hematite Product from Experiment RT56 at Different Magnifications(x4000 left, x20,000 right).

4.6. Corrosion Problems

Aqueous ferric chloride solutions are very corrosive [77]. To avoid corrosion on the agitators, a corrosion resistant Teflon layer was coated over the two titanium impellers and the stainless steel rod on which they were mounted. However, the coating was not applied very thoroughly, and this led to corrosion attack between the rod and the impeller.

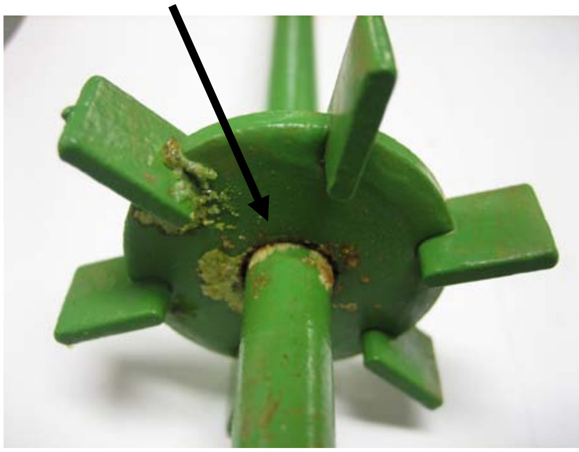

Figure 28: Teflon coated stirrer after ~15h of application.

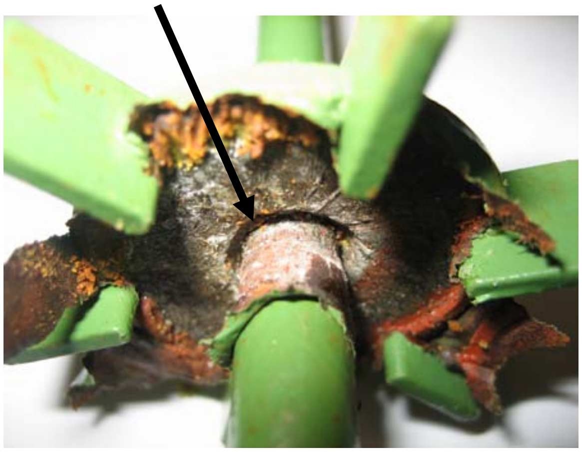

Figure 29: Crevice corrosion at the stirrer (Teflon coating removed).

Figure 28 shows the stirrer after about 15 hours service life in the reactor during oxidation experiments. No severe corrosion signs are evident. The arrow indicates the small area which had not been sealed well with the Teflon coating. After removing manually the Teflon coat (depicted in Figure 29) severe corrosion attack on the stirring rod and the titanium disk became obvious. This type of corrosion has the apparent characteristics of crevice or more specifically filiform type of corrosion that refers to corrosion attack under protective films –here Teflon. The parts where the Teflon layer was properly applied, however, were not affected by crevice corrosion. This leads to the conclusion, that for further industrial application of the process, Teflon coated reactor parts are highly recommended.

Chapter 5: Hydrolytic Distillation of $FeCl_3$ Solutions

5.1. Introduction

This chapter deals with the investigation of the hydrolytic distillation as it is applied to ferric chloride solutions, to produce hematite and recover HCl by distillation. The reaction involved in the case of $FeCl_3$ solutions originally conceived and patented by *Kovacs* as the PORI Process [11-13] is:

$$2\ FeCl_3\,(aq) + 3\ H_2O\,(l) \longrightarrow 6\ HCl\,(g) + Fe_2O_3\,(s) \qquad (25)$$

5.2. Anatomy of a Typical Test

Because of the non-conventional nature of the hydrolytic distillation process it was deemed necessary as an opening to this chapter to describe in detail a typical test. Figure 30 shows a standard reaction profile. On this Figure the evolution of temperature in the liquid phase, vapor phase and oil bath as well as the strength of HCl in the collected condensate, %conversion and the amount of iron reporting to the condensate is depicted.

Basically 1 L $FeCl_3$ solution (in this case having 3.08 M or 500g/L $FeCl_3$ concentration) was heated to reach (after about 30 min) its boiling point (in this case 108ºC) under atmospheric pressure while water evaporates. Evaporation of the water continued and after about 20 min the boiling temperature of the solution is seen to start rising as a result of solution concentration. This continued for 40-50 min before HCl started reporting to the condensate (T~120ºC and 100 min). The temperature continued to rise reaching a plateau at ~180ºC (t = 130 min). When the solution reached the reaction temperature of 180ºC, it was calculated that it consisted of $FeCl_3\cdot 2H_2O$. At this point water started being pumped (2.0-2.3 mL/min) into the reactor to compensate for the evaporated water and maintain the hydrolysis reaction at ~180ºC. With the initiation of water addition the distillation of HCl produced by hydrolysis of $FeCl_3$ increased yielding very high strength acid in the condensate (nearly 9 M HCl). At the same time iron precipitates as Fe_2O_3 (see reaction 25). When conversion (measured here on the basis of chloride units, from $FeCl_3$, reporting to the condensate as HCl) has reached 95% after 480 min water addition and heating were stopped. It is obvious that with the interruption of water addition and the exhaustion of $FeCl_3$ the strength of HCl in the condensate vertically drops. It can be seen in Figure 30 that a certain amount of iron (as $FeCl_3$) reports in the condensate. It must be stated here that prior to cooling of the final reaction slurry water is added to bring its volume back to 1 L and so avoid solidification of the residual ferric chloride. An analysis and an interpretation of the reaction changes associated with this complex process system are provided in the subsequent sections of this chapter.

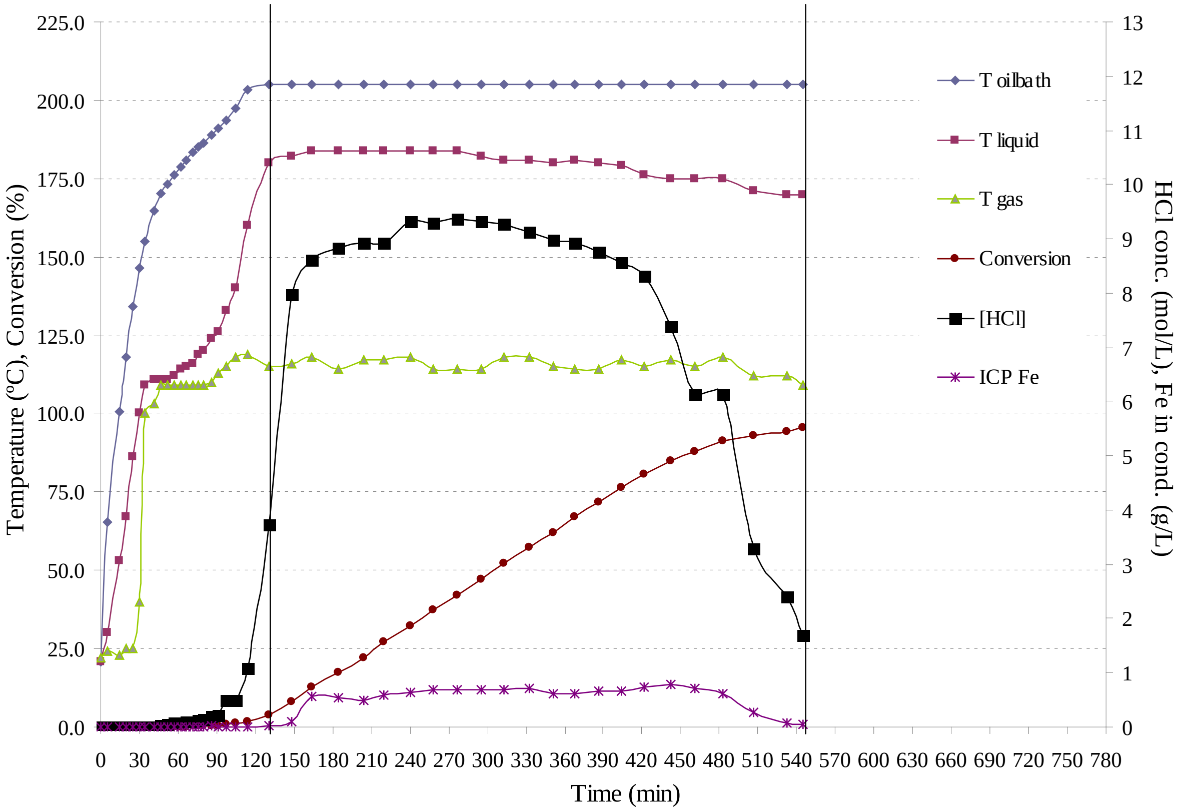

Figure 30: Standard Reaction Profile of a Hydrolytic Distillation Experiment (RT42). (Initial $FeCl_3$ Concentration: 3.08 M; Water Flow Rate: 2.3 mL/min. Vertical Lines denote the Start and End of Water Addition).

Table 7: Summary of $FeCl_3$-H_2O Hydrolytic Distillation Experiments and Results (180ºC).

Test ID	Reaction Time (min)	Initial $FeCl_3$ Concentration (M)	Max. HCl strength (mol/L)	Average HCl strength (mol/L)	Conversion[*] (%)
RT40	735	2.01^1	11.92	5.98	94.4
RT41	780	1.97^2	12.54	6.95	87.6
RT42	545	3.08^3	9.36	8.53	95.3
RT43	609	1.97^+	9.20	8.04	100+62.3
RT44	649	1.97^+	9.47	7.26	100+56.3
RT45	500	5.67^4	11.20	8.53	67.9
RT48	147	3.08	4.06	2.53	3.9
RT49	601	3.08	9.26	8.46	90.0

[*] Based on the amount of Cl found in the condensates

[+] In these experiments feed solution as opposed to water was added; Q_{43}=2.3 mL/min and Q_{44}=2.3 mL/min feed solution

[1] Initial solution contained also 4 g/L (0.014 M) $FeCl_2$; Q_{water}=1.3 mL/min

[2] Q_{water}=1.3 mL/min

[3] Q_{water}=2.3 mL/min

[4] This concentration corresponds to the saturation point of the solution at 22ºC; Q_{water}=2.4 mL/min

5.3. Results–Reaction Parameters

In the early stages of this work hydrolytic distillation experiments involving mixed 0.5 M $FeCl_3$-3.8 M $MgCl_2$ solutions were performed in continuation of previous research conducted in the hydrometallurgy laboratory at McGill University [69, 70, 73, 75]. The results from these tests are included in Appendix III of this thesis. As discussed and mentioned earlier in section 2.5.4 (Hydrolytic Distillation in chapter 2) the presence of $MgCl_2$ highly complicated the process hence the focus was shifted in the $FeCl_3$-H_2O system instead, which constitutes step 2 of the PORI Process (Equation 25). Table 7 summarizes the main hydrolytic distillation experiments performed with this system and the results obtained in terms of $FeCl_3$ conversion to HCl and Fe_2O_3 and HCl strength. Details about these tests can be found in Appendix II.

Among the reaction parameters studied were the initial concentration ($FeCl_3$) of the solution, the rate of water addition and the addition of feed solution instead of water.

5.3.1. *The Effect of the Water Addition Rate*

As described in 5.2 the hydrolytic distillation process (as applied to $FeCl_3$-H_2O solutions) is driven at 180ºC with the addition of water. This is a critical parameter as inadequate water addition would result in drying of the slurry inside the reactor or erratic HCl distillation while excess water would lead to production of weak strength HCl in the condensate. This is exemplified by comparing the results obtained from RT41 involving 1.3 mL/min water addition to that of RT42 involving 2.3 mL/min water addition.

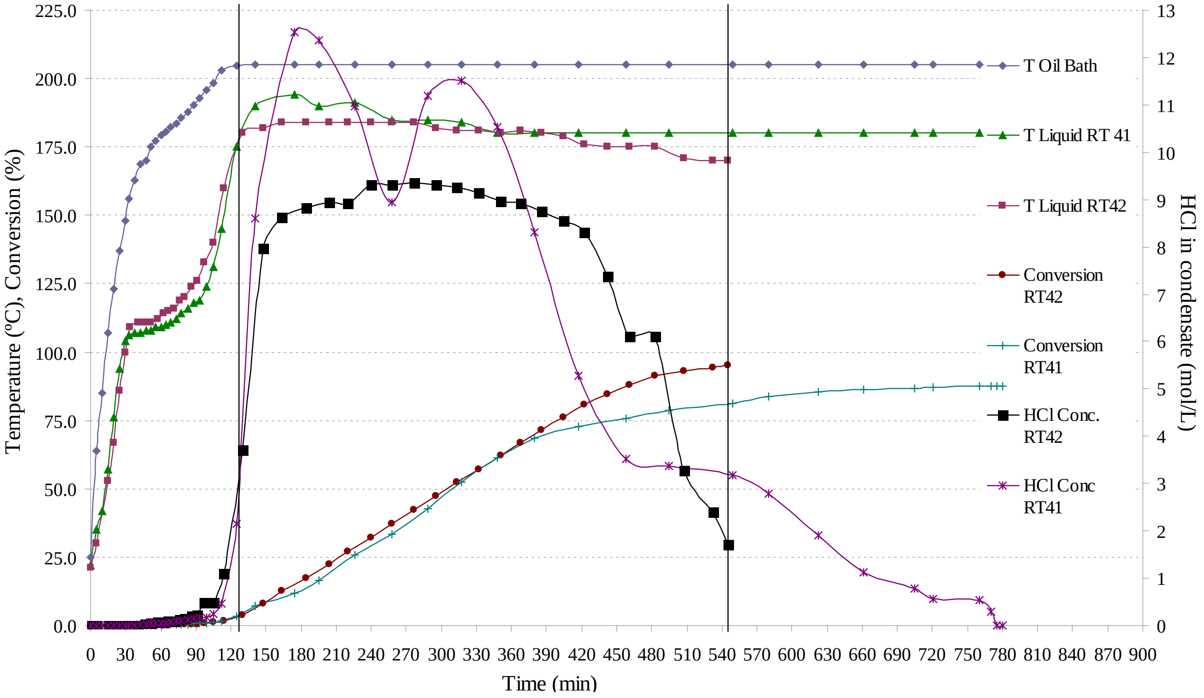

Figure 31: Superimposed Reaction Profiles of the Hydrolytic Distillation Experiments Involving Different Water Addition Rates (RT41: Initial $FeCl_3$ Concentration 1.97 M, Water Flow rate: 1.3 mL/min and RT42: Initial $FeCl_3$ Concentration: 3.08 M; Water flow rate: 2.3 mL/min). (The Vertical Lines denote the Start and End of Water Addition).

Figure 31 shows the superimposed reaction profiles of experiments RT41 and RT42. By examining the profile RT41 it can be seen the HCl strength in the condensate came to be exhibit sharp peaks (erratic behavior). Thus at time (t = 180 min) a spike in acid strength at ~12 M is observed followed by a drop down to 8.5 M before it shoots up again to 11.5 M thereafter constantly decreasing. At the same time the temperature of the reaction mixture is seen to initially rise up to 190ºC before it stabilizes at ~180ºC. The first vertical line denotes the start of water addition for both experiments (RT41 with a rate of 1.3 mL/min and RT42 with a rate of 2.3 mL/min). The second line indicates the end of water addition. Following the first HCl concentration peak of RT41 it was observed the solution/slurry inside the reactor to start solidifying signaling that the amount of water added was not adequate. At this point the origin of the second spike in HCl strength is not known as the same water addition rate (1.3 mL/min) was kept constant throughout the test. The second elevation of the acid strength most likely reflects a solid phase transformation event such as the formation of FeOCl (refer to section 2.4 and Appendix I). The overall conversion within the reaction period was only ~78% after 540 min (compare to 95% for RT42) reaching 87% after 780 min.

By increasing the water addition rate to 2.3 mL/min (experiment RT42) hydrolytic distillation was stabilized producing constant strength HCl at ~8.5 M and the conversion was higher and faster, i.e. 95% after 545 min. Hence proper selection of water addition rate is the key for the success of the hydrolytic distillation process.

5.3.2. The Effect of Solution Pre-Concentration

The initial $FeCl_3$ concentration in the solution increases upon evaporation of water ultimately reaching (at 180ºC) the concentration that corresponds to a “$FeCl_3 \cdot 2H_2O$”-composition as demonstrated later in section 5.5.1. The experiments described earlier (RT41 and RT42) had an initial $FeCl_3$ concentration of 2 and 3 M respectively. With the view of (i) shortening the required evaporation time and (ii) testing the limits of the process, a test (RT45) was performed using a solution with initial $FeCl_3$ concentration equal to 5.67 corresponding to the saturation point at room temperature. Figure 32 shows the reaction profile for experiment RT45. It can be seen that the water evaporation phase was shorter (~110 minutes instead of ~130 minutes) and that the acid concentration increased to 11 M. However, after 300 minutes the acid concentration dropped significantly leveling down to a ~6 M level just before the end of the water addition period. Of interest is the observation that at the same the temperature profile went through a hump and then started to decline below 175ºC after 300 min as well. The overall conversion obtained in this experiment was only 68%. It is tentatively assumed that the observed deteriorated performance may be due to the large (almost thrice as much as vis-à-vis RT42) mass of iron oxide solids produced that caused the viscosity-thickness of the slurry to increase. Hence this is another process parameter that needs to be properly selected in an eventual application for optimum results.

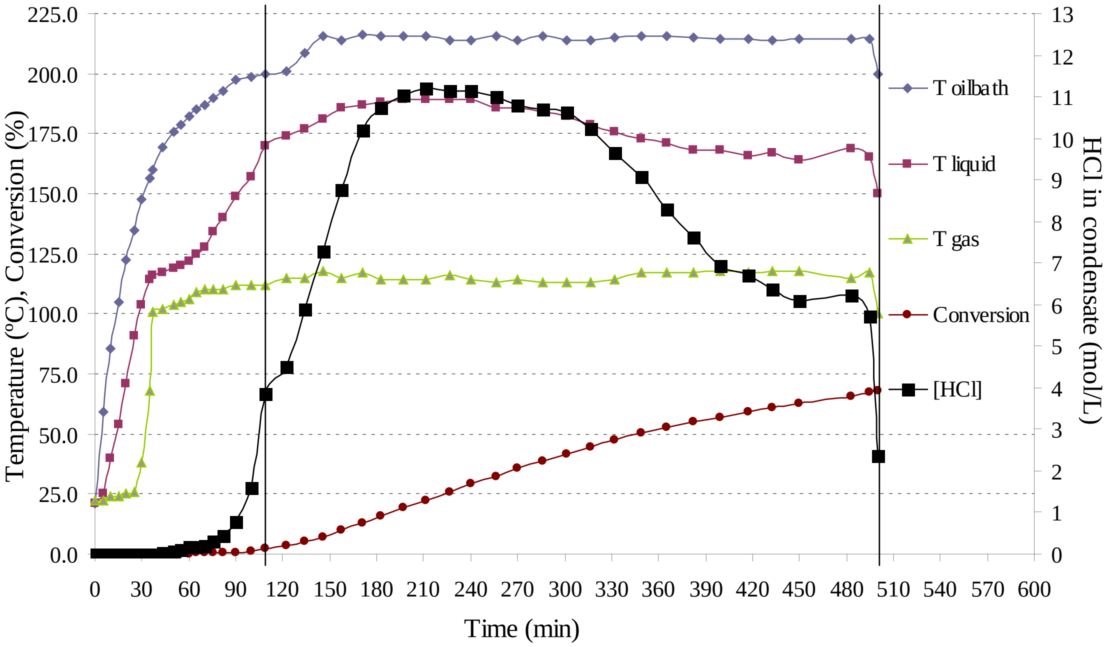

Figure 32: Reaction Profile of Experiment RT45. (Initial $FeCl_3$ Concentration: 5.67 M; Water Flow Rate: 2.4 mL/min. Vertical Lines denote the Start and End of Water Addition).

It would be interesting to see how this experiment works with continuous removal of the solids and simultaneous addition of concentrated feed solution. Unfortunately, the reactor was not designed to accommodate those conditions.

5.3.3. Reproducibility

From the above description it becomes clear that the best performance was obtained (Test RT42 –refer to Figure 31) using a $FeCl_3$ solution with initial concentration of 3 M and a water addition rate equal to 2.3 mL/min. In order to verify the reproducibility of the obtained results of test RT42 a duplicate test (RT49) was carried out. The results of the 2 tests are compared in Figure 49 where the conversion of iron chloride to hydrochloric acid and the HCl concentration are superimposed.

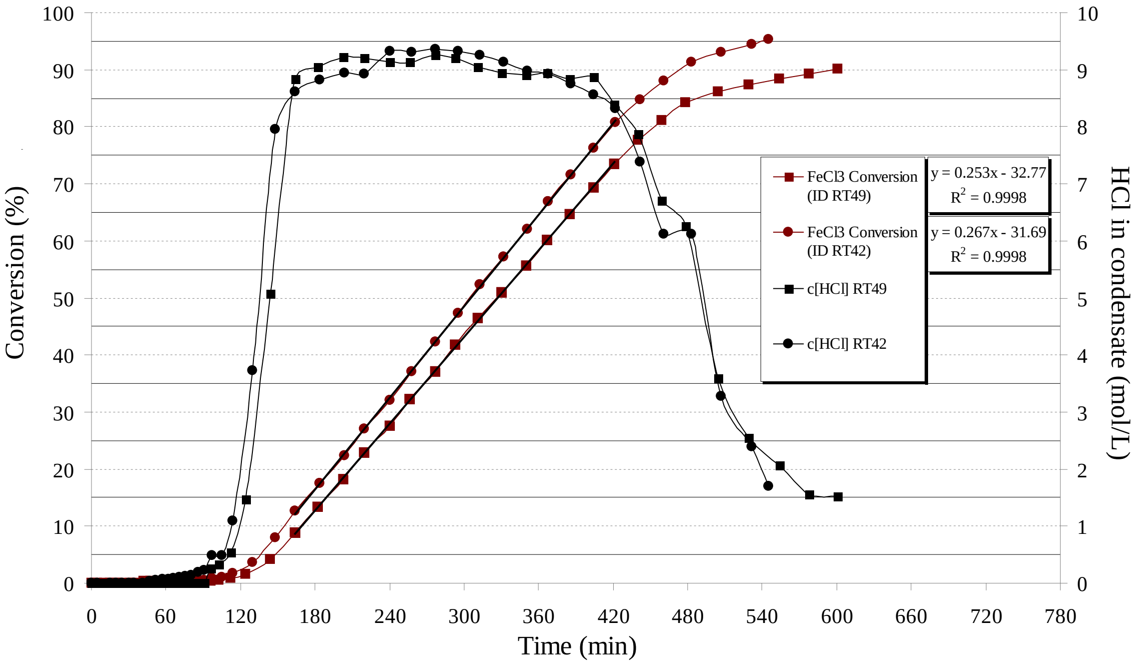

Figure 33: Reproducibility Check: Comparison of tests RT42 and RT49 (Initial $FeCl_3$ concentration: 3 M; Water Flow Rate: 2.3 mL/min; 180°C).

It should be mentioned that the water inflow had been activated 4 minutes later in RT42 than in RT49. This is perhaps the origin of the observed small deviation between the two tests. All in all however, the above Figure shows good reproducibility that renders confidence in the obtained results.

5.3.4. Substitution of Feed Solution for Water Addition

The hydrolytic distillation process was also run with feed addition (2 M $FeCl_3$ solution) instead of water addition. This option was investigated as it may be appropriate for continuous operation at large scale in a possible industrial application. Figure 34 shows the evolution of HCl concentration in the condensate and associated conversion efficiency.

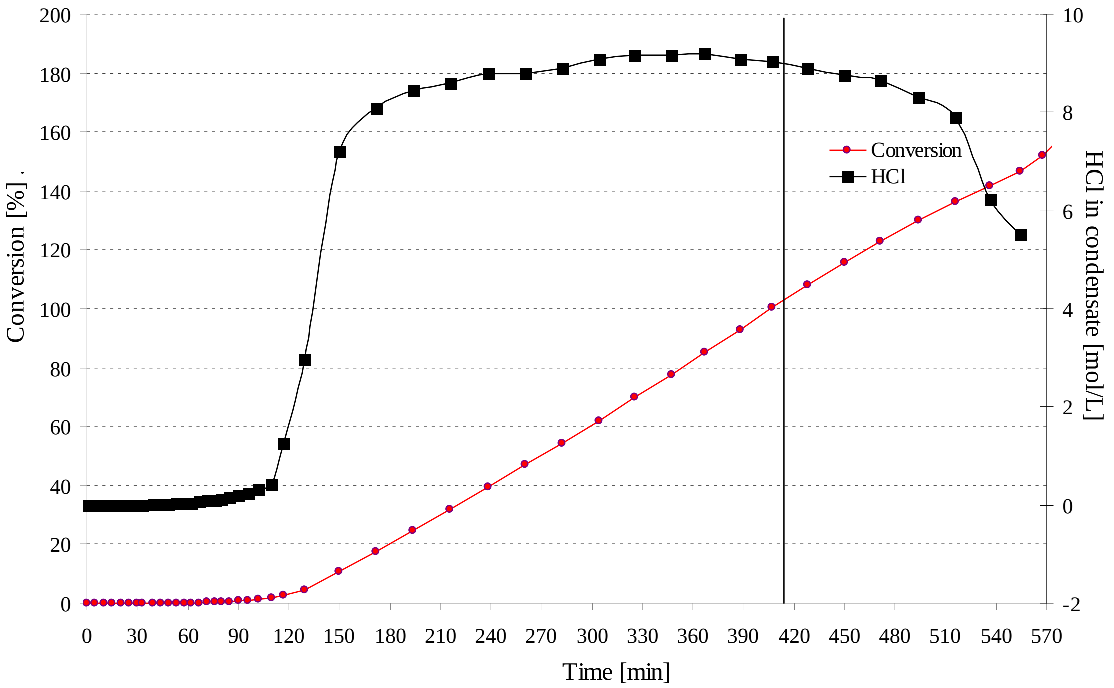

Figure 34: Conversion and Acid Strength of a Hydrolytic Distillation Experiment involving Feed Solution Addition. (Feed Rate: 2.3 mL/min; Initial Iron Concentration 1.97 mol/L; (RT43)).

The line at 407 minutes indicates the intersection where all the ferric chloride of the initial solution (one liter) has been transformed to iron oxide precipitate and HCl (conversion at 100%). The acidity of the condensate was at the same level (above 8 M) as with the test involving water addition (RT42-Figure 31) This implies that the process can be operated with either water addition or feed solution addition. The slope of the conversion line is the same before and after this intersection. This is evidence, that the reaction can be driven continuously by the addition of feed solution. It is clarified that conversion values higher than 100% are recorded as it is the initial $FeCl_3$ solution content that is taken as basis for defining conversion.

It is interesting to note that reaction test RT43 was repeated (RT44) but this time using a higher addition rate (3 mL/min) –refer for details to Appendix II. The recovery/ strength of HCl in the condensate did not exhibit a stable (pseudo steady-state) profile as in Figure 34. This is another manifestation of the importance of fine tuning the addition of water/feed solution as discussed in section 5.3.1.

5.3.5. *Iron in the Condensate*

The condensates collected during the hydrolytic distillation reaction contained a small amount of soluble iron (as $FeCl_3$). This iron chloride contamination gave the condensates their characteristic yellow color. Under optimum operating conditions (refer to Figure 30 and Appendix II) a bit less than 1 g/L Fe (as $FeCl_3$) was found to report in the condensate in a profile that parallels that of the HCl. By analyzing the data of other experiments it was observed the carry-over of $FeCl_3$ into the condensate to be linked to HCl concentration in the condensate. This is best explained with the data of reaction test RT41 (discussed in section 5.3.1, Figure 31 and Figure 35). The correlation between HCl and Fe concentration is remarkable. In this case the iron carry over was as high as 3x with reference to test RT42 operated at optimum conditions. As described earlier (section 5.3.1) the key difference between the two tests was the rate of water addition. The iron carry-over data further strengthen the view that the rate of water addition is critical in this type of process. Finally it is interesting to note that the iron concentration transferred to the condensate when feed solution as opposed to water was added (RT43 refer to section 5.3.4 and Appendix II) was at the level of 0.3 g/L, i.e. slightly lower than that (0.7 g/L) reported with water addition (RT42-Figure 30).

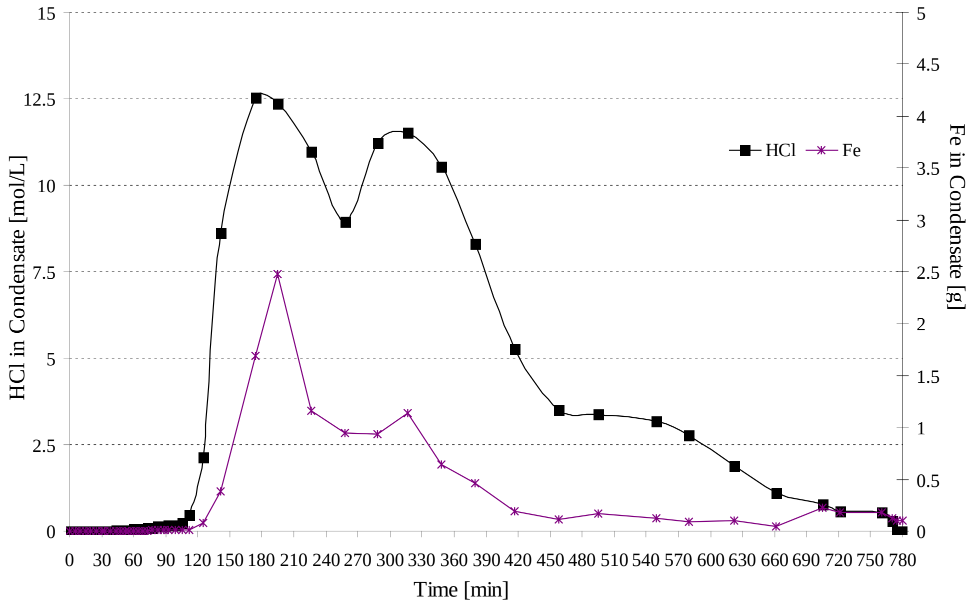

Figure 35: Iron and HCl Concentration-Time Profiles (RT41: Initial $FeCl_3$ Concentration: 1.97 M, Water Flow Rate 1.3 mL/min).

5.3.6. Scale Formation

The produced hematite precipitate is characterized in section 5.4. Here it is important to note that typically about 80% of the precipitate was recovered. 20% (RT42) of the product was observed to deposit on the reactor's wall forming a ring shaped scale. Figure 36 and Figure 37 help to visualize the extent of scale formation. It has to be noted, that no scale occurred directly underneath the impeller.

Figure 36: Scale in the Reactor after the Removal of the Reaction Products (RT42).

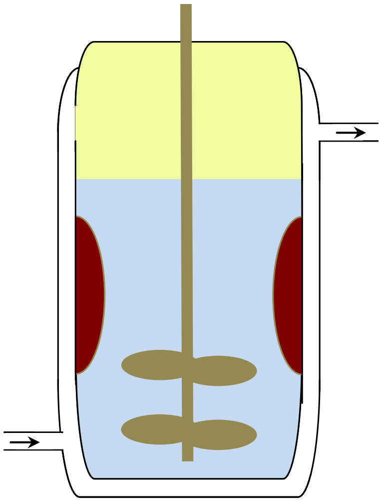

Figure 37: Schematic Cross Section of the Reactor with Ring-Shaped Scale on the inside of the Walls.

The introduction of baffles into the reactor setup was not tested but should receive attention in a new reactor design. Baffles could reduce the extent of scale and thus improve the total yield of the reaction. Similarly the use of hematite seeding as another means of scale prevention should be investigated.

5.4. Results–Product Characterization

General: Upon completion of a test while the reaction slurry was still hot it was diluted with water to its original volume to avoid solidification during cooling. The diluted slurry was agitated while cooling and the following day filtered through a 0.1 μm nitro cellulose filter under 50 psi pressure, washed with 1L of water to remove the residual soluble material (unreacted ferric chloride) and subsequently dried over night at ambient pressure in an oven (55˚C). This drying procedure resulted in 2.8-9.5% weight loss as a result of water removal. In contrast to the hematite produced from the oxidation experiments at 150ºC (refer to section 0) the hematite product from the hydrolytic distillation tests (refer to Equation 25 in section 5.1) was black. A picture of the solid product can be seen in Figure 38. This type of hematite was easily filterable: For example 240 g precipitate filtered within 2 minutes from 1 liter slurry through a filter with 0.1 μm pore size and 159 cm^2 surface area under 50 psi pressure. That corresponds to a filtration rate of 450 $kg \cdot m^{-2} \cdot h^{-1}$ of iron oxide.

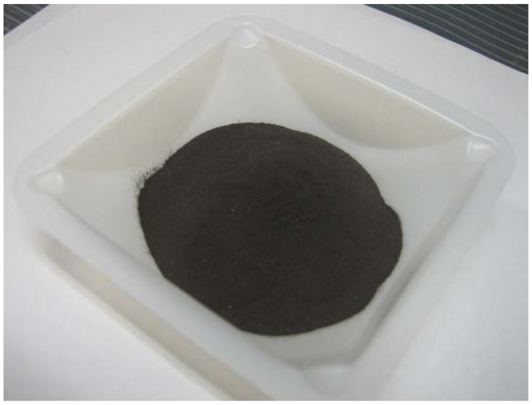

Figure 38: Dried Precipitate after Filtration.

Different methods were applied to acquire information about the chemical and physical properties of the precipitates. The full characterization data is presented in the following paragraphs.

Phase Identification: Figure 39 shows the XRD pattern of the precipitated product, formed during the hydrolytic distillation reaction with water addition. With the help of reference patterns in the database it could be clearly identified as hematite (α-Fe_2O_3). The high intensities and sharp peaks suggest the produced hematite is highly crystalline. As the detection limit of the XRD technique used was only 5% a higher sensitivity method –Raman Spectroscopy was employed as well (1% detection limit).

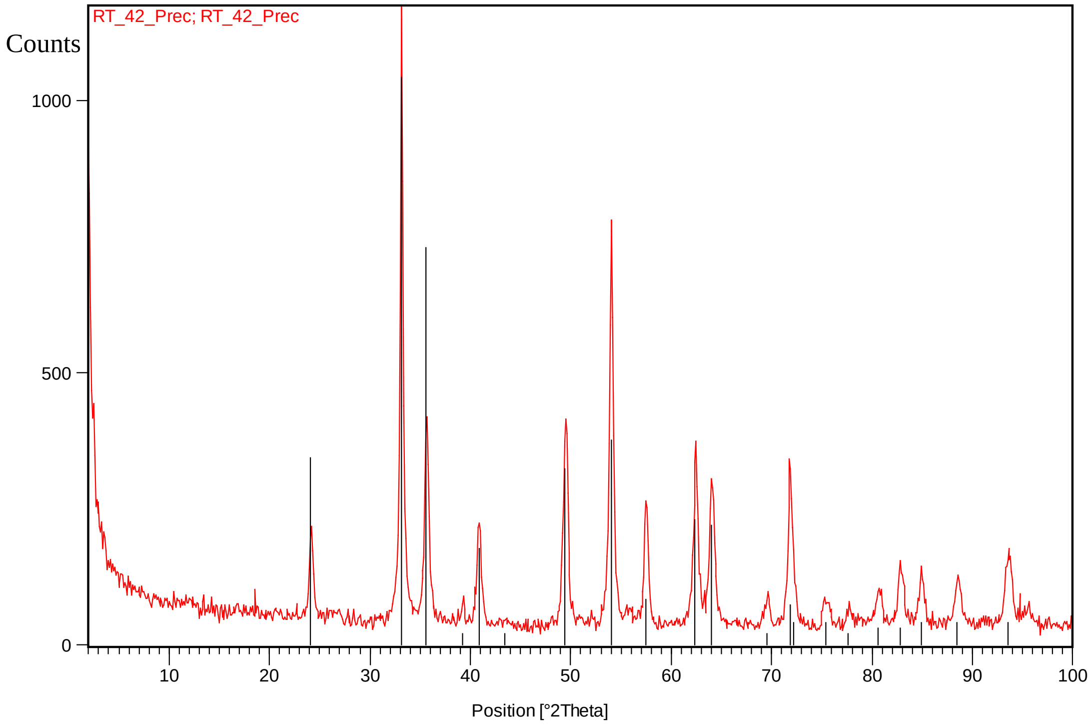

Figure 39: XRD-Pattern of the hematite product (RT42) (Ref. #: 00-024-0072).

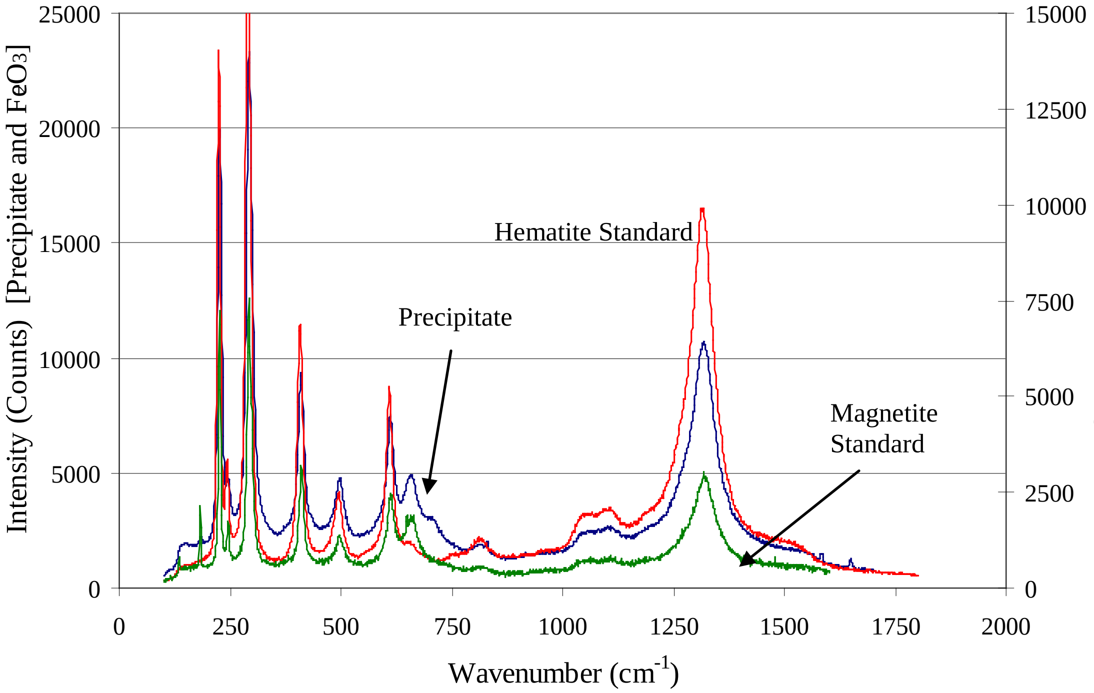

Figure 40: Raman Spectrum of the Precipitate Compared to Hematite and Magnetite Standards (RT42).

Raman spectroscopy confirmed hematite to be the major phase but also revealed that a small amount of magnetite (Fe_3O_4) might be present (Figure 40). As a reminder magnetite was also found to form during hematite precipitation by the oxidation of ferrous chloride solutions (refer to section 0). The presence of magnetite is indicated by the peak at 680 cm^{-1} [76].

Composition: Table 8 provides chemical composition data in terms of %Fe and %H_2O content for various hematite precipitation products as determined by digestion(%Fe) and TGA (%H_2O). The hematite product contained on average 69.4% iron, which is slightly lower than the theoretical value of 69.94% for pure Fe_2O_3. By titration of the HCl digestion liquor it was further determined the hematite to contain 0.65% of iron(II) which is attributed to the minor amount of magnetite detected by the Raman analysis. Finally digestion of the precipitate in HF and titration with $AgNO_3$ revealed the presence of ~3% Cl content. However, thorough washing (10 g solids in 30 L water) completely removed all chloride suggesting no structural incorporation in hematite.

Table 8: Chemical Composition Analysis and Surface Area of Hematite Products from Selected Hydrolytic Distillation Experiments.

Test ID	Reaction Time (min)	Initial $FeCl_3$ Conc. (M)	Water Content (%)	Iron Content (%)	BET Surface Area (m^2/g)
RT42	545	3.08	3.3	68.15	7.2
RT43	609	1.97	4.0	71.58	15.6
RT49	601	3.08	2.5	68.49	6.2

Thermo gravimetric analysis of various iron oxide precipitates produced the weight loss vs. temperature curves shown in Figure 41. It can be concluded that after the initial weight loss of 2.8-9.5% (due to drying in the oven over night at 55ºC) the precipitate lost another 3.5-4.0% (upon heating to 600ºC). Of the latter water content ~1% is attributed to surface water while the rest to structural water, most likely as OH. Hence the total water content of the produced hematite cake after pressure filtration can be estimated to be 6.3-13.5%.

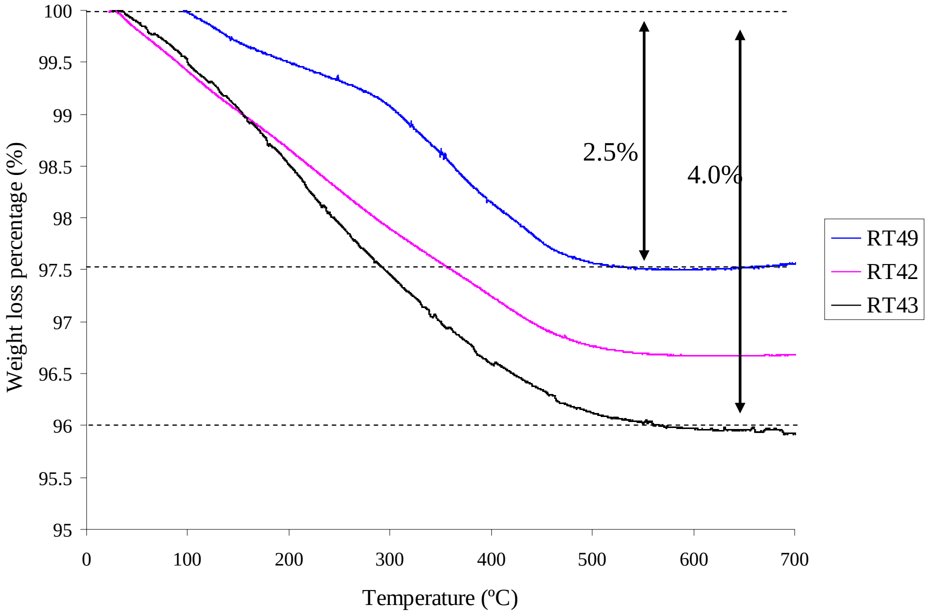

Figure 41: TGA of Iron Oxides Obtained by Hydrolytic Distillation; Heating Rate 10˚C/min.

Physical Characteristics: The particle size distribution of a representative product sample (from test RT42) can be seen in Figure 42. The mean particle size was 42 μm significantly larger that that of the red hematite (1.7 μm) provided by oxidation (refer to section 4.5) which explains the color difference between the two hematite particles [20]. The hematite produced by water addition (RT42 and RT49) was found to have a BET surface area (data shown in Table 8) in the range of 6-7 m^2/g, as opposed to the hematite produced be feed solution addition (RT43) that had a higher surface area (15 m^2/g). By using Equation 32 (given in section 0) the equivalent isometric dense particle size was calculated to be only 0.16 μm for experiment RT42 product (7 m^2/g). This is some 260 times smaller than the apparent particle size (42 μm) (see Figure 42) suggesting a porous particle structure.

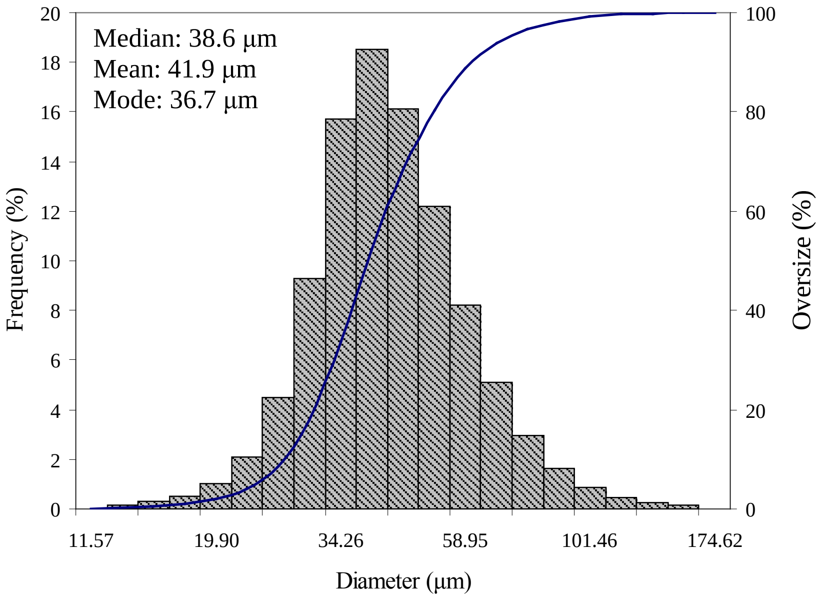

Figure 42: Volume Based Particle size Distribution for the Iron Oxide Precipitate (RT42).

VP SEM imaging was used to examine the morphological features of the hematite precipitate. As it can be seen in Figure 43 the precipitate mostly consists of uniform shaped coarse particles. The majority of the spherical particles had the morphology of the particle shown in Figure 45. Occasionally, however, some irregular shape particles with different texture were observed as the one in Figure 44. The latter was suspected not to be hematite per say but rather unreacted $FeCl_3{\cdot}nH_2O$ or FeOCl (refer to section 2.4 and Appendix I).

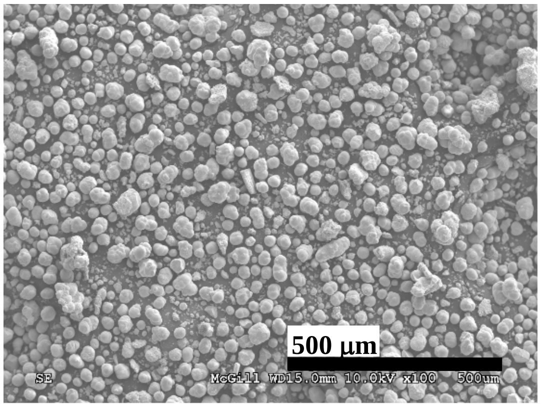

Figure 43: VP SEM Image of the Precipitate, Magnification x100 (RT42)

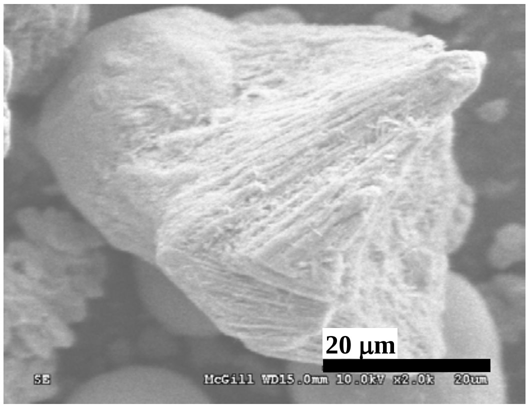

Figure 44: SEM Image of a Layer on Top of a Particle, Magnification x2000 (RT42).

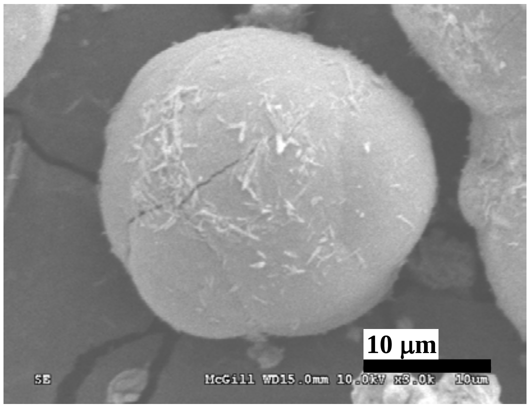

Figure 45: SEM Image of a Typical Hematite Particle, Magnification x3000 (RT42).

This was indirectly confirmed be performing EDS analysis (refer to Figure 46). Thus by comparing the peaks for the two different particles (punctual scan method), it is seen the particle of Figure 44 to contain significantly more chloride ("High Cl") that the particle of Figure 45 ("Low Cl").

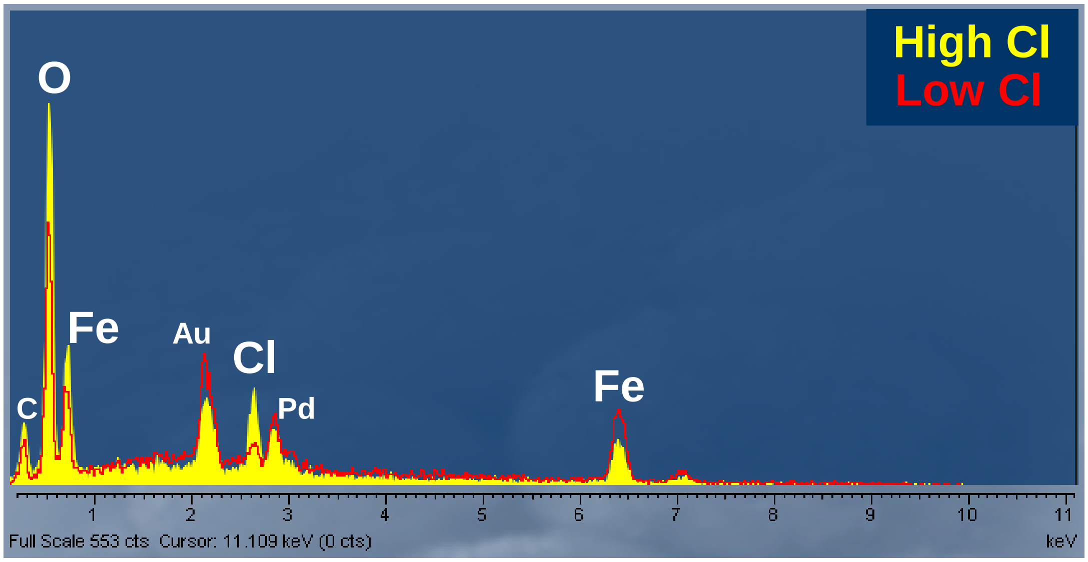

Figure 46: EDS Analysis of the Particles of Figure 44 (high Cl) and Figure 45 (low Cl). Both RT42. (Note: C, Au and Pd signals originate from sample preparation)

Finally with the view of verifying the BET results that pointed to a porous internal particle shape, a feature that was not evident from the SEM picture of Figure 45, cross sections of the hematite powder were prepared for further examination. Figure 47 shows a back-scattered electron image of a representative particle cross section. It can be seen the interior core of the particles to be fragmented revealing an agglomerate structure. The cross section of the main particle further revealed the presence of an outer ring with significant void space between the outer ring and the inner core. It is possible that the void was created by loss of loose sub-micron fragments as a result of the polishing procedure. The image shows nevertheless, that the particles are very brittle and that they have grown via aggregation of primary particles formed initially homogeneously that were finished via heterogeneous deposition towards the end of the precipitation process as elucidated by the ring formation. Such complex aggregated particle structure is common in batch crystallization processes operating under variable supersaturation regimes [32].

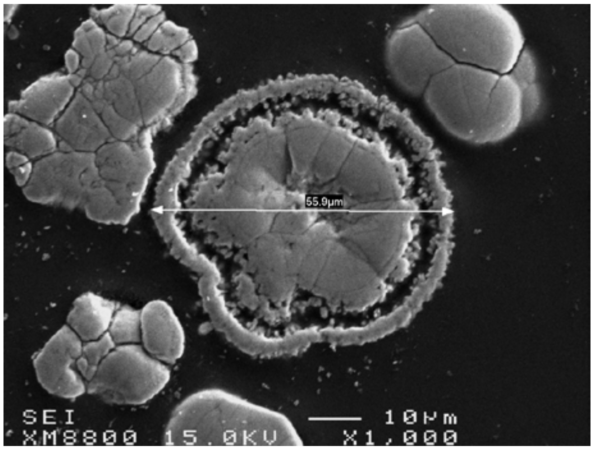

Figure 47: Cross section of a precipitate particle (RT42).

5.5. Results–Analysis and Discussion

In this section the obtained results are analyzed in terms of mass balances for water, iron and chlorine and kinetics and discussed from a reaction mechanism point of view.

5.5.1. Mass Balances

To better understand the hydrolytic distillation process mass balances for water and for the two main elements of the process (iron and chlorine) were established as described in the following paragraphs.

Water Balance: In the previous sections it was reported that optimum results were obtained by raising the temperature of the $FeCl_3$ aqueous solution to 180ºC (via evaporation) and subsequent addition of water (or feed solution) to drive the hydrolytic distillation process (refer to section 5.2 and Figure 30). Though the hydrolytic distillation tests were conducted under various conditions, it became clear that temperature and the right ratio of water to $FeCl_3$ were crucial to drive the reaction (Equation 25) to completion while producing super azeotropic (8-9 M) hydrochloric acid. To this end, a test was conducted (RT48) up to the point that usually water addition would start in order to determine the composition of the liquid phase. By accounting for the water collected as condensate the molar mass of water remaining inside the reactor was calculated. This is plotted in Figure 48 (data from RT48) as a function of time. On the same graph the temperature in the liquid phase and HCl concentration of the condensate are plotted As demonstrated below the obtained data revealed that the liquid phase at 180ºC had the composition of $FeCl_3{\cdot}2H_2O$.

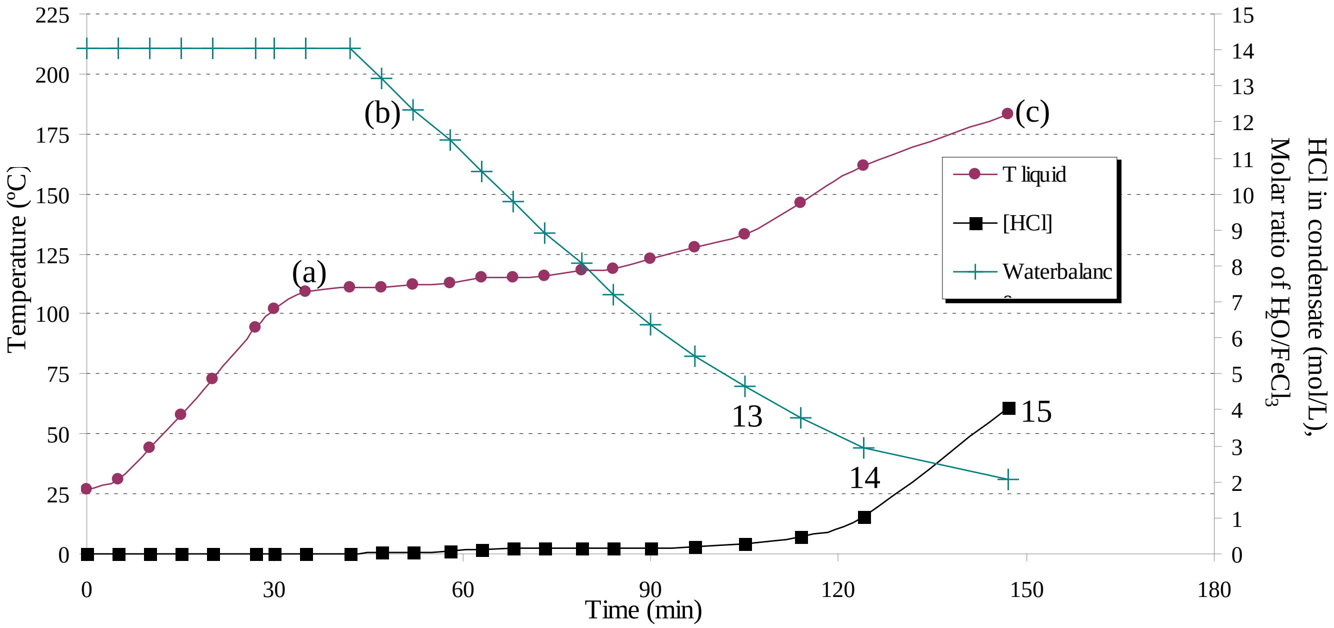

Figure 48: Monitoring of the Molar Ratio of Water to $FeCl_3$ in the Liquid Phase until Hydrochloric Acid Starts to Flash Off (RT48).

The point (a) of the temperature curve signifies the boiling point of the solution. Until this point, no water had evaporated from the system. About 15 minutes later (point (b)) the first condensate of 47.5 mL was collected and titrated. The concentration of hydrochloric acid in this sample was close to zero and remained below 1 mol/L for the first 13 samples. With sample 13 (each condensate sample had the same volume equal to 47.5 mL) already 617.5 mL water had been collected in the condensate. Sample 14 was the first sample with an HCl concentration of about 1 mol/L. Thereafter it took 23 minutes to obtain the next sample 15. This shows an increasing difficulty of removing water from the system. After sample 15 was collected, only an extremely low amount of condensate came out of the reactor. Thus, beyond this point (c) water addition had to be turned on with a flow rate of about 2.3-2.5 mL per minute. This rate as explained in section 5.3.1 proved to be best to maintain stable conditions inside the reactor. At the point of water addition, the reactor had already reached the reaction temperature of about 180ºC.

The water content of the liquid phase at this point (just before water addition will start) was calculated by subtracting the amount of condensate from the amount of water in the initial solution. This calculation was done for several experiments. Table 9 shows the liquid phase at this point to contain on average value of 2.09 mol water per mol of ferric chloride. This composition needs to be reached and maintained by water (or feed solution) addition in order to allow production of superazeotropic strength acid.

Table 9: Calculation of the reaction slurry composition, as superazeotropic HCl starts to flash off.

ID	Initial Iron Concentration (M)	Condensate Collected (mL)	Cryst. Water Remaining (mL)	Molar H_2O/ $FeCl_3$ ratio
RT42	3.08	720.0	107.47	1.94
RT43	1.97	807.5	82.08	2.31
RT44	1.97	822.0	67.58	1.90
RT45	5.67	464.0	218.54	2.14
RT48	3.08	712.5	114.97	2.07
RT49	3.08	705.0	122.47	2.21
			Average	**2.09**

Figure 49: Black Liquid inside the Reactor at the Beginning of Hydrolytic Distillation (RT48).

The liquid phase with composition 2 mol H_2O/1 mol $FeCl_3$ was thick black as it can be viewed in Figure 49. To obtain this picture, the experiment was stopped and the reactor opened. A sample was taken which looked like crude oil. It was highly viscous and did not crystallize after cooling down to room temperature. However, after 3 days it solidified inside the sample tube.

Chlorine Balance: To gather information about the pathways for chlorine in the reaction, a balance was set up. Basically the chloride units of $FeCl_3$ are converted to HCl and report to the condensate. In general (refer to tests RT42 and RT44 in Table 7) somewhere between 90 and 95% of chloride units report to the condensate as HCl –this was verified by acid titration. Direct analysis of the Cl^- content of the condensate by the AgCl gravimetric method gave 93.8%. As per analysis of the precipitate (refer to section 5.4) an amount of 3.7% of the total chlorine amount was calculated to be present in the washed cake. It was further determined the filtrate and the wash water to contain 2.3%. Figure 50 provides a graphical breakdown of chlorine deportment.

An issue that remains unresolved is if any of the chloride (Cl^-) input converted to Cl_2 (gaseous or dissolved). Detection of chloride using KI and hexanes failed to reveal its presence. Its formation, however, cannot be completely ruled out because of the finding of a minor amount of ferrous iron (0.65%) in the hematite precipitate. Equation 33 shows a possible reaction for the formation of chlorine during hydrolytic distillation but its thermodynamic feasibility was not verified.

$$2\ FeCl_3 \longrightarrow 2\ FeCl_2 + Cl_2 \tag{33}$$

Given that the amount of Fe^{2+} in the precipitate corresponds to 1% maximum of the $FeCl_3$ input (3 M) it is estimated that the amount of Cl_2 produced according to Equation 33 would be 0.015 M or 1 g/L, a rather small amount that perhaps remained undetected.

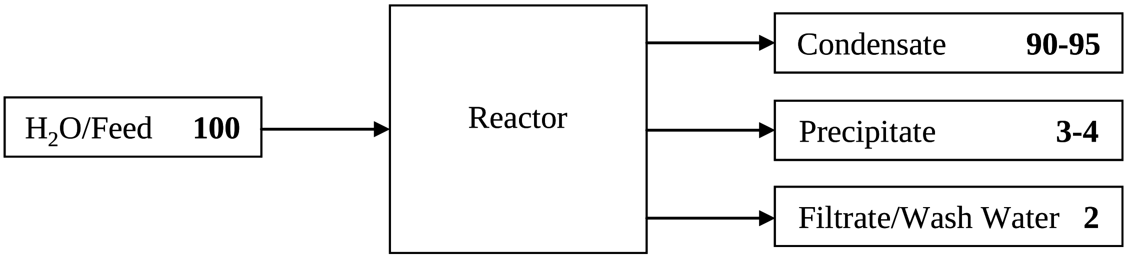

Figure 50: Deportment of Chlorine Units.

Iron Balance: A balance for iron (RT42 and RT 49) was set up to gather information about its reaction pathways (refer to Figure 51). The iron content of the condensate was found to be 0.67 g/L or 0.39% of the iron in the initial solution.

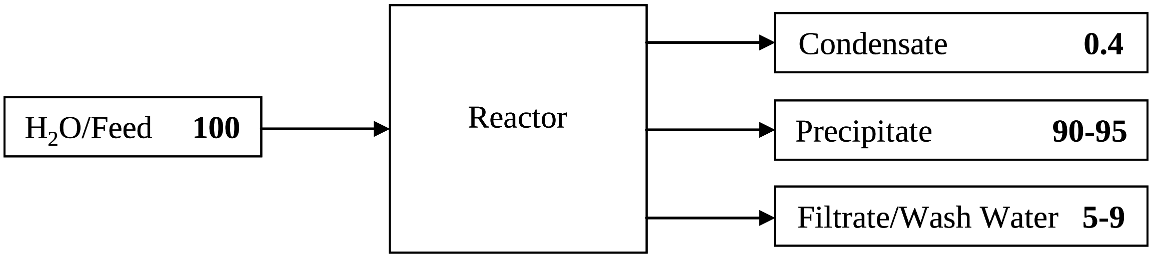

Figure 51: Deportment of Iron Units.

Based on the stoichiometry of the reaction (Equation 25) and the measured conversion efficiency of 90-95% for Cl^- it is extrapolated that also 90-95% of the iron reports to the hematite product. The balance is most probably left in the filtrate. This breakdown does not take into account the amount of iron as precipitate that reports as scale on the reactor walls. As mentioned earlier up to 20% of the iron oxide precipitate is estimated to form scale.

5.5.2. Reaction Kinetics

The reaction kinetics of the most promising experiments were analyzed. Figure 52 shows the cumulative amount of HCl recovered in the product and the average concentration on HCl in the product as a function of time for tests RT42 and RT49 involving water addition (refer to section 5.3.3) and test RT43 involving feed addition. All three tests had produced similar acid concentration profiles and were operated at similar addition rates (2-2.3 mL/min).

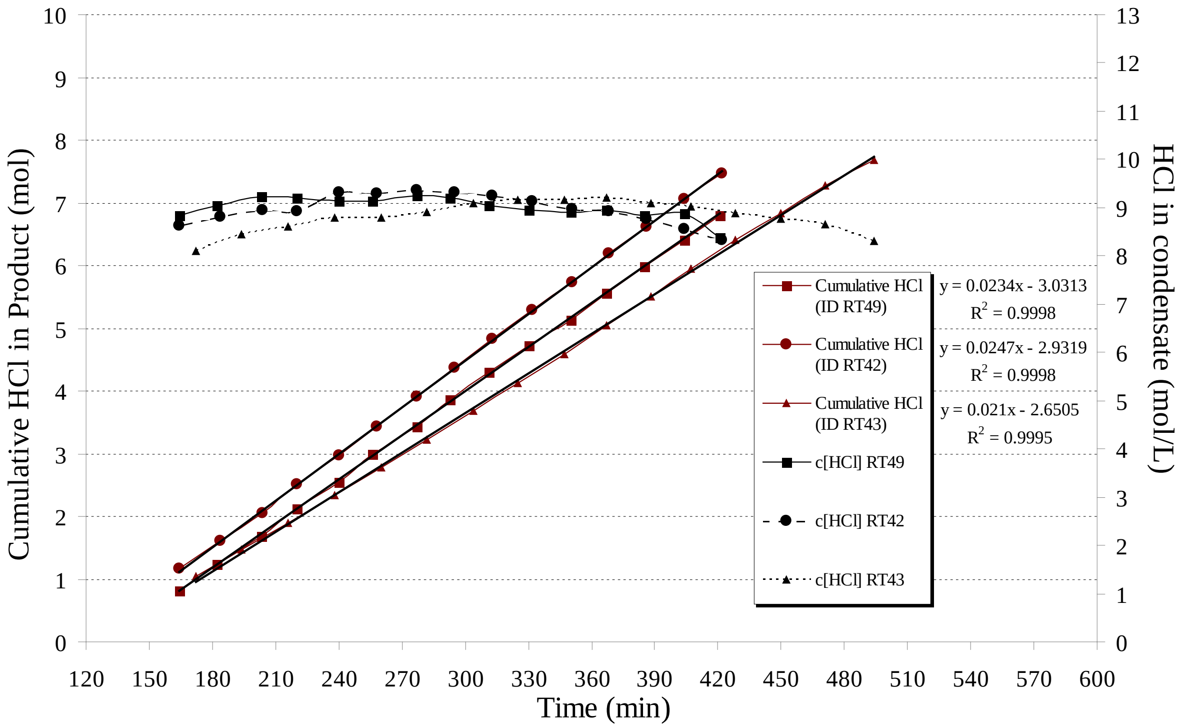

Figure 52: Comparison of HCl Recovery and Concentration as a Function on Time: Water Addition (RT42 and RT49) and Feed Solution Addition (RT43); Water/Feed Addition Rate=2-2.3 mL/min.

The trend lines were fit by regression and their corresponding equations are given in Figure 52. The slopes of these linear plots represent the rate of HCl production (refer to Equation 25). Equation 34 shows the rate r_{HCl} for the production of HCl in mol/min.

$$r_{[HCl]} = \frac{\Delta n_{[HCl]}}{\Delta t} \tag{34}$$

Where: $\Delta n[HCl]$ = change in the number of moles of HCl
Δt = time range

It can be seen, that the slopes of all three straight lines are in a very close range, i.e. all three experiments exhibit the same HCl production rate. The constant rate of HCl production[4] implies that the reaction is independent of ferric chloride concentration. Hence, the reaction has the appearance of zero order in C_{FeCl3}. The linear kinetics of HCl

---

[4] The ferric chloride concentration is assumed to decrease with time only in the case of water addition (RT42 and RT49). In the case of feed addition the concentration is essentially constant (pseudo steady-state) as the units of iron that are removed as hematite are replaced by the incoming $FeCl_3$.

production appears therefore to be limited to the constant rate of water addition (this was 125 mL water or feed solution added per hour). The calculated rates of HCl production in mol/h (or g/h) are given in Table 10 along with the linked rates of Fe_2O_3 production, $FeCl_3$ consumption and H_2O reaction according to the stoichiometry of Equation 25. The estimated amount of H_2O reacted in Equation 25 was found to be $^1/_{10}$ of that added at constant rate. The remaining $^9/_{10}$ apparently evaporate and report to the condensate. In other words the rate of HCl production is controlled by the rate of water addition. This can be conveniently expressed with the aid of Equation 35:

$$r_{[HCl]} = k \cdot c^0_{FeCl_3} \cdot a_{H_2O} \cdot n_{H_2O} \tag{35}$$

Where: k = rate constant (min^{-1})
C_{FeCl_3} = concentration of ferric chloride
a_{H_2O} = “activity” of water = 0.1
n_{H_2O} = amount of water added (mol)

In this equation the “activity” term a_{H2O} is introduced to denote the fact that only $^1/_{10}$ of the water added participates in the reaction. It must be further stated that the equation applies only for specific conditions applying to Figure 52.

Table 10: Conversion Rates of the Species involved in the Hydrolytic Distillation Process.

	mol/h (RT42)	**g/h (RT42)**	**mol/h (RT49)**	**g/h (RT49)**	**mol/h (RT43)**	**g/h (RT43)**
r(HCl)	1.48	54.04	1.40	51.19	1.25	45.72
r(Fe_2O_3)	0.25	39.44	0.23	37.37	0.21	33.37
r($FeCl_3$)	0.49	80.13	0.47	75.91	0.42	67.80
r(H_2O)$_{react}$	0.74	13.35	0.70	12.65	0.63	11.30
r(H_2O)$_{added}$	6.94	125	6.94	125	6.3$^{\#}$	112

r(H_2O)$_{react}$: amount of water spent by iron chloride
r(H_2O)$_{added}$: amount of water added
\# : this was estimated by assuming the amount of water in 1 L of feed solution is 0.9 L (2 M $FeCl_3$)

5.5.3. Reaction Mechanism Sequence

As described earlier the overall reaction involved in the hydrolytic distillation process of $FeCl_3$ is given by Equation 25:

$$2\ FeCl_3\ (aq) + 3\ H_2O\ (l) \longrightarrow 6\ HCl\ (g) + Fe_2O_3\ (s) \qquad (25)$$

On the basis of the presented data and observations and insight from the thermal decomposition of $FeCl_3$ salts literature the following reaction steps are postulated to characterize the hydrolytic distillation process:

$$FeCl_3\ (aq) + x\ H_2O\ (l) \longrightarrow FeCl_3{\cdot}xH_2O\ (l) \qquad (36)$$

$$FeCl_3{\cdot}xH_2O\ (l) \longrightarrow FeCl_3{\cdot}2H_2O\ (l) + (x\text{-}2)\ H_2O\ (g) \qquad (37)$$

$$FeCl_3{\cdot}2H_2O\ (l) \longrightarrow FeOCl{\cdot}H_2O\ (s\ or\ l) + 2\ HCl\ (g) \qquad (38)$$

$$FeOCl{\cdot}H_2O\ (s\ or\ l) \longrightarrow HCl\ (g) + FeOOH\ (s) \qquad (39)$$

$$2\ FeOOH\ (s) \longrightarrow Fe_2O_3(s) + H_2O\ (g) \qquad (40)$$

Equation 36 describes the formation of “liquid crystals” of heated ferric chloride as a result of water evaporation. This step occurs over the temperature range 110-180ºC (refer to 5.2, Figure 30). At 180ºC further de-hydration of the salt leads to formation of the liquid dihydrate ($FeCl_3{\cdot}2H_2O$) – Equation 37 as determined by the water balance analysis –refer to Table 9 in section 5.5.1. The next step of the hydrolytic distillation process (Equation 38) that involves the production of hydrochloric acid by water addition is postulated also to lead to iron oxychloride formation as an intermediate phase. Although the formation of FeOCl was not as such directly identified in this work the parallel study involving thermal decomposition experiments (described in Appendix I) gives credibility for this postulation. Gaseous hydrogen chloride dissolves in the water vapor condensate, forming superazeotropic strength acid. The effect of removing gaseous hydrogen chloride facilitates the hydrolytic decomposition reaction by shifting the equilibrium (refer to Equation 25) to the right side of the equation. Due to the high temperatures involved, the formed hydrated iron oxychloride apparently immediately decomposes generating hydrogen chloride and iron oxyhydroxide as another intermediate phase-Equation 39. The final step of the process involves the transformation of iron oxyhydroxide to hematite and water –refer to Equation 40. The formation of intermediate iron oxyhydroxide (in this case most likely akaganeite, i.e. β-FeOOH) and subsequent transformation to hematite is a well known reaction pathway [32].

Chapter 6: Global Conclusions

In this work the recovery of HCl from ferrous and ferric chloride solutions by hydrolytic distillation and simultaneous precipitation of hematite has been investigated. Experiments were conducted in two main areas, namely (1) oxidation of aqueous ferrous chloride solution (2) hydrolytic distillation of ferric chloride solutions. In addition to these areas a side study on the transformation of ferric chloride salt to iron oxychloride was conducted and reported in Appendix I of this thesis. The most important results from this work are summarized in the following paragraphs.

Oxidation of ferrous chloride solutions was successfully achieved with continuous sparging of oxygen at atmospheric pressure under reflux conditions –an approach never considered before. After screening various solution compositions a mixed 2 M $FeCl_2$-2 M $FeCl_3$ solution was found to provide the best results. This initial solution composition was heated to evaporate approximately $^2/_3$ of the water to raise the boiling point to 150ºC at which temperature $^2/_3$ of $FeCl_2$ were converted to $FeCl_3$ and $^1/_3$ to Fe_2O_3. The kinetics of the process are controlled by oxygen mass transfer hence reactor design becomes an essential consideration for any future work. Finally it should be mentioned that the produced hematite (red in color) consisted of aggregates of sub-micron crystallites with a mean particle size of 1.7 μm and a specific surface area of 12-28 m^2/g. No scale formation was observed. Its chemical composition was nearly 70% Fe with evidence of a trace amount of magnetite (<5%) and essentially free of chloride contamination (~0.1%). Oxidation could also take place at lower temperature (110-115ºC) but in that case goethite was producted exhibiting very poor filtration properties.

Aqueous ferric chloride solutions with initial concentration 2-5.67 mol/L were successfully transformed by hydrolysis to superazeotropic strength acid and hematite following pre-concentration by evaporation. The process was run at ~180ºC at which the pre-concentrated liquid phase was determined to consist of "$FeCl_3 \cdot 2H_2O$". For optimum and smooth operation of the hydrolytic process a constant water addition rate of 2-2.5 mL/min or equivalent 7 mol H_2O/h had to be applied. A lower water addition rate would result in drying of the reaction mass and erratic HCl distillation/release behavior, while a higher water addition rate would result in sub-azeotropic strength acid production. Feed solution (2 M $FeCl_3$) addition can successfully substitute water addition. The kinetics of HCl production were found to be linear controlled by the rate of water addition. It was possible to consistently produce 8-9 mol/L hydrochloric acid and obtain 95% conversion efficiency. A minor amount (~0.5 g/L) of iron (as $FeCl_3$) was found to be carried over to the produced acid

The hydrolytic process at 180ºC produced well grown and crystalline black-colored hematite particles with 68.5% Fe, ~4% H_2O/OH and ~3% Cl^- content. The chloride content, most likely as unconverted $FeCl_3$ or FeOCl impurity was upon thorough washing completely removable, hence it was not structurally incorporated in hematite. The average particle size of the precipitate was 40 μm and upon SEM examination and BET surface area measurement it was confirmed to be in the form of compact spherical aggregates. The product exhibited excellent filtration (450 $kg{\cdot}m^{-2}{\cdot}h^{-1}$) and washing properties, but a measurable amount of it (up to 20%) was found to form scale in the reactor –an issue that needs to be addressed in future work.

Further research should focus on the optimization of the oxidation of ferrous chloride with the view of selecting proper reactor design that will improve mass transfer kinetics, hence reducing the rather high agitation speed employed in the current work that demands high power. As regards the hydrolytic precipitation/distillation step, further work is required with the aim of reducing the occurrence of scale formation. Use of seed is an obvious option to consider, but also the introduction of baffles in a new designed reactor vessel. Along this line, the performance of integrated oxidation (at 150ºC) and hydrolytic distillation (at 180ºC) tests where the red hematite product of oxidation acts as seed during the hydrolytic distillation/precipitation reaction can be investigated as well. Finally, from an experimental point of view, a modification of the water addition/dispersion system and an automation of temperature and HCl concentration (conductivity) data acquisition could be considered for faster and more accurate data acquisition.

References

1. Strobbe, M., Luts, P., Vermeiren, C., Elemental Chlorine-free Conversion of Waste HCl Liquor by Oxidation and Concentration to form Aqueous Ferric Chloride Solution. *European Patent No. 0968961*, **2000**.

2. Demopoulos, G. P., Li, Z., Becze, L., Moldoveanu, G., Cheng, T. C., Harris, B., New Technologies for HCl Regeneration in Chloride Hydrometallurgy. *Erzmetall-World of Metallurgy* **2008**, 62, (2), 89-98.

3. McBain, J. W., Oxidation of Ferrous Solutions by Free Oxygen. *The Journal of Physical Chemistry* **1901**, 5, (9), 623-638.

4. Kobe, K. A., Dickey, W., Oxidation of Ferrous Sulfate Solutions with Oxygen. *Industrial & Engineering Chemistry* **1945**, 37, (5), 429-431.

5. Reedy, J. H., Machin, J. S., The Oxidation of Ferrous Sulfate to Ferric Sulfate by Means of Air. *Industrial & Engineering Chemistry* **1923**, 15, (12), 1271-1272.

6. Huffman, R. E., Davidson, N., Kinetics of the Ferrous Iron-Oxygen Reaction in Sulfuric Acid Solution. *Journal of the American Chemical Society* **1956**, 78, (19), 4836-4842.

7. Iwai, M., Majima, H., Awakura, Y., Oxidation of Fe (II) in sulfuric acid solutions with dissolved molecular oxygen. *Metallurgical and Materials Transactions B* **1982**, 13, (3), 311-318.

8. Battino, R., *IUPAC Solubility Data Series - Oxygen and Ozone Edition*. Pergamon Press, Oxford, UK: **1981**.

9. Tromans, D., Temperature and Pressure Dependent Solubility of Oxygen in Water: A Thermodynamic Analysis. *Hydrometallurgy* **1998**, 48, (3), 327-342.

10. Sechenow, M., Über die Konstitution der Salzlösungen auf Grund ihres Verhaltens zu Kohlensäure. *Zeitschrift für Physikalische Chemie* **1889**, 4, 117-125.

11. Kovacs, G. L., Treatment of Waste HCl Pickle Liquor. *US Patent No. 3,682,592*, **1972**.

12. Kovacs, G. L., Verfahren zur Herstellung von Eisen(III)-chlorid aus Eisen(II)-chlorid. *Deutsches Patent No. 2136303*, **1973**.

13. Kovacs, G. L., Process for Producing Ferric Chloride. *UK Patent No. 1365093*, **1974**.

14. Kovacs, G. L., Process for Partial Oxidation of $FeCl_2$ to $FeCl_3$. *European Patent No. 0173133*, **1985**.

15. Burtch, J. W., Hydrochloric acid from industrial waste streams. The PORI process. *CIM Bull.* **1975**, 68, 96-100.

16. Sylva, R. N., The Hydrolysis of Iron III. *Rev. Pure Appl. Chem.* **1972**, 22, 115-132.

17. Aprahamian, V. H., Demopoulos, G. P., The Solution Chemistry and Solvent Extraction Behaviour of Cu, Fe, Ni, Zn, Pb, Sn, Ag, As, Sb, Bi, Se and Te in Acid Chloride Solutions Reviewed from the Standpoint of PGM Refining. *Mineral Processing and Extractive Metallurgy Review* **1995**, 14, (3), 143 - 167.

18. Senanayake, G., Muir, D., Speciation and Reduction Potentials of Metal Ions in Concentrated Chloride and Sulfate Solutions Relevant to Processing Base Metal Sulfides. *Metallurgical and Materials Transactions B* **1988**, 19, (1), 37-45.

19. Chiarizia, R., Danesi, P. R., Mass Transfer Rate in Liquid Anion Exchange Processes-II : Kinetic of iron(III) transfer in the Biphasic System Trilaurylamine Hydrochloride-Aromatic Diluent, HCl-Water. *Journal of Inorganic and Nuclear Chemistry* **1978**, 40, (10), 1811-1816.

20. Cornell, R. M., Schwertmann, U., *The Iron Oxides: Structure, Properties, Reactions, Occurences and Uses*. 2nd ed.; Wiley-VCH Verlag GmbH & Co. KGaA: Weinheim, **2003**.

21. Dutrizac, J. E., Monhemius, A. J., *Iron Control in Hydrometallurgy*, Ellis Horwood, Chichester, U.K., **1986**.

22. Dutrizac, J. E., Harris, G. B., *Iron Control and Disposal*, CIM, Montreal, Canada, **1996**.

23. Dutrizac, J. E., Riveros, P., *Iron Control Technologies*, CIM, Montreal, Canada, **2006**.

24. Cheng, T. C. M., Demopoulos, G. P., Analysis of the Hematite Precipitation Process from a Crystallization Point of View, *EPD Congress TMS*, Warrendale, PA, USA, **1997**; pp 599-617.

25. Cheng, T. C., Demopoulos, G. P., Shibachi, Y., Masuda, H., The Precipitation Chemistry and Performance of the Akita Hematite Process—An Integrated Laboratory and Industrial Scale Study, *Hydrometallurgy 2003*, Vancouver, **2003**; pp 1657-1674.

26. Demopoulos, G. P., Cheng, T. C., The Hematite Process - New Concepts for Increased Throughput and Improved Product Quality. *Pressure Hydrometallurgy*, Collins, M. J., Papangelakis, V. G., Eds. CIM: Montreal, **2004**; pp 965-980.

27. Biederman, G., Chow, J. T., Studies on the Hydrolysis of Metal Ions. Part 57. Hydrolysis of the Iron(III) Ion and the Solubility Product of $Fe(OH)_{2.7}Cl_{0.3}$ in 0.5 M $(Na^+)Cl^-$ Medium. *Acta Chem. Scand.* **1966**, 20, 1376.

28. Powder, Diffraction, File, *International Centre for Diffraction Data* **2001**.

29. Riveros, P. A., Dutrizac, J. E., The Precipitation of Hematite from Ferric Chloride Media. *Hydrometallurgy* **1997**, 46, (1-2), 85-104.

30. Dutrizac, J., Riveros, P., The Precipitation of Hematite from Ferric Chloride Media at Atmospheric Pressure. *Metallurgical and Materials Transactions B* **1999**, 30, (6), 993-1001.

31. Filippou, D., Choi, Y., A Contribution to the Study of Iron Removal from Chloride Leach Solutions, Van Weert, G., Peek, E. M. L., Eds. *Chloride Metallurgy*, CIM, Montreal, Canada, **2002**; p 729 Vol. 2.

32. Demopoulos, G. P., Aqueous Precipitation and Crystallization for the Production of Particulate Solids with Desired Properties. *Hydrometallurgy* **2009**, 96, (3), 199-214.

33. Voigt, B., Göbler, A., Formation of Pure Haematite by Hydrolysis of Iron (III) Salt Solutions under Hydrothermal Conditions. *Crystal Research and Technology* **1986**, 21, (9), 1177-1183.

34. Goñi-Elizalde, S., Garcia-Clavel, M. E., Tejedor-Tejedor, M. I., Mechanism of Akaganeite-Hematite Transformation via Solution. *Reactivity of Solids* **1987**, 3, (1-2), 139-154.

35. Goñi-Elizalde, S., García-Clavel, M. E., Thermal Behaviour in Air of Iron Oxyhydroxides Obtained from the Method of Homogeneous Precipitation: Part II. Akaganeite sample. *Thermochimica Acta* **1988**, 129, (2), 325-334.

36. Thorpe, T. E., Bothamley, C. H., Wilson, A. E., Ingle, H., Kennedy, C. L., Johnstone, M. N., Contributions to the History of the Mineral Waters of Yorkshire. From the Laboratory of the Yorkshire College. *Journal of the Chemical Society* **1881**, 39, 497-516.

37. Rousseau, G., Crystallised Ferric Oxychloride. *Journal of the Chemical Society* **1890**, 58, 1063.

38. Schäfer, H., Untersuchungen am System Fe_2O_3-$FeCl_3$-H_2O-HCl I. Die Einwirkung von Chlorwasserstoff auf alpha-Eisenoxyd und die Auswertung der Reaktionsgleichgewichte. *Zeitschrift für anorganische Chemie* **1949**, 259, (1-4), 53-74.

39. Schäfer, H., Untersuchungen am System Fe_2O_3-$FeCl_3$-H_2O-HCl II. Vergleichende kritische Betrachtung der Literaturangaben Über die Einwirkung von Chlorwasserstoff auf Eisenoxyd. Bemerkungen und Versuche zur Gasentmischung bei der

Gleichgewichtsmessung nach der "Schiffchenmethode". *Zeitschrift für anorganische Chemie* **1949**, 259, (1-4), 75-85.

40. Schäfer, H., Untersuchungen am System Fe_2O_3-$FeCl_3$-H_2O-HCl III. Chlorierungsgleichgewichte mit Eisenoxychlorid als Bodenkörper. *Zeitschrift für anorganische Chemie* **1949**, 259, (5-6), 265-277.

41. Schäfer, H., Untersuchungen am System Fe_2O_3-$FeCl_3$-H_2O-HCl IV. Das Vierphasen-System FeOCl, $FeCl_3$ fest, ($FeCl_3 \cdot n\ H_2O$) flüss., Gas. *Zeitschrift für anorganische Chemie* **1949**, 260, (1-3), 127-140.

42. Schäfer, H., Untersuchungen am System Fe_2O_3-$FeCl_3$-H_2O-HCl V. Die präparative Darstellung von Eisenoxychlorid. *Zeitschrift für anorganische Chemie* **1949**, 260, (4-5), 279-294.

43. Schäfer, H., Untersuchungen am System Fe_2O_3-$FeCl_3$-H_2O-HCl VI. Das System Fe_2O_3-FeOCl-$FeCl_3$-H_2O-HCl zwischen etwa 100 und 1000°C. *Zeitschrift für anorganische Chemie* **1950**, 261, (3-4), 142-152.

44. Schäfer, H., Untersuchungen am System Fe_2O_3-$FeCl_3$-H_2O-HCl VII. Über den Hydrolytischen Abbau des Eisenoxychlorids unter der Einwirkung von feuchter Luft bei Raumtemperatur. *Zeitschrift für anorganische und allgemeine Chemie* **1951**, 264, (5-6), 249-254.

45. Schäfer, H., Gann, W., Untersuchungen am System Fe_2O_3-$FeCl_3$-H_2O-HCl VIII. Die Wasserdampfdrucke über Eisen(III)-Chlorid-Hydrat-Schmelzen. *Zeitschrift für anorganische und allgemeine Chemie* **1952**, 270, (5-6), 304-316.

46. Schäfer, H., Wittig, F. E., Jori, M., Untersuchungen am System Fe_2O_3-$FeCl_3$-H_2O-HCl IX. Die Thermochemische Beständigkeit des Eisenoxychlorids FeOCl. *Zeitschrift für anorganische und allgemeine Chemie* **1956**, 287, (1-2), 61-70.

47. Berlin-Lübecker-Maschinenfabriken, Kontinuierliche Produktion von Eisenoxychlorid. *Belg. Patent No. 452,131*, **1943**.

48. Marinovic-Cincovic, M., Wang, G., Fedoroff, M., Saponjic, Z., Vilonic, S., Nedeljkovic, J., Ferrioxychloride and Hematite Nanoparticles: Synthesis and Phase Transformation. *Materials Science Forum* **2006**, 63-66.

49. Peek, E. M. L., Chloride Pyrohydrolysis: Lixiviant Regeneration and Metal Separation. *PhD Thesis Delft University Press* **1995**.

50. Baerhold, F., Lebl, A., Statrcevic, J., Recovery of Metal Oxides and Associated Acid From Process Solutions Using Water as Reagent. *Iron Control Technologies,* Dutrizac, J., Riveros, P., Eds. CIM, Montreal, Canada, **2006**; Vol. 3, pp 789-803.

51. Kamal, A., Lee, C., Minimizing Fuel Costs During Thermal Regeneration of the Hydrochloric Acid Lixiviant. Hatch, Mississauga, Ontario, Canada.

52. Van Weert, G., Peek, E. M. L., Reagent Recovery in Chloride Hydrometallurgy - Some Missing Links. *Hydrometallurgy* **1992**, 29, (1-3), 513-526.

53. Adham, K., Lee, C., Small, D., Energy Consumption for Iron Chloride Pyrohydrolysis: A Comparison Between Fluidized Beds and Spray Roasters. *Iron Control Technologies*, Dutrizac, J., Riveros, P., Eds. CIM, Montreal, Canada, **2006**.

54. Harris, G. B., Magee, T. J., Lakshmanan, V. I., Sridhar, R., The Jaguar Nickel Inc. Sechol Laterite Project Atmospheric Chloride Leach Process. *International Laterite Nickel Symposium—2004*, Imrie, Ed. The Minerals, Metals and Materials Society: Warrendale, PA, USA, **2004**; pp 219-241.

55. Allen, C., Kondos, P., Payant, S., Van Weert, G., Van Sandwijk, A., Production of Zinc Oxide from Complex Sulphide Concentrates using Chloride Processing. *US Patent No. 6,395,242*, May 28, **2002**.

56. Girgin, S., Demopoulos, G. P., Production of the High Value Material, alpha-$CaSO_4$ Hemihydrate out of Spent $CaCl_2$ Solutions by Reaction with H_2SO_4. *EPD Congress 2004*, Schlesinger, M. E., Ed. TMS: Warrendale, PA, USA, **2004**; pp 627–639.

57. Al-Othman, A., Demopoulos, G. P., Gypsum Crystallization and Hydrochloric Acid Regeneration by Reaction of Calcium Chloride Solution with Sulfuric Acid. *Hydrometallurgy* **2009**, 96, (1-2), 95-102.

58. Moyes, A. J., The Intec Laterite Process. *ALTA Nickel/Cobalt 10*, Perth, Australia, **2005**.

59. Smit, J. T., Steyl, J. D. T., Leaching Process in the Presence of Hydrochloric Acid for the Recovery of a Value Metal from an Ore. *Int. Patent No. WO 2006/043158*, April 27, **2006**.

60. Brown, C. J., Olsen, D. R., Regeneration of Hydrochloric Acid Pickle Liquors by Crystallization, Dutrizac, J., Riveros, P., Eds. *Iron Control Technologies*, CIM, Montreal, Canada, **2006**; pp 831-843.

61. Connolly, D. W., Manufacture of Ferric Sulfate and Hydrochloric Acid from Ferrous Chloride. *US Patent No. 5,417,955*, May 23, **1995**.

62. Harris, G. B., White, C. W., Demopoulos, G. P., Iron Control in High Concentration Chloride Leach Processes. *3rd International Symposium on Iron Control in Hydrometallurgy*, Montreal, Canada, **2006**.

63. Burtch, J. W., The PORI Process. Regeneration of Hydrochloric Acid from Spent Pickle Liquor. *Wire Journal* **1976**, 9, (2), 57-59.

64. Burtch, J. W., PORI Hydrochloric Acid Regenaration Process. *SEASI Quarterly* **1973**, 2, (4), 52.

65. Harris, G. B., White, C., Demopoulos, G. P., Ballantyne, B., Recovery of Copper from a Massive Polymetallic Sulphide by High Concentration Chloride Leaching. *Proceedings of the Conference Copper - Cobre 2007*, *Hydrometallurgy of Copper*, CIM, Montreal, Canada, **2007**.

66. Harris, G. B., White, C., Ballantyne, B., Chloride Leaching of Polymetallic Massive Sulphide. *ALTA Copper 10*, Perth, Australia, **2006**.

67. Harris, G. B., White, C., Demopoulos, G. P., Ballantyne, B., Recovery of Copper from a Massive Polymetallic Sulphide by High Concentration Chloride Leaching. *Canadian Metallurgical Quarterly* **2008**, 3, (47).

68. Harris, G. B., A New Approach to the High Concentration Chloride Leaching of Nickel Laterites. *ALTA Nickel/Cobalt 11*, Perth, Australia, **2006**.

69. Demopoulos, G. P., Li, Z., Recovery of Hydrochloric Acid and Preparation of Hematite from Concentrated Magnesium Chloride Solutions II. *Hydrometallurgy Laboratory McGill University*: Montreal, **2006**.

70. Demopoulos, G. P., Li, Z., Recovery of Hydrochloric Acid and Preparation of Hematite from Concentrated Magnesium Chloride Solutions III. *Hydrometallurgy Laboratory McGill University*: Montreal, **2006**.

71. Harris, G. B., White, C., Process for Recovering Iron as Hematite from a Base Metal Containing Ore Material. *Int. Patent No. WO 2007/017020 A1*, June 28, **2006**.

72. Harris, G. B., White, C., Process for Recovering a Base Metal from a Sulfide Ore Material. *Int. Patent No. WO 2007/017021 A1*, June 28, **2006**.

73. Demopoulos, G. P., Becze, L., Study of Hematite Precipitation and Hydrochloric Acid Recovery from Magnesium Chloride Solution. *Hydrometallurgy Laboratory McGill University*: Montreal, **2007**.

74. Baldwin, S. A., Cheng, T. C., Demopoulos, G. P., A contribution to the Measurement of Oxygen Mass Transfer in a Laboratory Pressure Reactor. *Journal of Chemical Technology & Biotechnology* **2000**, 75, (8), 665-672.

75. Demopoulos, G. P., Moldoveanu, G., Recovery of Hydrochloric Acid and Preparation of Hematite from Concentrated Magnesium Chloride Solutions I. *Hydrometallurgy Laboratory McGill University*: Montreal, **2006**.

76. Faria, D. L. A., Venâncio Silva, S., Oliveira, M. T., Raman Microspectroscopy of some Iron Oxides and Oxyhydroxides. *Journal of Raman Spectroscopy* **1997**, 28, (11), 873-878.

77. http://www.jtbaker.com/msds/englishhtml/f1080.htm, Material Safety Data Sheet $FeCl_3$. (**13.04.2009**),

78. Kanungo, S. B., Mishra, S. K., Thermal Dehydration and Decomposition of $FeCl_3 \cdot 6H_2O$. *Journal of Thermal Analysis* **1996**, 46, 1487-1500.

Appendix I: The $FeCl_3 \cdot nH_2O$-FeOOH-Fe_2O_3 System

I.1 Introduction

In this Appendix, the results of an auxiliary study on the mechanism of thermal decomposition of hydrated ferric chloride crystals (no aqueous solutions were used here) are described. The work involved the production of FeOCl via the thermal decomposition of $FeCl_3 \cdot nH_2O$ and the investigation of the reaction of FeOCl with water that led sequentially to transformation to FeOOH and Fe_2O_3.

I.2 Transformation of $FeCl_3 \cdot nH_2O$ to FeOCl

FeOCl was synthesized according to the procedure in section 3.2.2. A mould filled with $FeCl_3 \cdot 6H_2O$ solids (lumps) was placed into a pre-heated oven at 100ºC. After one hour the picture was taken shown in Figure I.1:

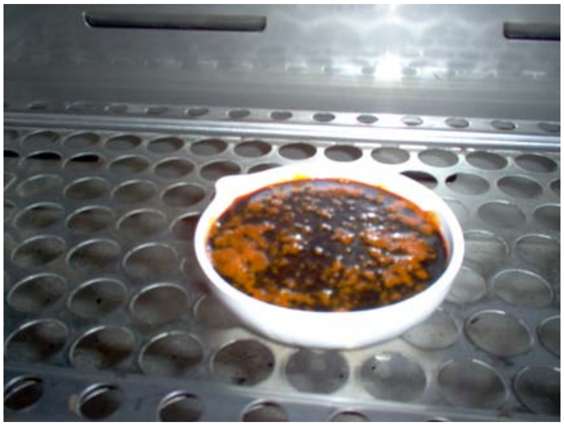

Figure I.1: Picture Showing the Molten $FeCl_3 \cdot 6H_2O$ (l) after 1h Retention Time.

At this point, the salt had become liquid with no HCl or water vapour yet released. It took several hours to transform the ferric chloride salt into iron oxychloride. Table I.1 summarizes the collected data in terms of weight loss over time. It can be seen, that after about 15 hours heating, the salt had lost about one third of its mass. The material was still liquid at this time. It started to partially solidify as black needles after 25 hours and had thus to be stirred with a spatula from time to time. Simultaneously the pungent odour of gaseous hydrogen chloride could be smelled pointing to conversion of $FeCl_3 \cdot nH_2O$ to FeOCl and HCl (g) as per Equation I.1:

$$FeCl_3 \cdot 6H_2O\ (l) \longrightarrow FeOCl\ (s) + 2\ HCl\ (g) + 5\ H_2O\ (g) \qquad (I.1)$$

It is conceivable that the hexahydrate loses some water (6<n≤1) before in situ hydrolysis leads to FeOCl formation. The conversion of $FeCl_3 \cdot 6H_2O$ to FeOCl can be described in Equation I.2:

$$FeCl_3 \cdot H_2O\ (l) \longrightarrow FeOCl\ (s) + 2\ HCl\ (g) \qquad (I.2)$$

As it was difficult to elucidate/identify the exact reaction step sequence it may be tentatively assumed that at least in the intermediate reaction period a mixture of iron oxychloride product and molten liquid $FeCl_3 \cdot xH_2O$ salt coexist.

Table I.1: Weight Loss of the Ferric Chloride salt during the Transformation to Iron Oxychloride.

Time (h)	**Weight (g)**	**Weight loss (%)**	**Phase**
0	90	0	$FeCl_3 \cdot 6H_2O(s)$
15.75	60.10	33.22	*
20.75	54.54	39.4	*
25.43	50.03	44.41	*
42	35.88	60.13	*
44	35.66	60.37	FeOCl(s)

* The exact formula cannot be determined since water vapor and hydrogen chloride gas escaped simultaneously the reactor

The experiment ended after 44 hours, when the product in the mould was fully solidified. It had a black appearance. However, after crushing the sample gently with a spatula, it turned to a crystalline brown powder (Figure I.2). The final ground product is seen in Figure I.3.

Figure I.2: Picture of the Solid Phase (FeOCl) obtained after 44 h Heat Treatment at 100 ^{o}C (Note: The picture on the Right was taken after Agitating the solid with a Spatula).

Figure I.3: Thermal Composition Product (FeOCl) after Grinding.

I.3 Characterization of FeOCl

The weight loss of 60.37% that was measured after 44 hours heating (Table I.1) corresponds exactly to the theoretical weight loss (60.30%) of HCl and water predicted by Equation I.1. This was the first indication that the obtained product was FeOCl. This was confirmed by XRD analysis (Figure I.4) and determination of the products %Cl content via digestion in HNO_3 and precipitation as AgCl. The latter analysis gave with only 2% deviation the expected theoretical value for the chloride content in FeOCl. An SEM image of the FeOCl product can be seen in Figure I.5.

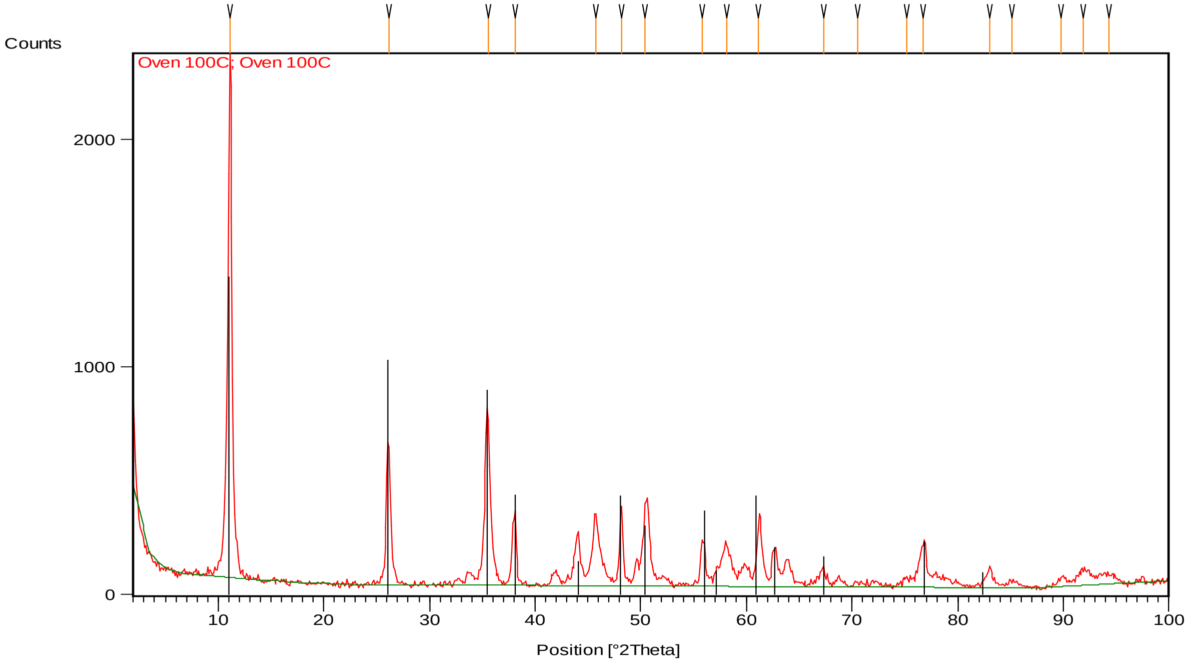

Figure I.4: XRD Pattern of the FeOCl product (Ref. code: 00-024-1005).

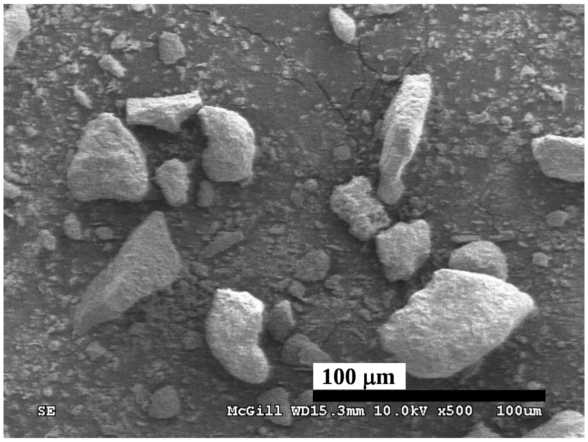

FigureI.5: VP SEM Image of the Produced FeOCl.

I.4 Transformation of FeOCl to FeOOH and Fe_2O_3

The transformation of FeOCl to FeOOH and later to Fe_2O_3 is investigated, and the results are discussed in this section.

Transformation of FeOCl (s) to FeOOH (s): To further investigate the system, a sample of the provided iron oxychloride was placed in a beaker with water and the whole slurry heated to 100ºC for 2 hours in the oven. As the picture in Figure I.6 illustrates a reaction of the FeOCl (s) with took place that led to precipitation of β-FeOOH.

Figure I.6: Hydrothermal Transformation of FeOCl to β-FeOOH after 2 Hours Heating at 100ºC.

Upon filtration and drying over night at 50ºC, the obtained solid product was characterized by XRD and identified as β-FeOOH (Figure I.7).

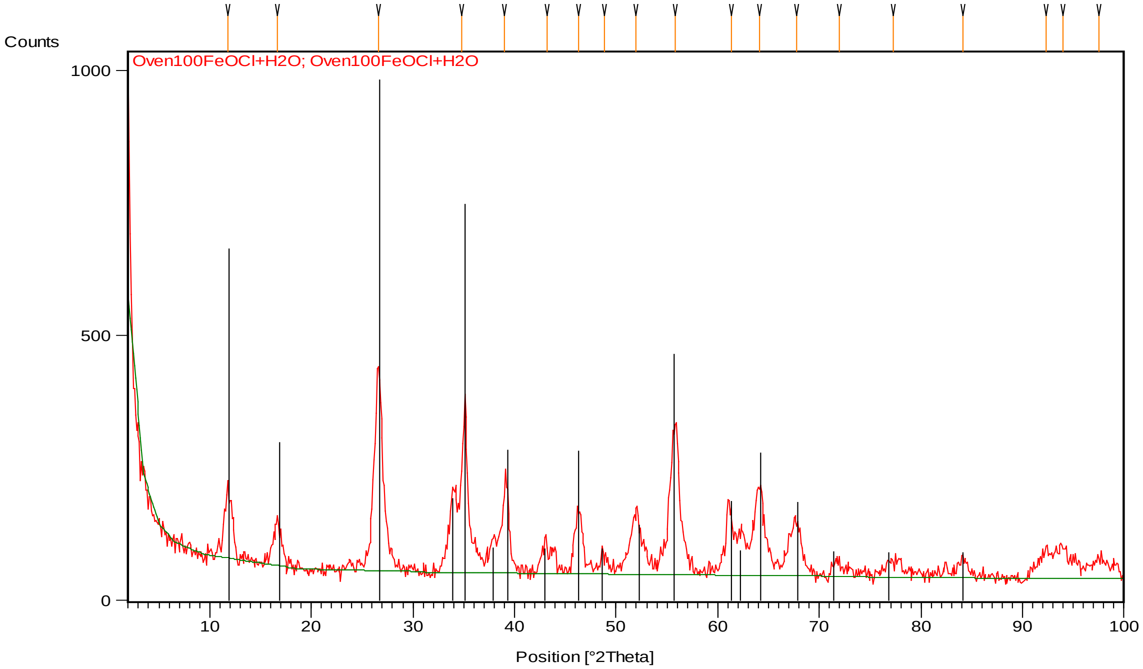

Figure I.7: XRD Pattern of the Obtained Tranformation Product (β-FeOOH) (Ref. 00-001-0662).

The hydrothermal conversion of iron oxychloride to iron oxy-hydroxide may be represented by Equation I.3.

$$3\ FeOCl\ (s) + H_2O\ (l) \longrightarrow 2\ FeOOH\ (s) + FeCl_3\ (aq) \qquad (I.3)$$

$$FeOCl\ (s) + H_2O\ (l) \longrightarrow FeOOH\ (s) + HCl\ (aq) \qquad (I.4)$$

Alternatively Equation I.4 may take place as proposed by *Kanungo* and *Mishra* [78]. No attempt was made to analyze the solution and verify which of the two occurs as it was beyond the scope of this work.

Transformation of FeOOH to Fe_2O_3: FeOOH (s) is not stable above 150ºC. After heating the phase in the oven, it transformed to hematite and water vapor according to the following equation:

$$2\ FeOOH\ (s) \longrightarrow Fe_2O_3\ (s) + H_2O\ (g) \qquad (I.5)$$

Appendix II: Hydrolytic Distillation of $FeCl_3$ Solutions-Supplementary Data

This Appendix contains additional information on a number of experiments that have been conducted during the investigation of the ferric chloride system.

Experiment – RT40

Purpose and Conditions of the Experiment: Experiment RT 40 was the first experiment without $MgCl_2$ in the reactor. It was kept out of the solution to investigate just the ferric chloride system and the PORI process. The reactor was fed with a 1.97 mol/L ferric chloride solution and 0.07 mol/L ferrous chloride. The speed of agitation was 300 rpm.

Characterization: The solid products were characterized by XRD and Raman, the slurry by particle size analysis. The iron content of the condensates and the filtrates was analyzed by ICP.

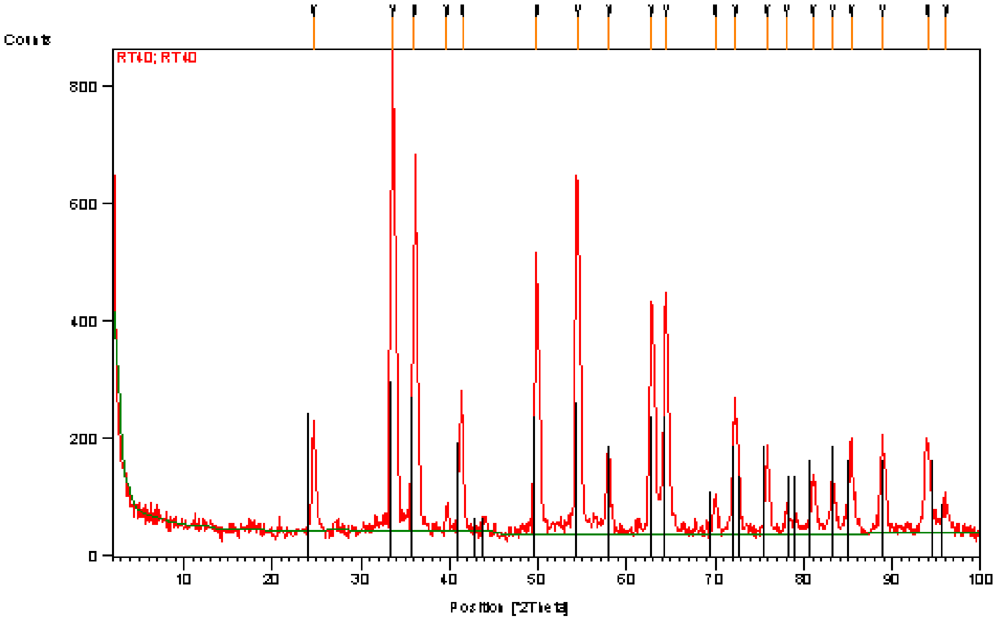

Figure II.1: XRD-Pattern of RT40.

The XRD pattern (Figure II.1) shows the formation of hematite as the main product as it does Raman spectroscopy of Figure II.2.

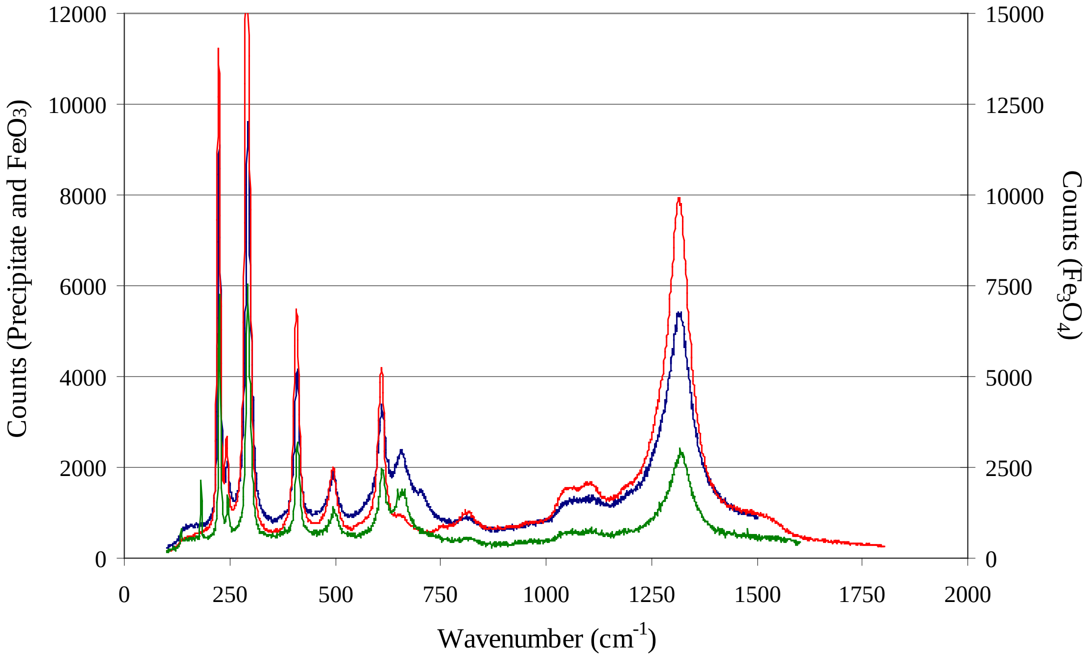

Figure II.2: Raman of RT40 Compared to Those of Hematite as Magnetite References.

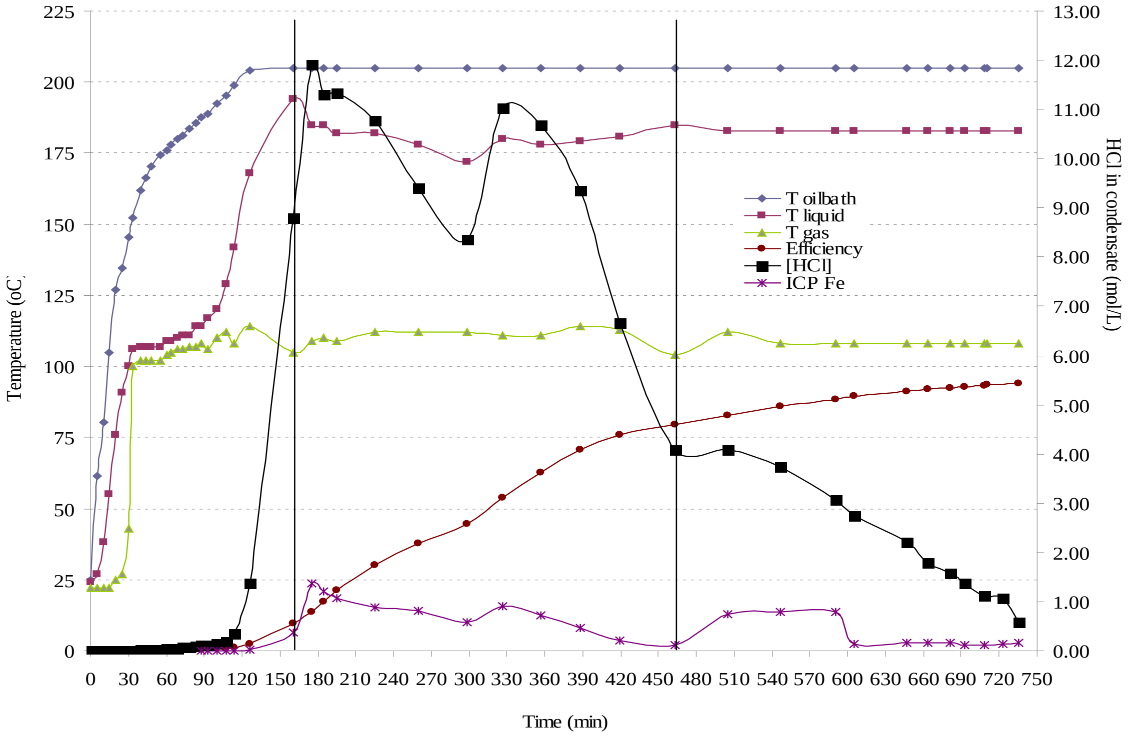

Figure II.3: Reaction Profile of Experiment RT40.

Reaction Profile: Figure II.3 shows the reaction profile, containing all the data that has been collected during the experiment. The highest temperature of the oil bath was 205ºC. The vertical lines indicate the time when the peristaltic pump for the water addition has been switched on or off. During the first 160 min, the evaporation of 850 mL water took place. Then the concentrated HCl (up to 12 M) started to flash off. It should be noted, that at the same time, the highest value for iron in the condensate was measured by ICP. The condensates were collected and water was added simultaneously at about 1.3 mL per minute. After reaching the 12 M HCl level, the acid concentration of the condensate started to go down. This is because the reactor content started to solidify. The second elevation of the acid concentration is due to a solid-liquid reaction which has to be further investigated. The overall efficiency was 93% for the HCl recovery. The total yield of solids was 74%. The balance (~25%) of the precipitate was in the form of scale.

Experiment – RT41

Purpose and Conditions of the Experiment: This Experiment was basically a repetition of experiment RT40. The only difference was that ferrous chloride was left out in the initial solution. It consisted just of 360 g/L (1.97 mol/L) ferric chloride.

Characterization: The XRD in Figure II.4 shows stronger reflexes for hematite than Figure II.3.

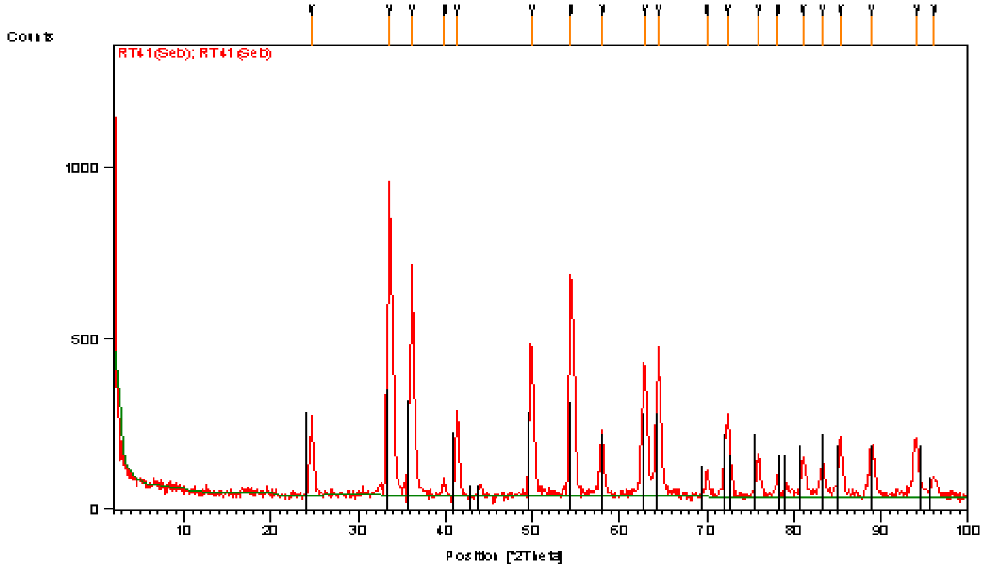

Figure II.4: XRD-Pattern of RT41.

The following picture shows the particle size distribution of the solids for experiment RT41. The particle size distribution has two maxima. This could indicate the presence of at least two different reaction mechanisms taking place. Moreover, the picture shows a relatively high particle size for the precipitates. As a consequence the filtration time for the solids was very short, under one hour.

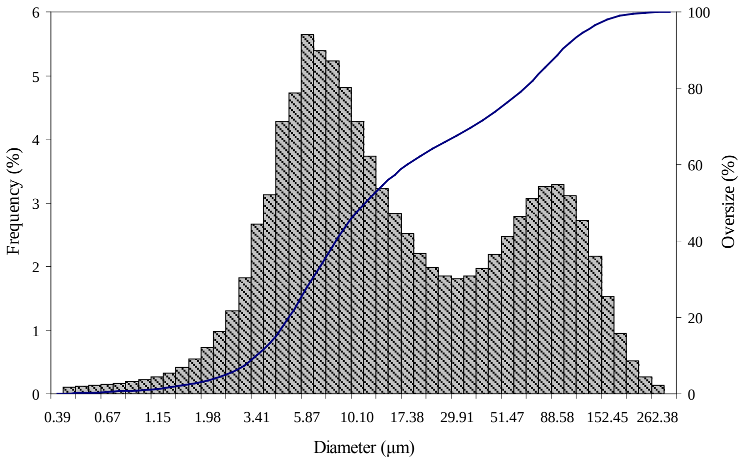

Figure II.5: Particle Size Distribution of RT41.

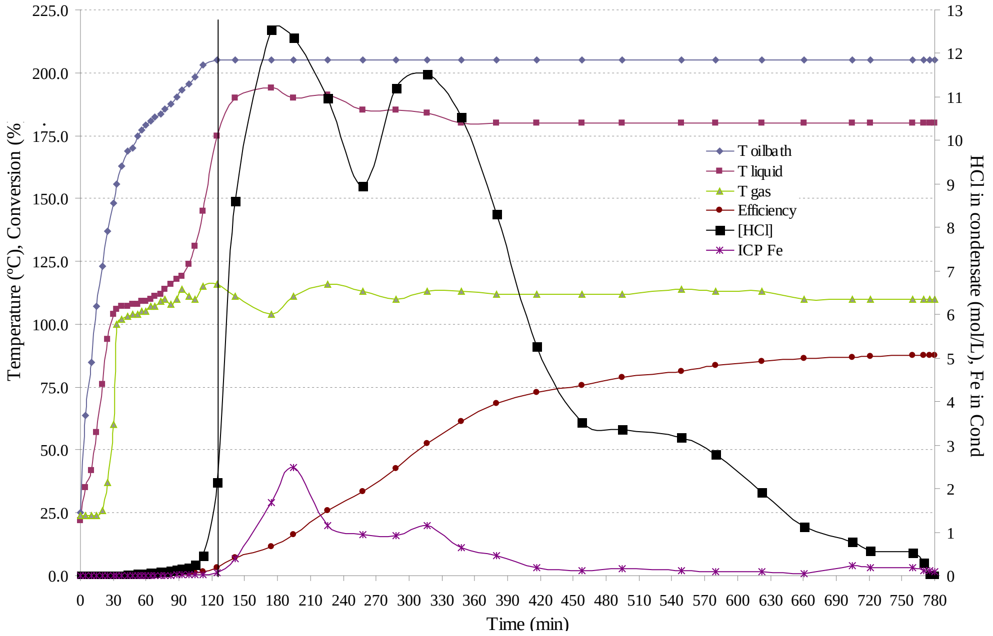

Figure II.6: Reaction Profile of Experiment RT41.

A detailed description of this Experiment can be found in section 5.3.1

Experiment – RT42

Purpose and Conditions of the Experiment: This experiment was conducted at higher water addition rate (2.3 ml/min) as an effort to avoid the problems encountered with tests RT40 and RT41. Moreover, the iron concentration was increased to 172 g/L (3 mol/L). The speed of agitation was elevated to 375rpm.

Results and Discussion: The higher flow rate for the water addition had a deep impact on the reaction profile. A higher efficiency could be reached in a much shorter period of time than in experiment RT41. The concentration of HCl in the condensate could be kept over 8 M for more than five hours and 800 mL condensate was collected. After having transformed almost all the ferric chloride, the concentration of the acid in the condensate dropped and the reaction was stopped. A detailed discussion of this experiment can be found in section 5.1. Figure II.7 serves to demonstrate the correlation between HCl strength and iron contamination found in the condensate.

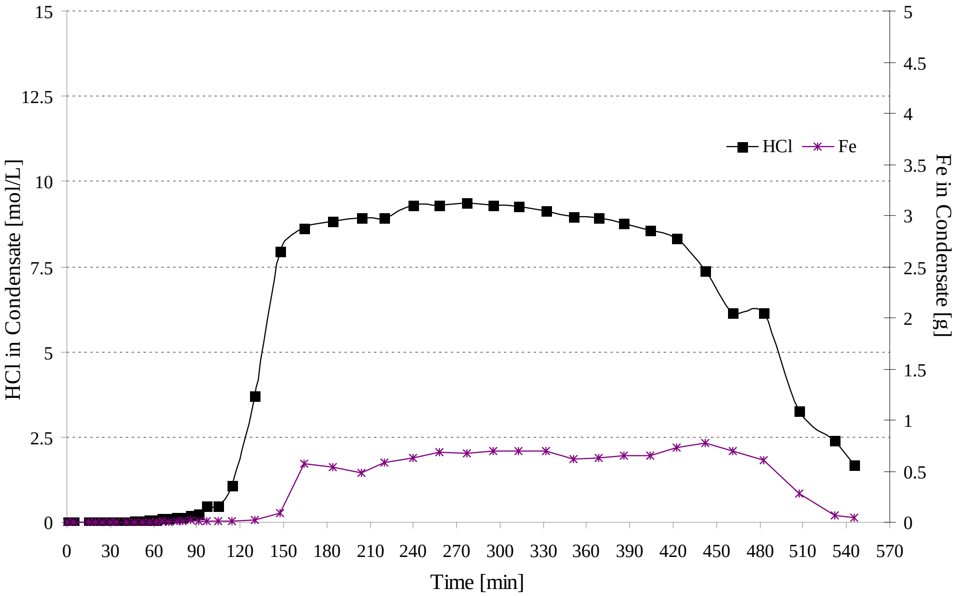

Figure II.7: Iron and HCl Concentration-Time Profiles (RT42: Initial $FeCl_3$ concentration 3.08 M, Water Flow Rate 2.3 mL/min).

Experiment – RT43

Purpose and Conditions of the Experiment: In addition to the data presented and discussed in section 5.3.4 the iron and HCl concentration profiles in the condensate are given in Figure II.8

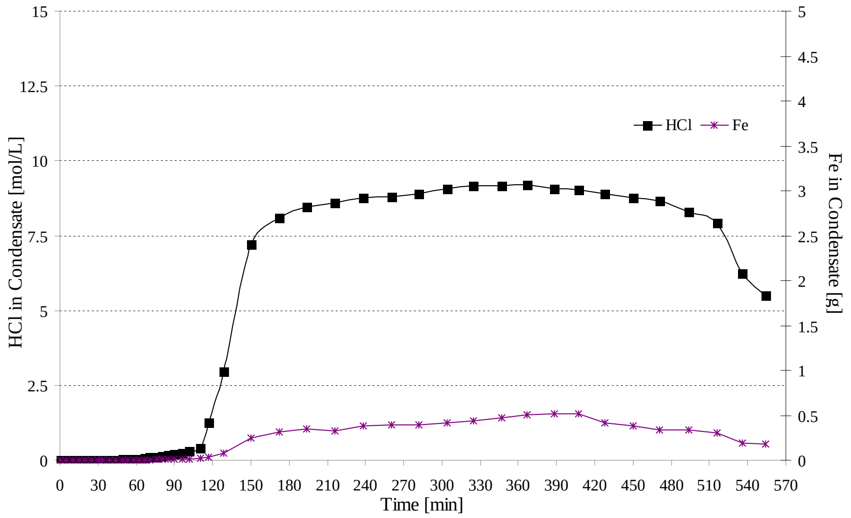

Figure II.8: Iron and HCl Concentration-Time Profiles (RT43: Initial $FeCl_3$ concentration 1.97 M, Feed Flow Rate 2 mL/min).

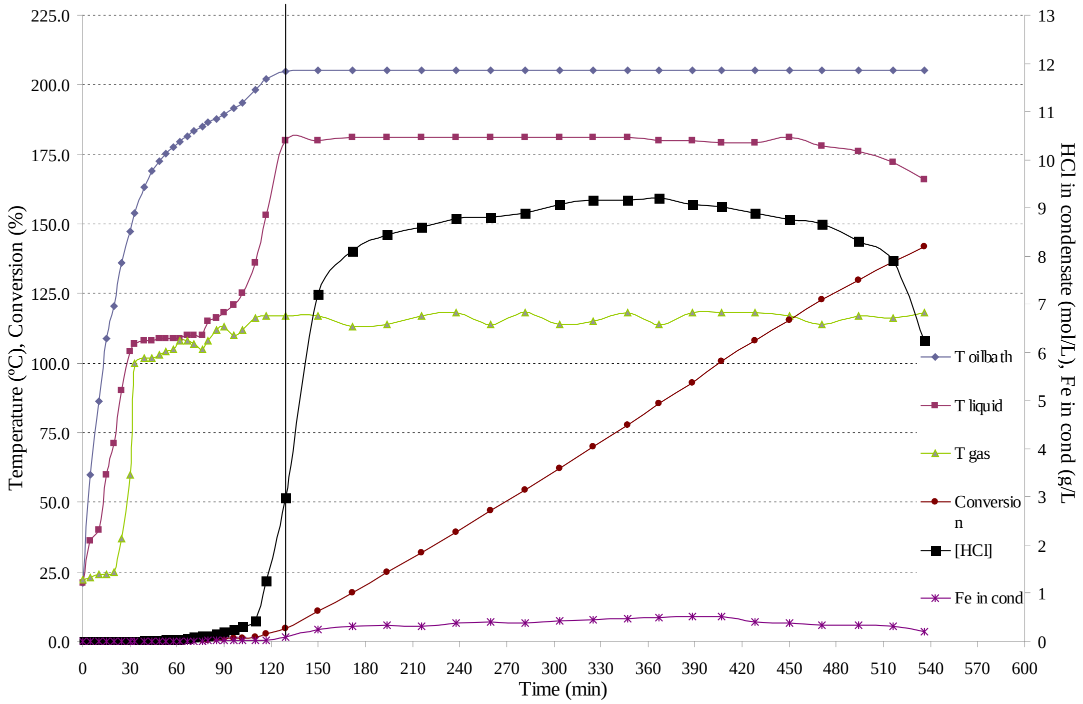

Figure II.9: Reaction Profile of Experiment RT43.

Experiment – RT44

Purpose and Conditions of the Experiment: This experiment was a repetition of experiment RT 43 (see also 5.3.4), i.e. the second trial of a hydrolytic distillation involving continuous addition of feed solution. The only difference was that this time a faster feed addition speed (about 3 mL/min) was investigated.

Results and Discussion: The higher flow rate of the feed addition (indicated by the first line in Figure II.10) lead to a drop in the acid concentration. Thus, the feed addition was slowed down (second line). Immediately the acid concentration rose, but could not remain stable for a longer period of time (as in 5.3.4). This suggests that the system can be easily disturbed. However, the conversion was 100% for the initial solution in the reactor and about 160% total conversion (with reference to initial solution) when the added feed is considered.

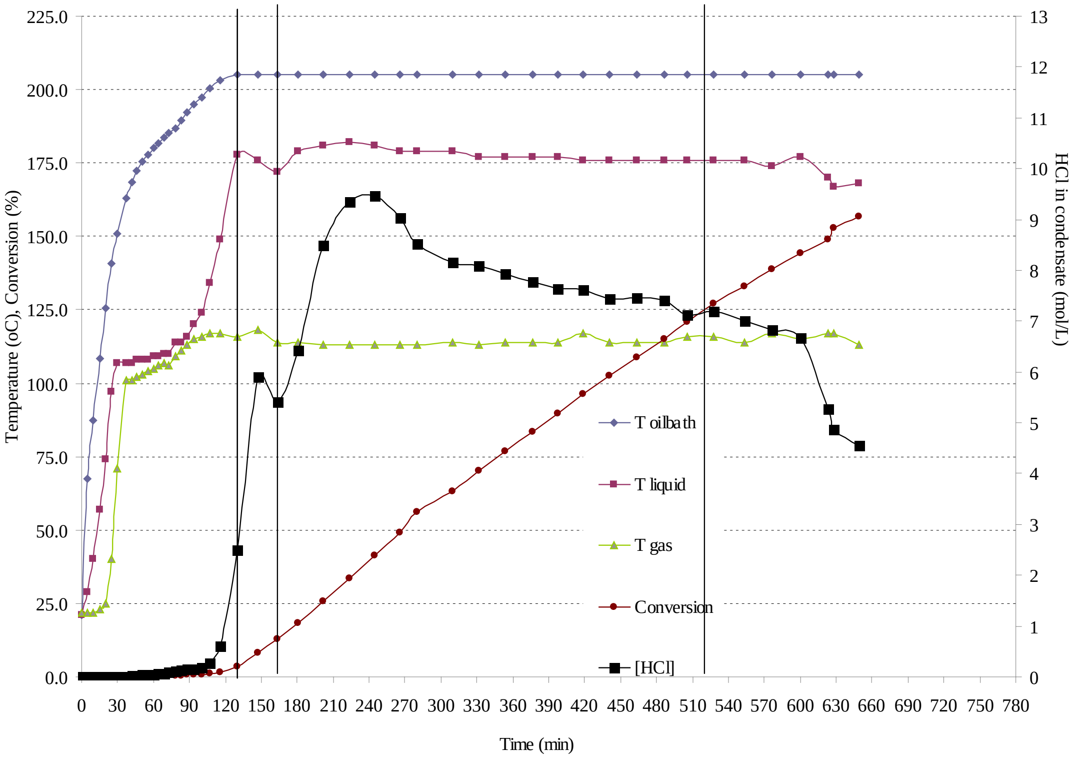

Figure II.10: Reaction Profile of Experiment RT44.

Experiment – RT45

Purpose and Conditions of the Experiment: In this a higher initial concentration of the ferric chloride solution was investigated. By dissolving 316.7 g iron (III) as 1533 g $FeCl_3 \cdot 6H_2O$ (or 5.67 mol/L) into water, the saturation point at room temperature could be reached. The results can be viewed in section 5.3.2.

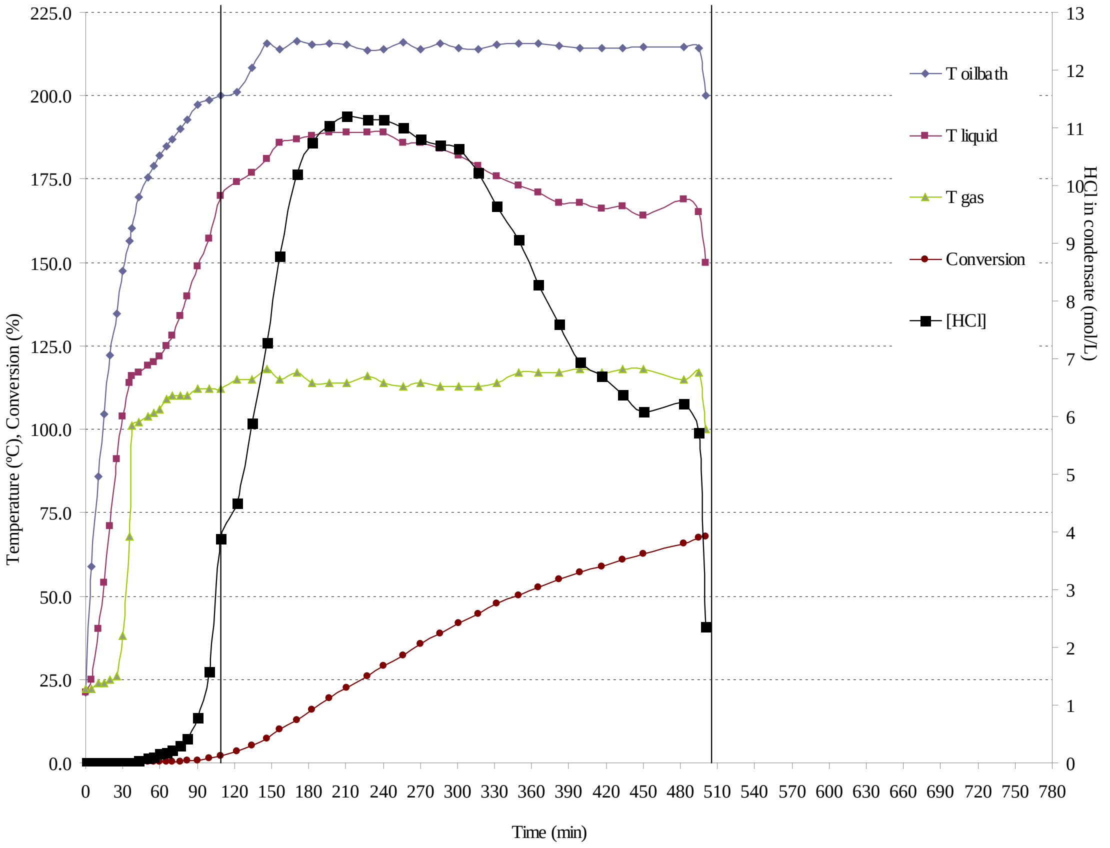

Figure II.11: Reaction Profile of Experiment RT45.

Experiment – RT48

Purpose and Conditions of the Experiment: This experiment was conducted to investigate the solution composition inside the reactor when hydrochloric acid starts to flash off. For a detailed discussion refer to 5.5.1.

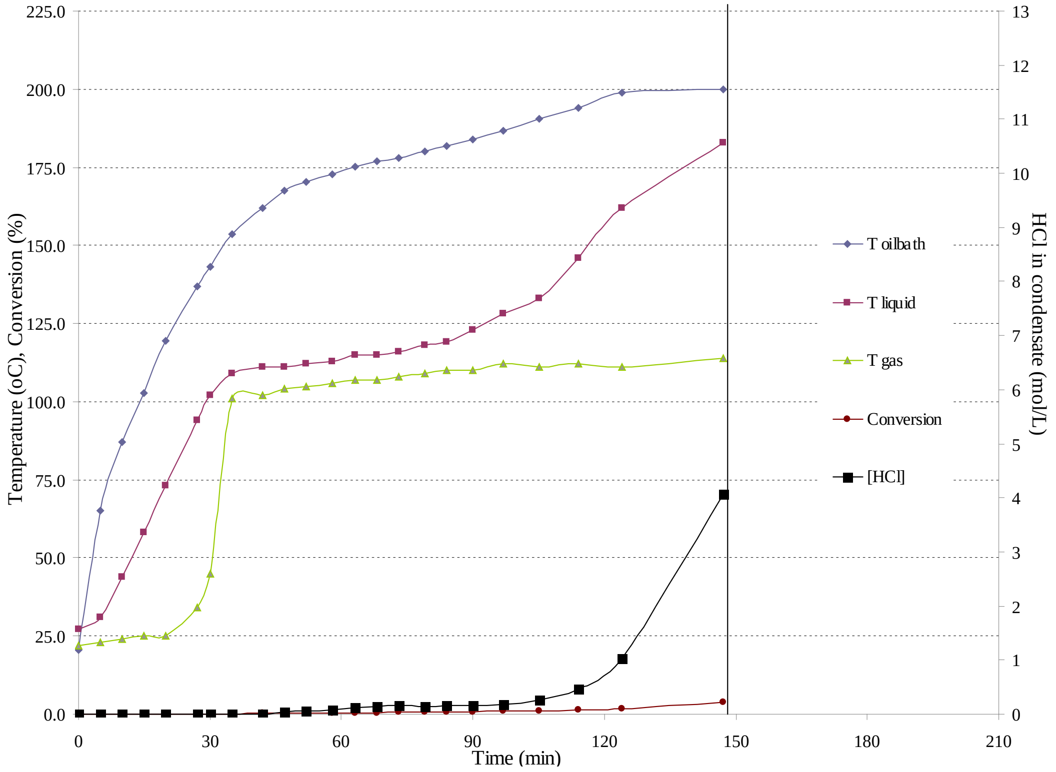

Figure II.12: Reaction Profile of Experiment RT48.

Experiment – RT49

Purpose and Conditions of the Experiment: This experiment was a repetition of experiment RT 42 and is further discussed in sections 5.3.1 and 5.3.3.

Appendix III: Hydrolytic Distillation of $FeCl_3$-$MgCl_2$ Solutions

As discussed in section 2.5.4 the initial hydrolytic distillation work involved iron-containing $MgCl_2$ solutions. The author at the early stages of his involvement with this project had the opportunity to conduct a few experiments with this system. The results from these tests are summarized in this Appendix.

III.1 Reaction Profiles

Experiment RT36: Figure III.1 shows the typical reaction profile for a hydrolytic distillation test involving magnesium chloride in the system (RT36).

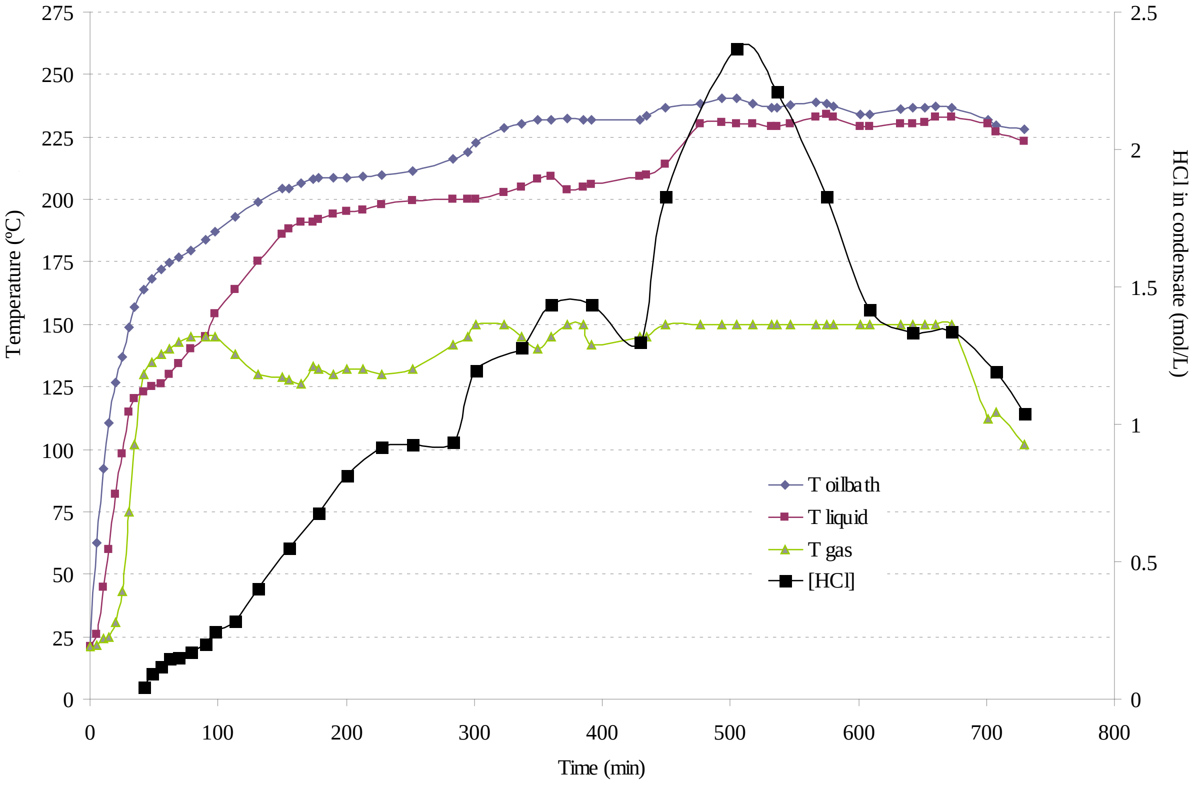

Figure III.1: Reaction profile of the $MgCl_2$-$FeCl_3$-H_2O system (RT36). (Initial Solution Composition 0.54 M $FeCl_3$-3.7 M $MgCl_2$; Water Addition Rate 1 mL/min).

The starting solution was almost saturated with magnesium chloride (3.7 mol/L = 360 g $MgCl_2$) and contained 30g/L (0.54 M) Fe(III) as ferric chloride. The reaction temperature was kept between 200 and 230ºC which is relatively high compared to 180ºC for pure ferric chloride solutions. In this experiment the highest acid strength that could be obtained was 2.3 molar (RT36) and clearly not satisfactory. It was hypothesized that due to the high amount of deposits on the walls, mostly caused by $MgCl_2$-crystallization, no constant reaction conditions could be obtained. Hence the acidic strength of HCl never reached a plateau but rather peaked, and fell afterwards.

Experiment RT38: Figure III.2 shows the temperature and HCl concentration profile during the reaction. The discussion that follows helps to illustrate the difficulties associated with the $FeCl_3$-$MgCl_2$ system which eventually led to the decision to remove $MgCl_2$ from the system and focus on $FeCl_3$ alone (refer to chapter 5).

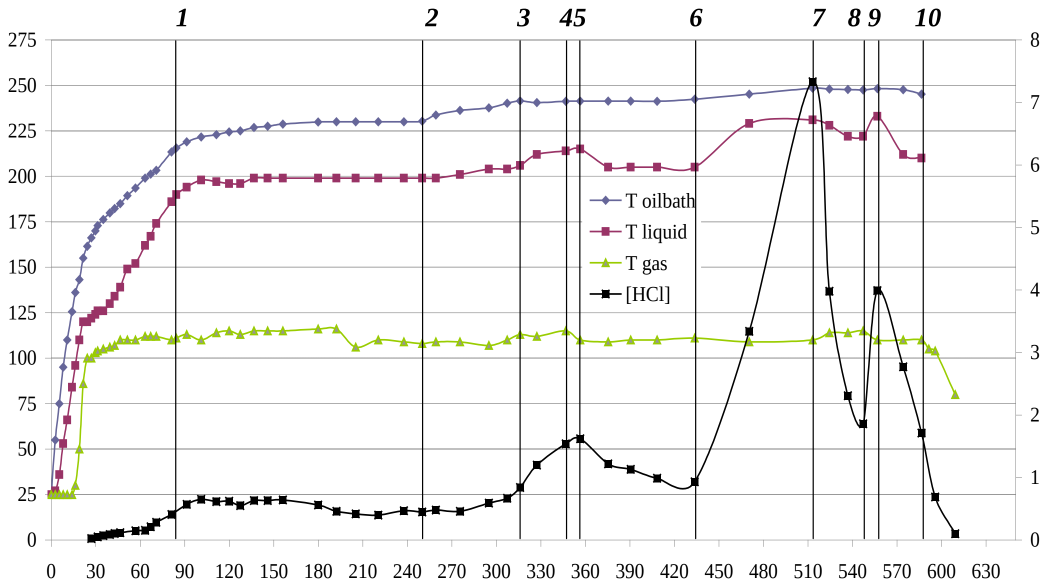

Figure III.2: Temperature and HCl Concentration vs. Time for Experiment RT38. (Initial Solution Composition: 0.54 M $FeCl_3$, 3.7 M $MgCl_2$; Water Addition Rate 1mL/min).

In this experiment an impeller with bigger blades than used in RT36 was employed so more intense mixing could be achieved. Furthermore, the oil bath was replaced by a new one with a higher flow rate. The system was ensured to be leak-proof, be applying Teflon plugs, clamps, gaskets and grease. The insulation was improved with new insulation tape and aluminum foil.

The numbers of Figure III.2 refer to several operations performed during the experiment:

1 after 81 minutes, 190ºC was reached and the addition of water (1 mL/min) began. The temperature rose until 199ºC. Then it remained constant.

2 after 250 minutes, the temperature of the oil bath was set to 250ºC, because no significant change in the reaction profile could be observed.

3 after 316 minutes, the impeller was stopped, because the reaction mixture was solid, and the impeller just moved above it, hindering the water dropping on the salt surface.

4 after 347 minutes, the reactor was opened and a sample of the solid was taken.

5 after 356 minutes, the water inlet was switched with the position of the thermometers’. This was necessary to figure out, if there is a “leaching effect” on the solid salt.

6 after 434 minutes, the water inflow was stopped, because the HCl concentration did not change significantly. Having done this, the distillate turned more and more to an intensive yellow greenish extract. It took much longer to get a sample than before.

7 after 513 minutes, the highest acidity (7.5 M) of the condensate could be obtained. It was hypothesized that the higher than azeotropic strength HCl collected might have been due to production of chlorine that followed HCl in the condensate. This could also have explained the color of the solution. However the presence of chlorine could not be substantiated. After no more condensate left the condenser, the water was turned on again. Immediately, the acidity concentration of the condensate decreased.

8 after 547 minutes, the water inlet was stopped again. After several minutes the acidity of the condensate increased again.

9 after 557 minutes, the water inflow was switched to its old position and turned on again. The concentration again decreased.

10 The water inflow was set to about 100 mL/min after 587 minutes to stop the reaction. The mixture was stirred over night and filtered two days later. The first filtration took

4 days, then the filtration cake was washed with 1L deionised water and filtered again. This filtration took more than 10 days.

The titration showed that 44.9g HCl were obtained. This translates to 76% HCl recovery.

Experiment RT46–$MgCl_2$ Alone: It is highly likely that the HCl did not only come from hydrolytic decomposition of ferric chloride but also from decomposition of $MgCl_2$ with water. To investigate this hypothesis, a pure aqueous solution of $MgCl_2$ was heated (RT46) presented in Figure III.3.

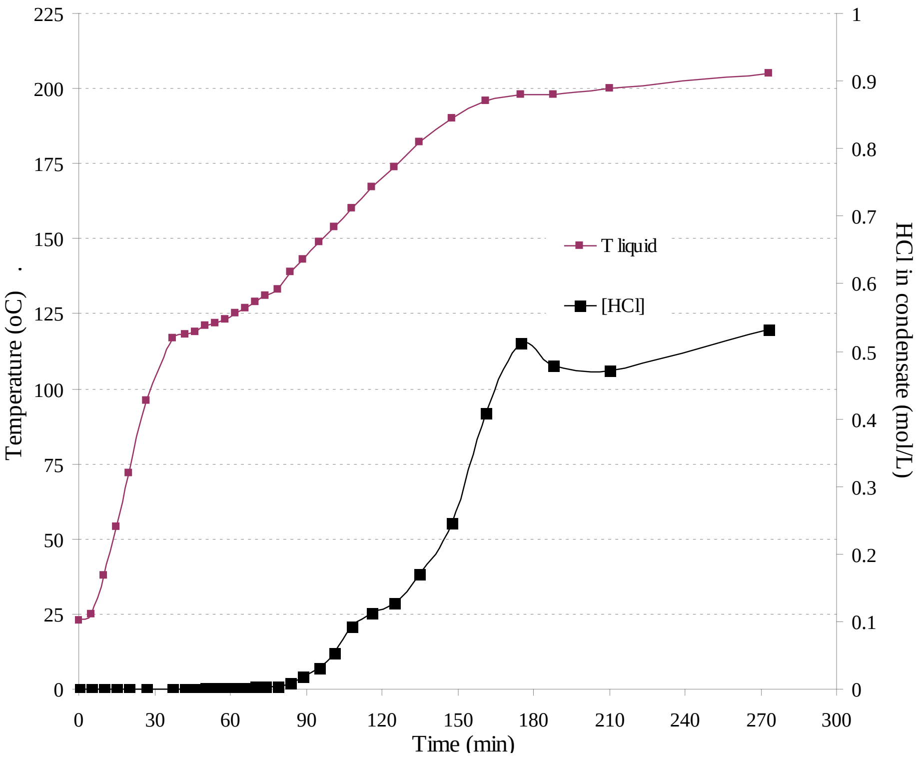

Figure III.3: Evolution of Hydrochloric Acid of Heated 3.7 M Aqueous $MgCl_2$-Solution (RT46).

As it can be seen a weak HCl acid condensate (0.5 mol/L) was produced. This suggests that magnesium chloride reacts with water to form hydrochloric acid and magnesium hydroxychloride according to the following equation:

$$MgCl_2\,(s) + H_2O\,(l,g) \longrightarrow MgCl(OH)\,(s) + HCl\,(g) \qquad (III.1)$$

Figure III.4 shows the solution transformation during the reaction. When a temperature of about 210ºC was reached inside the reactor, the magnesium salt started to crystallize. Within 30 minutes, the reactor was full of solids and the reaction had to be stopped. No water was added in this case.

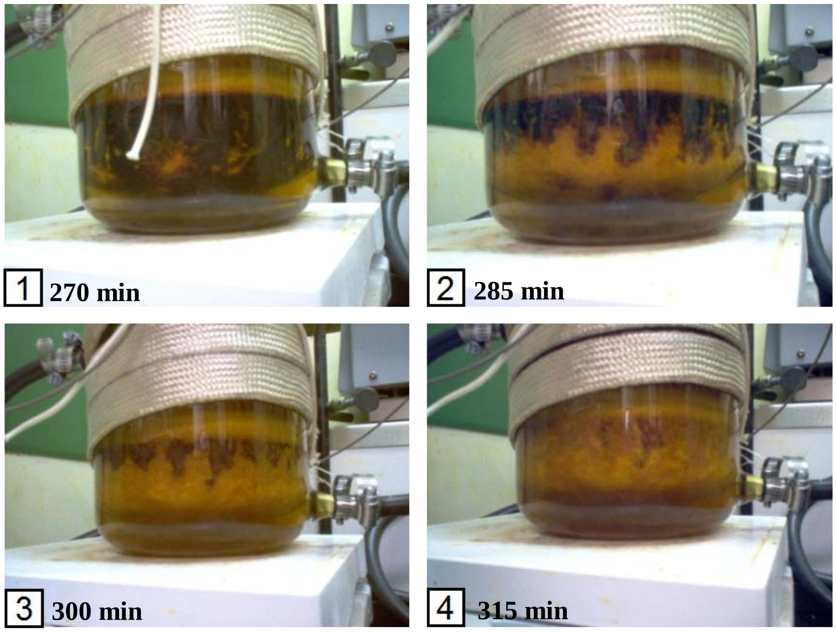

Figure III.4: Monitoring of the Transformation of a $FeCl_3$-$MgCl_2$ Solution (at 198-200ºC) (RT36).

Figure III.5 shows the scale formation in the reactor after removing the soluble contents by water leaching.

Figure III.5: Scale formation inside the reactor (RT38).

III.2 Precipitate Characterization

A typical iron oxide precipitate (Figure III.6) obtained from the hydrolytic distillation experiments involving $MgCl_2$-$FeCl_3$ Solutions (RT38) was characterized using various methods. As explained in the previous section the final slurry was very difficult to filter (>4days) and wash pointing to very fine particle characteristics. This was verified by particle size analysis (Figure III.7). Furthermore, BET analysis yielded a specific area of 108.4 m^2/g which is one order of magnitude larger than that of the iron oxide produced in the absence of $MgCl_2$ –refer to chapter 5. Moreover its red-brown color (Figure III.6) is another indication of its ultrafine size.

Figure III.6: Picture of the Hydro-Hematite Product (RT38).

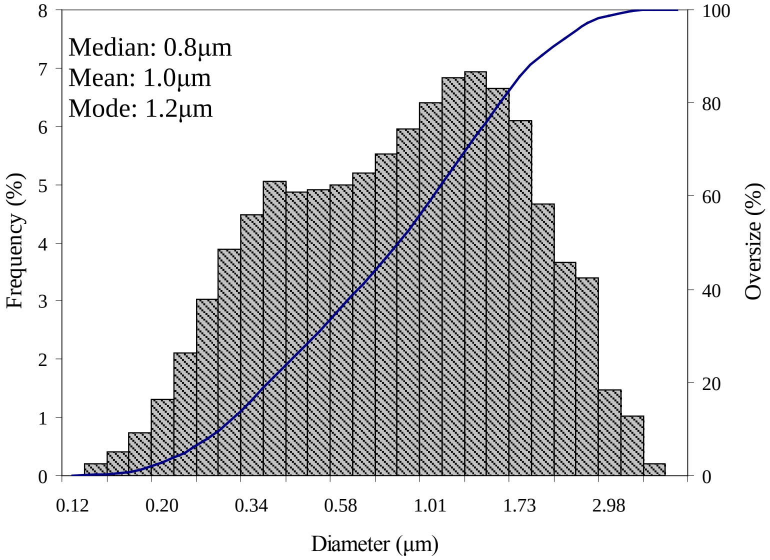

Figure III.7: Particle size distribution for the precipitate of the $MgCl_2$-$FeCl_3$-H_2O system (RT38).

An SEM picture of the precipitate is shown in Figure III.8.

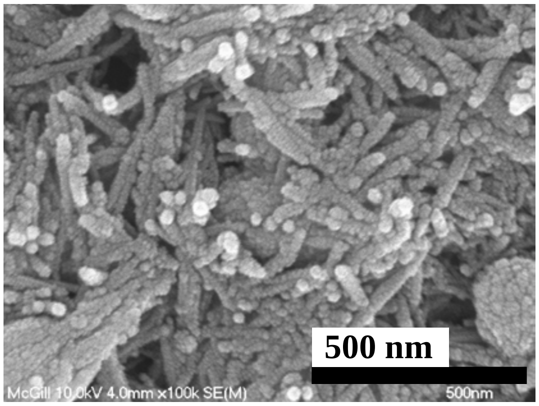

Figure III.8: VP-SEM picture for the precipitate of the $MgCl_2$-$FeCl_3$-H_2O system x100,000 (RT38).

It is highly likely that the ultra fine particle size is due to the magnesium salt matrix which interferes with the particle growth mechanism. In contrast the product from the $MgCl_2$-free system (chapter 5) had coarse particle size (~42 µm).

Raman spectroscopy (in addition to XRD-analysis) confirmed the product to be hematite (refer to Figure III.9). There was evidence of a trace amount of magnetite [76].

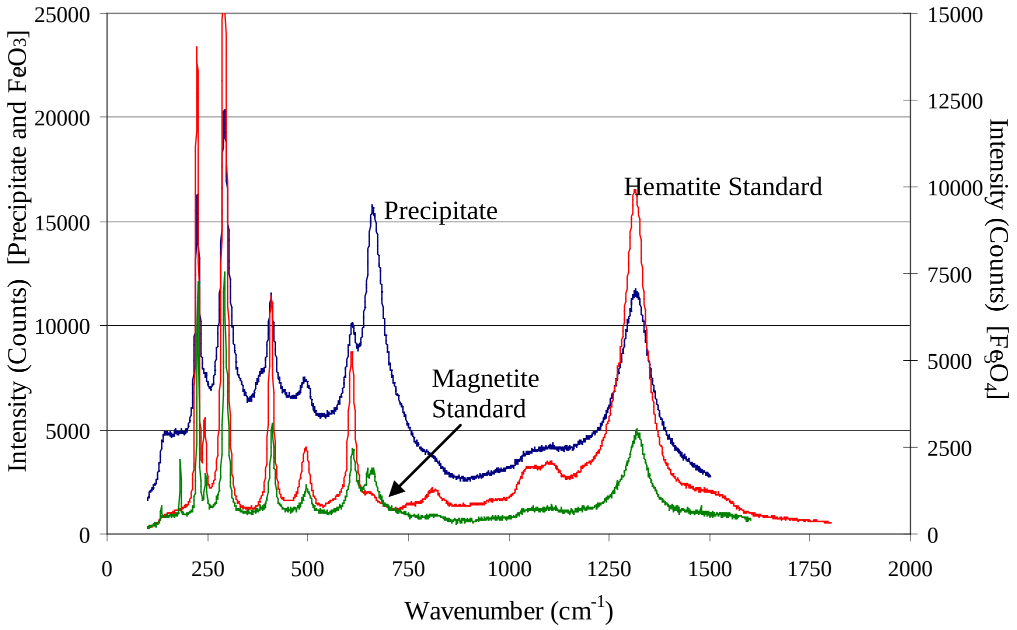

Figure III.9: Raman Spectrum of the Precipitate from the $MgCl_2$-$FeCl_3$-H_2O System and References.

Chemical analysis by digestion and ICP found the product to be highly contaminated containing only 55% iron compared to 70% theoretical iron content in pure Fe_2O_3.

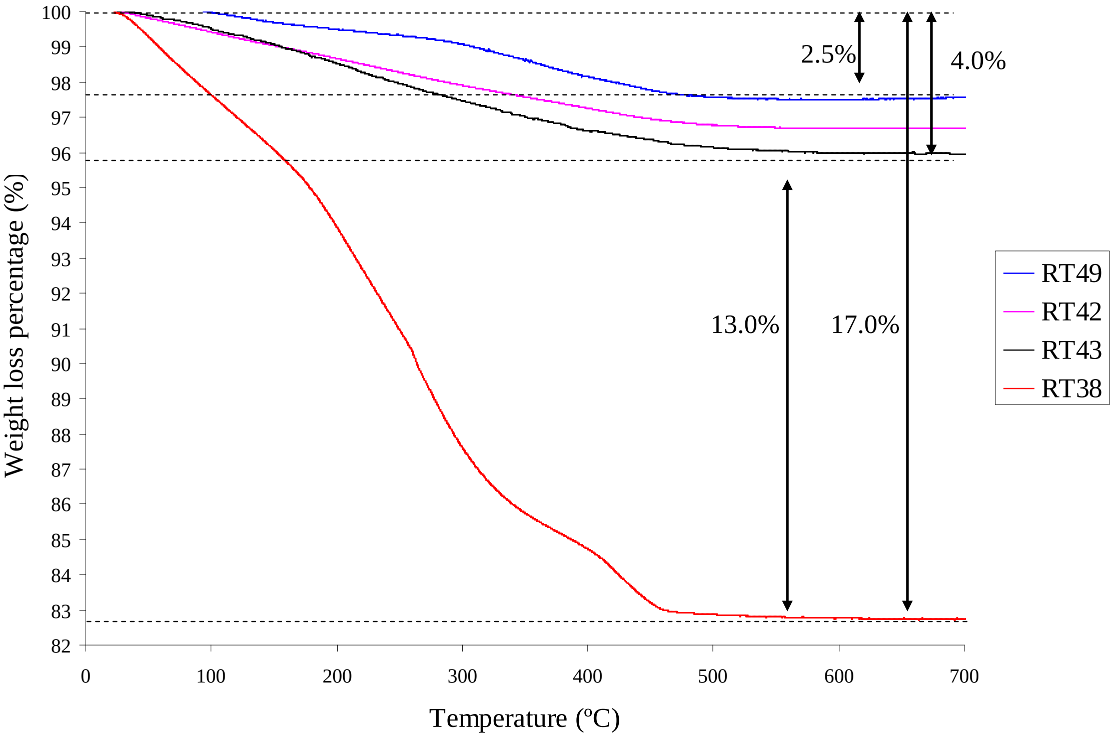

Figure III.10: TGA of Iron Oxide Precipitates with (RT38) and without (RT42-RT49) Magnesium Chloride Matrix; Heating Rate 10˚C/min.

TGA analysis revealed an unusual high content of water in the precipitated hematite product compared with other experiments (refer to Figure III.10). The loss of water during the TGA measurement was 17%, which is 13% more than for the reference experiments (with no $MgCl_2$). This suggests that the precipitated product is hydro hematite ($Fe_2O_3 \cdot H_2O$), which could also be an explanation for its ultrafine particle size.